Melting ice and cloud electrification

Peter F. Martin

MELTING ICE AND CLOUD ELECTRIFICATION

A thesis presented in candidature for the degree of Doctor of Philosophy in the University of Durham

by

Peter F. Martin B.Sc.

of Grey College

June 1971

FOREWORD

Although this thesis is primarily concerned with the electrical effects of melting ice a chapter on the electrification due to evaporating ice has been included as this could be readily studied with the apparatus.

The S.I. system of units has been used with two exceptions. The concentration of ions in solutions are gram molar concentrations and the electrical conductivity of solutions has been expressed in μmho cm^{-1}.

I should like to express my sincere thanks to all those people who have assisted me in any way during the course of my work at Durham. In particular I am grateful to my supervisor Dr. W.C.A. Hutchinson for his guidance throughout the investigation and to Professor G.D. Rochester, F.R.S. for the provision of research facilities in the Physics Department at Durham. I would also like to thank Mr. J. Moralee for his assistance during the construction of the wind tunnel and Mr. J. Scott for the construction of the glassware. I am grateful to the other members of the Atmospheric Physics group for their helpful comments and in particular to Dr. I.M. Stromberg and Dr. R. Dawson for their advice during the early stages of the work and Mr. K.M. Daily for his attempts to standardize my English.

Thanks are also due to the Natural Environment Research Council for the provision of a research studentship.

Finally I wish to thank Mrs. D. Anson for her speed and efficiency in the preparation of the typescript and Mr. J. Normile for carrying out the duplication of the thesis.

ABSTRACT.

A vertical wind tunnel has been constructed inside a cold room to simulate the fall of a frozen water drop from the 0°C level in a thundercloud. It was possible to freely support an ice sphere clear of the sides but the particle crashed early in the melting process. The ice spheres were frozen onto a 120 μm diameter platinum wire and during the final stages of melting the particle hung from the wire and was free to rotate about all 3 degrees of freedom. The spheres melted on this type of support produced the same amount of electrification as those melted on the wire loop support used by DRAKE (1968).

The charge on the meltwater was found to be always positive and to be highly dependent on the freezing rate, and water drops frozen in still air at between -10 and -15°C produced an order of magnitude less charging than drops frozen in an airstream flowing at 11 ms^{-1} at similar temperatures. Examination of the ice particles under a microscope suggested that this effect was due to air escaping from the ice at low freezing rates and smaller air bubbles being formed at high freezing rates. Evidence was found for the enhancement of electrification at high melting rates which DRAKE attributed to the onset of vigorous convection in the meltwater. The effect of carbon dioxide on melting electification was also discussed.

The electrification due to melting precipitation under ideal conditions in a thundercloud was estimated as 4 C km^{-3} which can be compared to 8 C km^{-3} found by SIMPSON and ROBINSON (1941). It was suggested that the importance of melting ice in thundercloud electrification cannot be established until more information is available on the nature of the solid precipitation, the environment in which it melted and the location and magnitude of the lower positive charge.

CONTENTS

CHAPTER 1

THE IMPORTANCE OF MELTING ICE IN CLOUD ELECTRIFICATION

1.1. INTRODUCTION

Many theories of the origin of the electric charges in thunderclouds have been based on theoretical and experimental work on the properties of ice and water. CHAPMAN (1953), DRAKE (1968) and IRIBARNE and KLEMES (1970) have described experiments to assess the importance of some of these cloud electrificiation theories by attempting to closely reproduce the natural environment of precipitation. DRAKE has shown that frozen water drops produce more electrification on melting than would be expected from studies of blocks of ice. The present work attempts to develop this approach to the laboratory study of cloud physics by trying to estimate the importance of melting ice in convective cloud electrification.

DINGER and GUNN (1946), MAGONO and KIKUCHI (1965), DRAKE (1968) and others have reported finding a positive charge of approximately 1000 pC g^{-1} on the meltwater produced from chemically pure ice. This electrification process is of the correct sign, and according to DRAKE the correct magnitude, to be responsible for the creation of the lower positive charge which is often found near the $0^{\circ}C$ level in thunderclouds. Melting electrification may also explain why RAMSAY and CHALMERS (1960) and REITER (1965) have found that precipitation current changes from positive to negative as steady rain turns to snow. I decided to study the melting of small frozen water drops, typically 4 mm in diameter, as they are of a size often found in convective clouds.

1.2. THE THUNDERSTORM

1.2.1. The thundercloud as a meteorological phenomenon

One of the most comprehensive studies of the dynamics of thunderclouds yet undertaken was the American 'Thunderstorm Project' in the late 1940s. The report of the observations made in Florida as part of this project (BYERS and BRAHAM, 1948) has been taken as the basis of a model thunderstorm

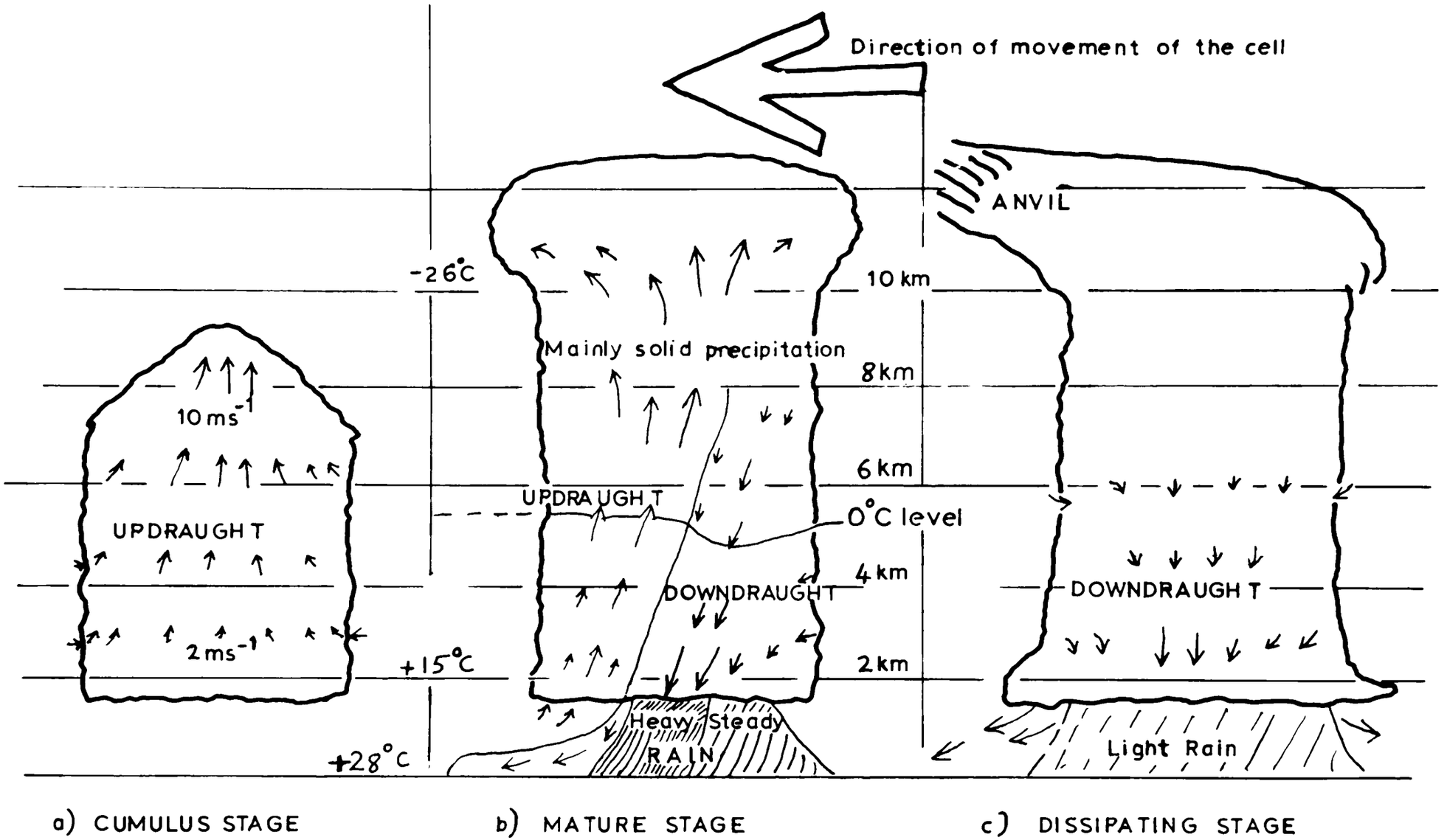

Fig.1.1 The growth of a Florida thunderstorm (After Byers and Braham, 1948, 1953)

ever since. By measuring the distribution of rainfall and observing radar echoes BYERS and BRAHAM picked out cells within a thunderstorm system which were typically 5 km across and contained an updraught and a downdraught. These cells were observed to pass through a well defined series of stages (Fig. 1.1) lasting a total of 30 minutes to one hour, starting from an apparently ordinary cumulus cloud (Fig. 1a). Due to a high level of vertical instability and a plentiful supply of moisture flowing into the cloud, the growth becomes more rapid and more extensive then for an ordinary cumulus. When the downdraught is started, the cloud passes into the mature stage (Fig. 1b) during which most of the lightning and precipitation occur. Finally the downdraught dominates and the cloud enters the dissipating or anvil stage (Fig. 1.1.c). An important feature of this description of the thundercloud is the role of the precipitation in causing the downdraught which then tends to limit the life of the cell.

1.2.2. Classification of thunderstorms

Thunderstorms may be classified as heat or air mass storms and frontal storms, depending on how the initial convergence necessary to start the vigorous updraught was produced. Most heat thunderstorms occur in the tropics overland, especially over mountains. Frontal thunderstorms are usually associated with cold fronts, and tend to persist for several hours as they move with the front, they are more frequent near the coast and can occur over the oceans outside the tropics (Admiralty Weather Manual 1938). The actual size, severity and life of the storm does not depend on its type, but rather on the total available energy, which will be determined by the degree and vertical extent of unstable air and the supply of moisture from below the cloud. Similarly the height of cloud base will be determined by the local meteorological variables especially humidity and will be much greater in the cool dry air of the Alps than in the warm moist air of the tropics.

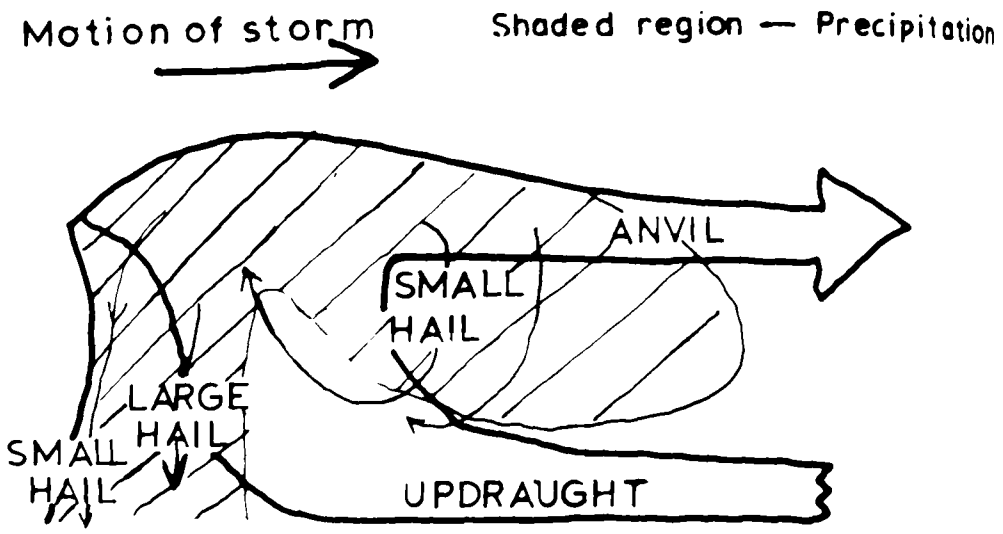

Fig.1.2 A steady state convective storm (Browning,1964)

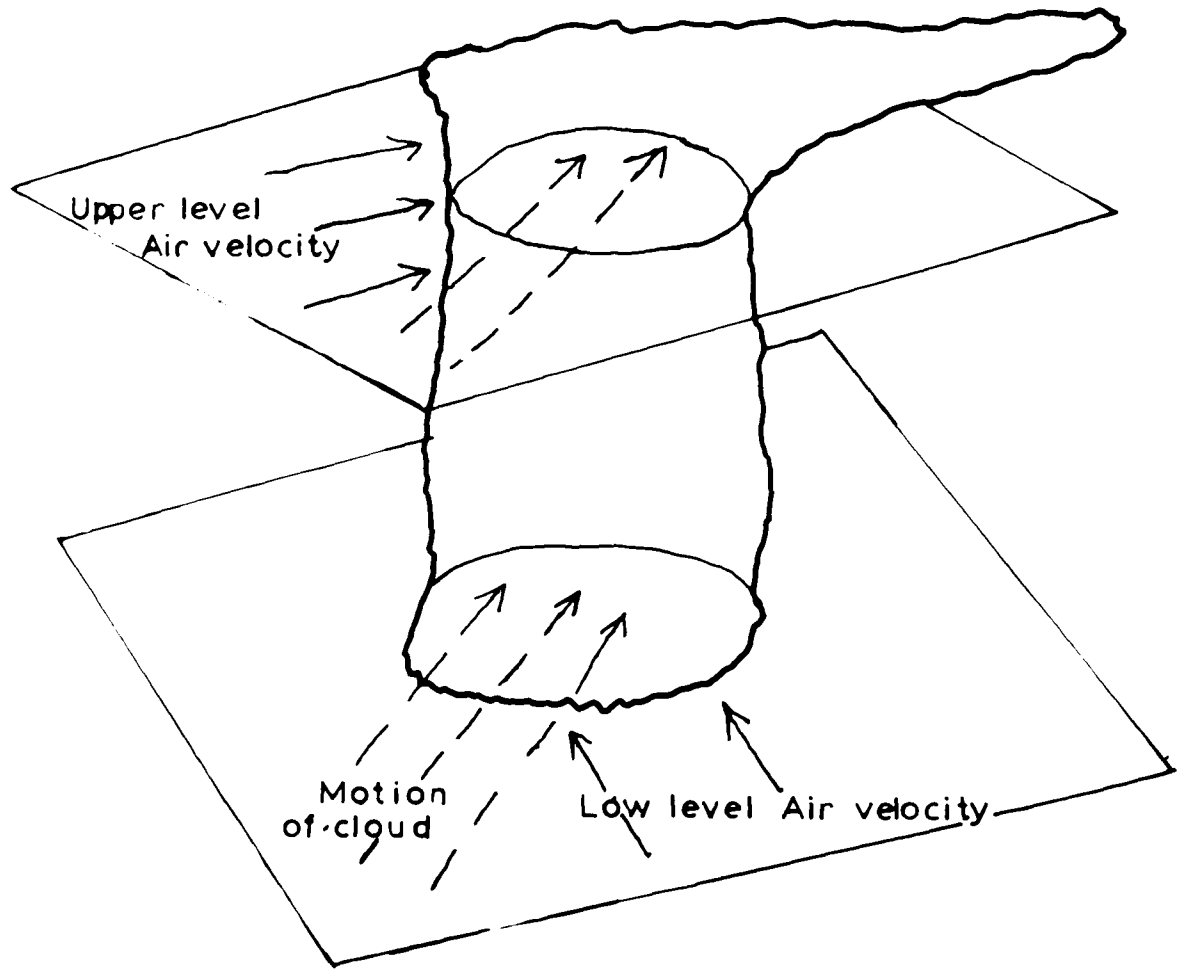

Fig.1.3 A schematic view of a thunderstorm in an environment in which the wind shears with height (Newton,1967)

1.2.3. Severe thunderstorms

There is some evidence thatsevere storms, often producing damaging hail, are associated with single cells or super cells, which persist for several hours. After studying a severe storm at Wokingham in 1959, BROWNING and LUDLAM (1962) described the essential feature of the severe storm as being the sloping of the updraught, enabling the precipitation to fall clear without forming a dominating downdraught as in the storms described by BYERS and BRAHAM (1948). New moist air could then be drawn in from the front of the storm as in Fig. 1.2, enabling the thunderstorm to persist and dominate its environment. According to NEWTON (1967) severe storms are most likely to occur when there are bands of strong winds flowing in different directions near the upper and lower levels of the cloud (Fig. 1.3).

If the storm moves with the velocity of the air in the mid-troposphere, there will be a relative movement between the cloud and its environment near both its top and base. From an analysis of the forces involved NEWTON and NEWTON (1959) suggested that with modest vertical motions a storm column could remain erect with relative horizontal motions between cloud and environment in excess of 10 ms^{-1}. It is probable that while severe storms are not very common, an appreciable number of thunderstorm cells are inclined to the vertical as the result of wind shear. From the Daily Weather Report and the Aerological Record it is possible to deduce values for the maximum relative velocities between cloud and environment when thunderstorms are in the region of the upper air wind sounding. Table 1.1. summarizes the results of this analysis for the British Isles during part of the summer of 1967. From these few results it seems that an appreciable fraction of British thunderstorms may have updraughts slightly inclined to the vertical.

TABLE 1.1 Maximum relative velocities between cloud and environment up to 10 km for summer storms over the British Isles

Relative velocity	Number of thunderstorm days
up to 10 ms^{-1}	9
from 10 to 15 ms^{-1}	11
more than 15 ms^{-1}	5

1.3 THE ELECTRICAL CHARGE DISTRIBUTION IN THUNDERSTORMS

The conventional picture of the thunderstorm having an upper positive and a lower negative charge is supported by the work of SIMPSON and SCRASE (1937) with an altielectrograph and MALAN and SCHONLAND (1951) who measured potential gradient changes due to lightning flashes. A subsidiary lower positive charge has often been observed near cloud base. SIMPSON and SCRASE in England, REYNOLDS and NEILL (1955) in U.S.A. and KUETTNER (1950) in the Alps suggest the negative charge is localised at some temperature between -8^{o} and $-16^{o}C$ depending on the height of the cloud base. However, measurements in South Africa by MALAN and SCHONLAND (1951) suggest that the negative charge is in the form of a column from the $0^{o}C$ level up to $-40^{o}C$. MALAN (1951) has pointed out that the South African storms were observed at Johannesburg 1.8 km above sea level and were generally isolated cumulinimbi as opposed to the English storms which were often of frontal origin and multicellular. However, the work of OGAWA and BROOK (1969) has suggested that the South African results exaggerate the vertical extent of the negative charge because they were single station observations of electric field changes compared to the multiple station measurements of REYNOLDS and NEILL and the vertical dimension probed by the altielectrograph.

TABLE 1.2 The magnitude and position of the main charge centres in thunderclouds

Observer	Positive		Negative	
	charge	height	charge	height
SIMPSON and ROBINSON (1940)	24C	6 km	20C	3 km
GISH and WAIT (1950)	39C	9.5 km	39C	3 km
MALAN (1952)	40C	10 km	40C	5 km

Typical values of the main charges in thunderclouds are found in Table 1.2. They are of the same order as those destroyed in single lightning flashes according to PIERCE (1955) and WORMELL (1939).

1.4 THE LOWER POSITIVE CHARGE

1.4.1 The evidence for a lower positive charge

SIMPSON and SCRASE (1937) found evidence for a local concentration of positive charge in the cloudbase of some thunderstorms usually in front of the main rain area. This lower positive charge has been observed by several other workers (Table 1.3) in some but not all storms. Because of the nature of the measurements and its relative size compared to the main charge centres a lower positive charge may be present in most thunderstorms but is only detected under favourable conditions. From the results of SIMPSON and ROBINSON (1940) and MALAN (1952) it would appear that the subsidiary charge is about one quarter of the magnitude of the main charges. Table1.3 also indicates that the vertical position of the charge seems to be independent of temperature but usually it is located in the lowest kilometre of cloud.

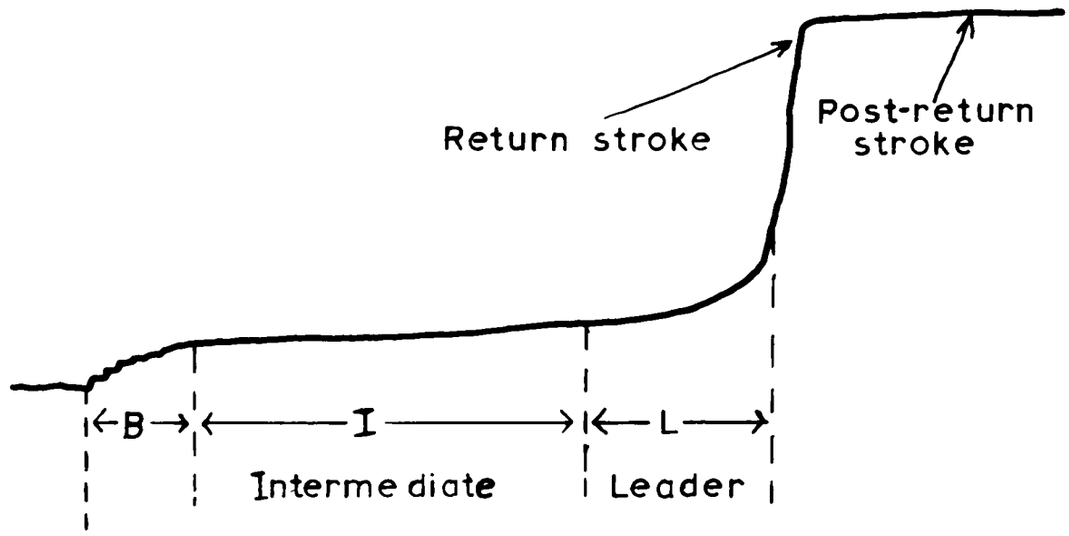

Fig.1.4 Typical electric field changes at 5 km from a discharge to ground (Clarence and Malan, 1957)

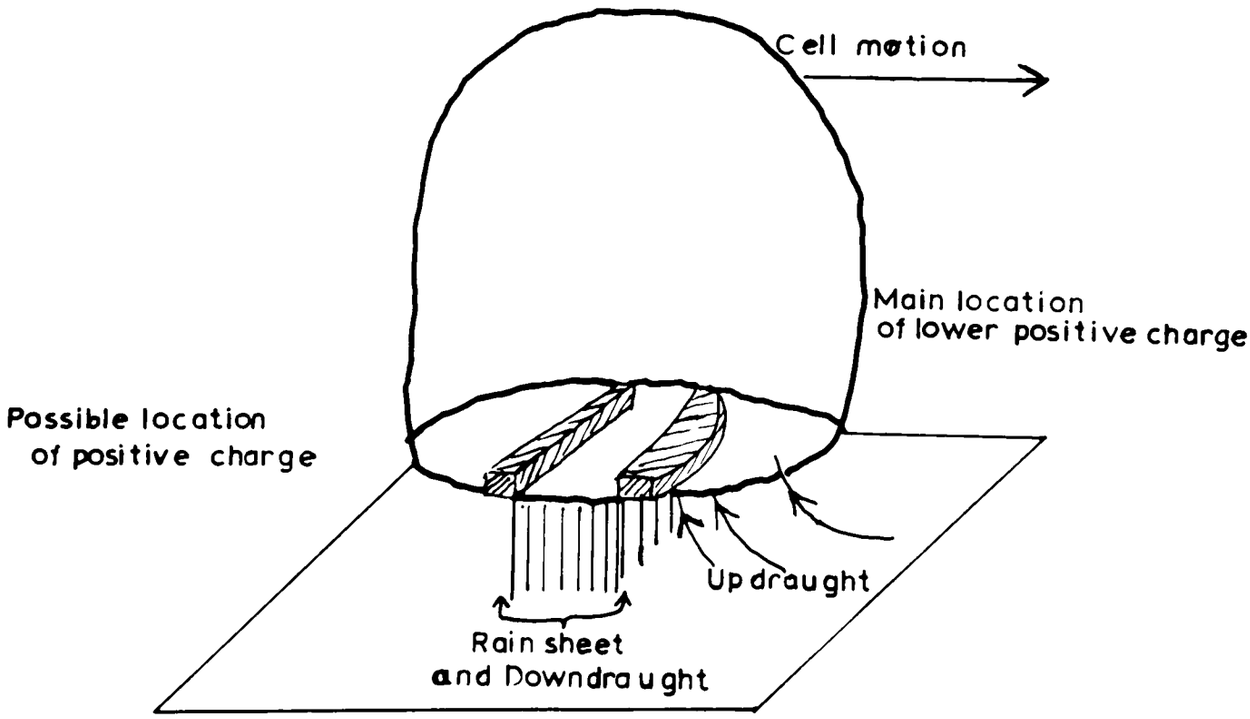

Fig.1.5 THE LOCATION OF THE LOWER POSITIVE CHARGE (WILLIAMS, 1958)

TABLE 1.3 The location of the lower positive charge

SOURCE		POSITION	TEMPERATURE
REYNOLDS and NEILL (1955)	New Mexico	1 km above cloud base	-3 °C
SIMPSON and ROBINSON (1941)	England	0.5 km " "	+8 °C
KUETTNER (1950)	Zugspitze	0.5 km " "	0 °C
MALAN (1952)	Johannesburg	cloud base	+5 °C
MALAN and SCHONLAND (1951)*	Johannesburg	0.5 km below cloud base	+8 °C
MALAN and CLARENCE (1957)*	"	0.5 km " " "	+8 °C

*Denotes that the bottom of the charged region was located.

1.4.2 The role of the lower positive charge in the lightning discharge

WHIPPLE (1938) suggested that lightning is not due to an exceptionally large potential difference between cloud and ground because it is possible to have cloud-ground lightning without point discharge under the active part of the cloud. He also tentatively suggested that lightning could be initiated by a build-up of positive point discharge ions in the base of the cloud.

CLARENCE and MALAN (1957) found evidence for this process by studying the electrostatic field changes that occurred before the first stroke in a lightning flash. Fig.1.4 shows the initial breakdown stage (B) lasting up to 10 ms which is followed by an Intermediate stage (I) lasting up to 400 ms after which the leader and the return stroke start the lightning discharge proper. At horizontal distances up to 2 km from the discharge the B field changes were observed to be negative while for distances in excess of 5 km they were positive, and between 2 and 5 km the field changes were equally likely to be positive or negative. CLARENCE and MALAN interpreted this initial breakdown as being due to a discharge in the cloud between a positive and a negative region where the maximum field at the ground due to these charges was located at 2 km and 5 km from the discharge. Using SIMPSON's (1927) result that the maximum field at the ground at a horizontal distance D from the charge passes through a maximum when the

charge passes through a maximum when the charge is at a height H

$$\text{where} \qquad H = \sqrt{2}\,D$$

CLARENCE and MALAN located the positive charge at 1.4 km and the negative at 3.6 km. These values agree well with the height of the cloud base and the lower region of the negatively charged column found by MALAN and SCHONLAND (1951). These results strongly suggest that the lower positive charge plays an essential part in the lightning discharge in at least some thunderstorms.

1.4.3 The location of the lower positive charge

WILLIAMS (1958) has compared the data in Table 1.3 and has drawn up a model of a thunderstorm cell (Fig. 1.5) in which the lower positive charge is located in the form of a prism 1 km wide on the boundary between the updraught and downdraught. He also suggested that there is a region of positive charge on the rear side of the downdraught. WILLIAMS found evidence for this model by analysing the experiment of FETERIS (1952) in which a dense network of ground observers reported the position and time of occurrence of every flash to ground from a single cell whose radar echo had a maximum diameter of 10 km. Assuming that the lower positive charge was involved in all the lightning flashes WILLIAMS used this analysis to confirm the horizontal distribution of the lower positive charge in his model.

1.5 THEORIES OF THE FORMATION OF THE LOWER POSITIVE CHARGE

1.5.1 Melting precipitation

CHALMERS (1965) suggests three ways in which the melting of solid precipitation may cause the charge separation necessary to produce the lower positive charge.

1) The bursting of air bubbles trapped in the ice (1.5.3)

2) large snowflakes or hail may melt to form waterdrops which are so large that they break up. (1.5.4)

3) when ice and water are in contact, the water may be positively charged, so any splashing, rubbing or shaking off of water from the surface of a melting particle will cause charge separation. (1.5.5)

1.5.2 The evidence for solid precipitation in thunderclouds

While it can probably be stated that the majority of thunderstorms in temperate climates extend above the 0°C level and have precipitation in the ice phase, there is a growing weight of evidence for the existence of warm thunderstorms with no ice present at all and whose precipitation growth is by the coalescence of water drops. FOSTER (1950), LANE-SMITH (1969), and MICHNOWSKI (1963) have reported seeing lightning from clouds whose tops did not extend above the 0°C level. The Admiralty Weather Manual (1938) states that thunderstorms often occur in Java with tops below the summits of nearby mountains which are all less than 3 km altitude. This implies that the tops of clouds are very close to the 0°C level. However in all the thunderclouds where the lower positive charge has been found the cloud extended for several kilometers above the 0°C level and it is not possible to say whether this charge is present in warm thunderstorms.

1.5.3 The air bubble theory of the lower positive charge.

The work of DINGER and GUNN (1946), MAC CREADY and PROUDFIT (1965a) and MAGONO and KIKUCHI (1965) provides strong evidence that when ice melts the meltwater acquires a positive charge of the order of 300 pC g^{-1} provided that air bubbles are released from the ice. DRAKE (1968) found that when frozen water drops of 1 to 6 mm in diameter are melted in an airstream vigorous convection may develop in the meltwater and the electrification is then enhanced by as much as an order of magnitude. The positively charged melting hail or snow will fall clear of the air which has become negatively charged so producing a net positive charge below the 0°C level. DRAKE estimated that this charging process could account for a positive charge

density of 10 C km^{-3}, which agrees well with the probable value of 8 C km^{-3} calculated by MASON (1957).

There are several objections to this theory, the most important being that it is very sensitive to ionic impurities and it may be argued that DRAKE considered water which was more pure than occurs in natural clouds. If this charging process can be explained by the IRIBARNE and MASON (1967) theory of bubble-bursting electrification, one would expect the spectrum of air bubbles sizes ~~the structure of the ice~~ to be an important factor. Finally it is not known whether vigorous convection would develop in real precipitation falling through a real atmosphere.

1.5.4. The drop-shattering mechanism

If large snowflakes or hailstones melt to form water drops which are larger than about 5 mm in diameter the resultant raindrops will break up as they gather speed under gravity. SIMPSON (1909) and CHAPMAN (1953) have found that breaking water drops separate charge, with the drops becoming positively and the air negatively charged. The actual magnitude of the charge depends on the severity of the shattering process and according to CHAPMAN can vary from 0.4 pC g^{-1} up to 1000 pC g^{-1} where the relative velocity of drop and airstream are as much as 5 ms^{-1}. CHAPMAN suggests that if there is enough microturbulence in the cloud to give drops a momentary velocity of 1 ms^{-1} relative to their surroundings then charges of 100 pC per drop are possible. This process could be important in the turbulent interface between updraught and downdraught where WILLIAMS (1958) has located the lower positive charge in thunderclouds.

A further advantage of this mechanism is that it is less sensitive to ionic impurities than the bubble bursting theory. MATTHEWS and MASON (1964) have found that when large drops are gently disrupted in an airstream, the electrification can be increased by a factor of a hundred to 300 pC g^{-1} by applying an electric field of the order of 3×10^4 V m^{-1}. As such a field would be expected in a thundercloud this process should be active to some extent below the $0^{\circ}C$ level.

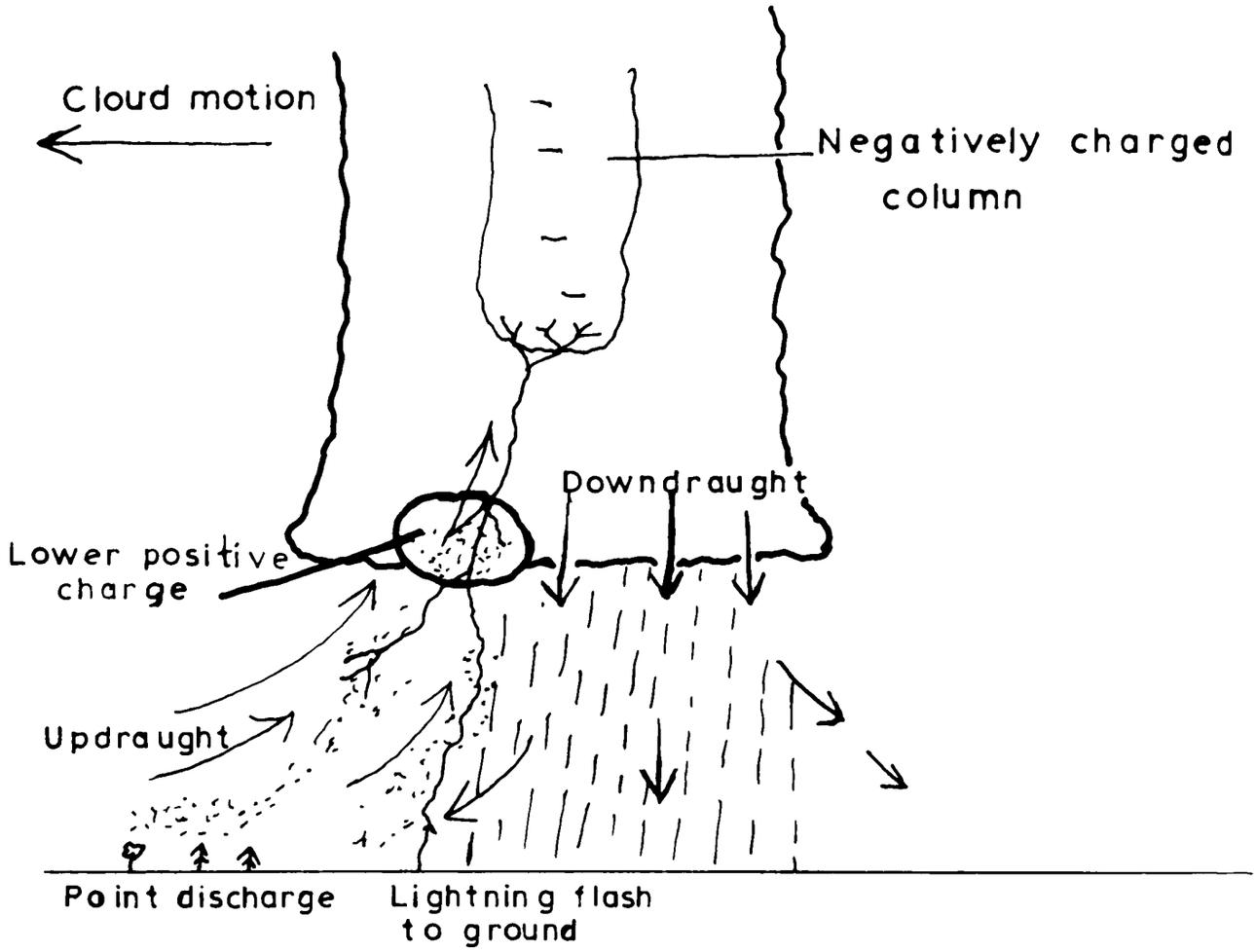

Fig. 1.6 The point discharge origin of the lower positive charge (MALAN, 1952)

1.5.4 The Ice-Water contact theory

Because the mobility of protons exceeds that of the hydroxyl ions in ice, and since for both ions the concentration is higher in water, there should be a tendency for the protons to pass through to the ice more easily than the hydroxyl ions, thus making a thin film of meltwater negatively charged. TAKAHASHI (1969) found this charge separation to be about 1500 pC cm^{-2} which for a 4 mm ice sphere corresponds to 75 pC spread over the surface. If water is shed during the melting process the melting particle will become positively charged. This mechanism could be important in the electrification of melting snowflakes, where air bubbles escape from a thin film of water.

1.5.5. The point discharge theory

WILLIAMS (1958) has pointed out that the lower positive charge has been observed to lie in the lowest kilometre of cloud and its location does not seem to be correlated with temperature. KUETTNER (1950) and REYNOLDS and NEILL (1955) located the charge at or above the 0°C level which does not allow the theories involving melting ice to be a satisfactory explanation, although it is not easy to estimate accurately the temperature inside clouds. MALAN (1952) has suggested that ions from point discharge may get caught in the updraught below the thundercloud (Fig. 1.6) and become immobilised by attachment to cloud particles in the base of the cloud. MALAN points out that most of the lightning flashes to ground in Johannesburg seem to take place to the front of the advancing storm where the point discharge ions are being caught in the updraught. This theory has only been explained in a qualitative way but it could explain the anomaly of the absence of an increase of field measured by the alti-electrograph below thunderclouds.

1.6 Laboratory Assessment of the Theories of the Formation of the Lower Positive Charge

Three theories of the lower positive charge have been outlined, which involve the electric surface or bulk properties of ice and water. The choice

between these theories does not seem to be determined by verifying these particular properties of the water substance, but rather by attempting to ascertain whether the mechanisms in which these properties are active do in fact occur in the region of the lower positive charge. It was therefore decided to try and simulate as closely as possible the conditions present in the thundercloud and at the same time make the necessary electrical measurements to assess the importance of melting ice in the lower regions of thunderclouds.

CHAPTER 2

PREVIOUS STUDIES OF MELTING ICE ELECTRIFICATION

2.1 EXPERIMENTS WITH BLOCKS OF ICE

DINGER and GUNN (1946) melted 2-ml ice blocks in a warm airstream and found that the meltwater acquired a positive charge of about 0.4 pC mg^{-1} if the ice was made from distilled water. The amount of charge separated decreased rapidly if the melting rate fell below 10 mg s^{-1} or carbon dioxide was dissolved in the ice. Small quantities of ionic impurities of the order of 20 mg l^{-1} were sufficient to reduce the charging by a factor of ten. DINGER and GUNN suggested that the charge separation mechanism was related to the escape of air bubbles trapped in the ice and pointed out that the reduction of charging with increased impurity levels was similar to the behaviour of the charge on air bubbles which had been investigated by McTAGGART (1914) and ALTY (1926).

MATTHEWS and MASON (1963) repeated Dinger and Gunn's experiment but failed to find any charging above 0.003 pC mg^{-1}. In two later notes MATTHEWS and MASON (1964) and DINGER (1964) suggest that this null result might be caused by the presence of a high concentration of carbon dioxide in the laboratory, due to the use of dry ice. McCREADY and PROUDFIT (1965) also repeated the Dinger-Gunn experiment and found that the meltwater acquired a positive charge of about 0.02 pC mg^{-1}. ROGERS (1967) melted 15-mm diameter ice spheres, supported on an air jet, and found that the partially melted spheres were negatively charged if water had been flung off and positively charged otherwise.

2.2. THE MELTING OF FROZEN WATER DROPS

DRAKE (1968) carried out a thorough study of the electrification accompanying the melting of frozen water drops over a wide range of melting conditions. The ice particles were frozen onto a 1mm loop of

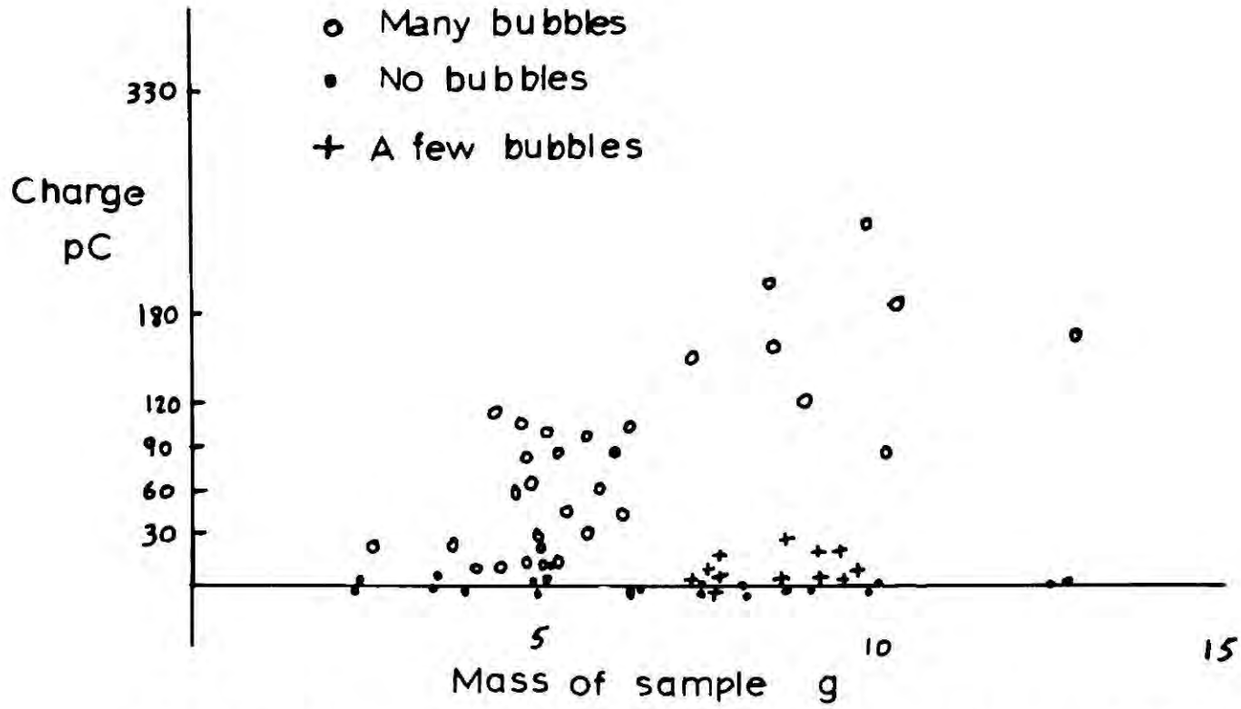

Fig.2.1 The effect of air bubbles on melting electrification

(After KIKUCHI,1965a)

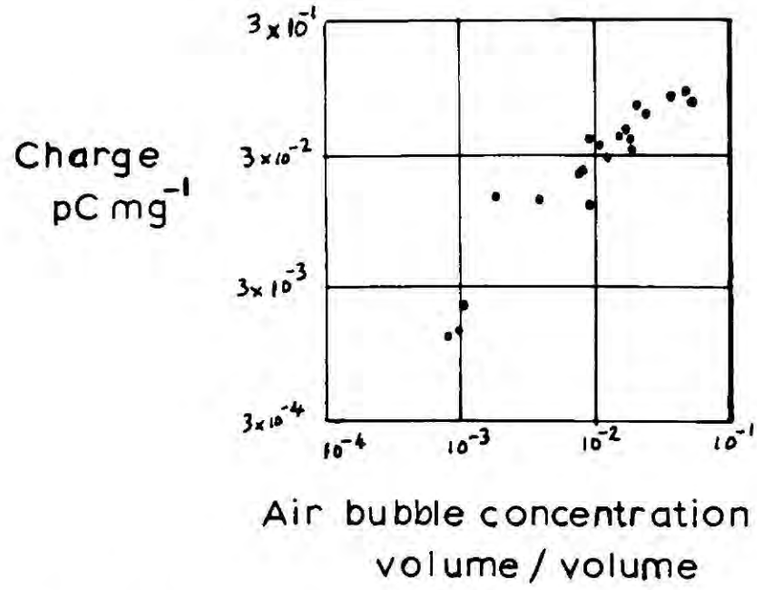

Fig.2.2 The relationship between air bubble concentration and melting electrification

constantan wire amd melted in a controlled airstream. DRAKE found that, when convection currents developed in the meltwater, the charging increased by an order of magnitude. He also found that carbon dioxide only inhibited charging if there was no convection in the meltwater and that high concentrations of carbon dioxide increased the charging. The actual amount of charging depended on the rate of heat flow to the melting ice and on the freezing temperature and purity of the water. For water with a concentration of impurity ions of less than 2 mg l^{-1} the charge separated lay typically between 1 and 2 pC mg^{-1}.

DRAKE found a good qualitative argeement with the amount of electrification predicted by the application of the IRIBARNE and MASON (1967) bubble bursting electrification experiments to the escape of trapped air bubbles from the melting ice. However, the enhancement of electrification with high concentrations of carbon dioxide did not fit this theory.

2.3. THE BUBBLE-BURSTING THEORY OF MELTING ELECTRIFICATION

2.3.1 The evidence for an air bubble mechanism.

KIKUCHI (1965a) showed that blocks of ice made from deionized water did not become charged on melting unless some air bubbles were present in the ice (Fig. 2.1). The level of charging was typically two orders of magnitude less than that found by DRAKE (1968), probably because of the different melting conditions. KIKUCHI also found that the higher theconcentration of air bubbles trapped in the ice, the greater the charging (Fig. 2.2). If large air bubbles of about 1 mm diameter were present, the charging was reduced, suggesting that the spectrum of bubble sizes was also important. Although KIKUCHI estimated the mean charge on an air bubble to be 3×10^{-4} pC, this cannot be directly compared with the result of the experiment of IRIBARNE and MASON (1967) who studied bubbles larger than 160 μm compared to the average diameter of 50 μm in the ice samples. This value for the charge

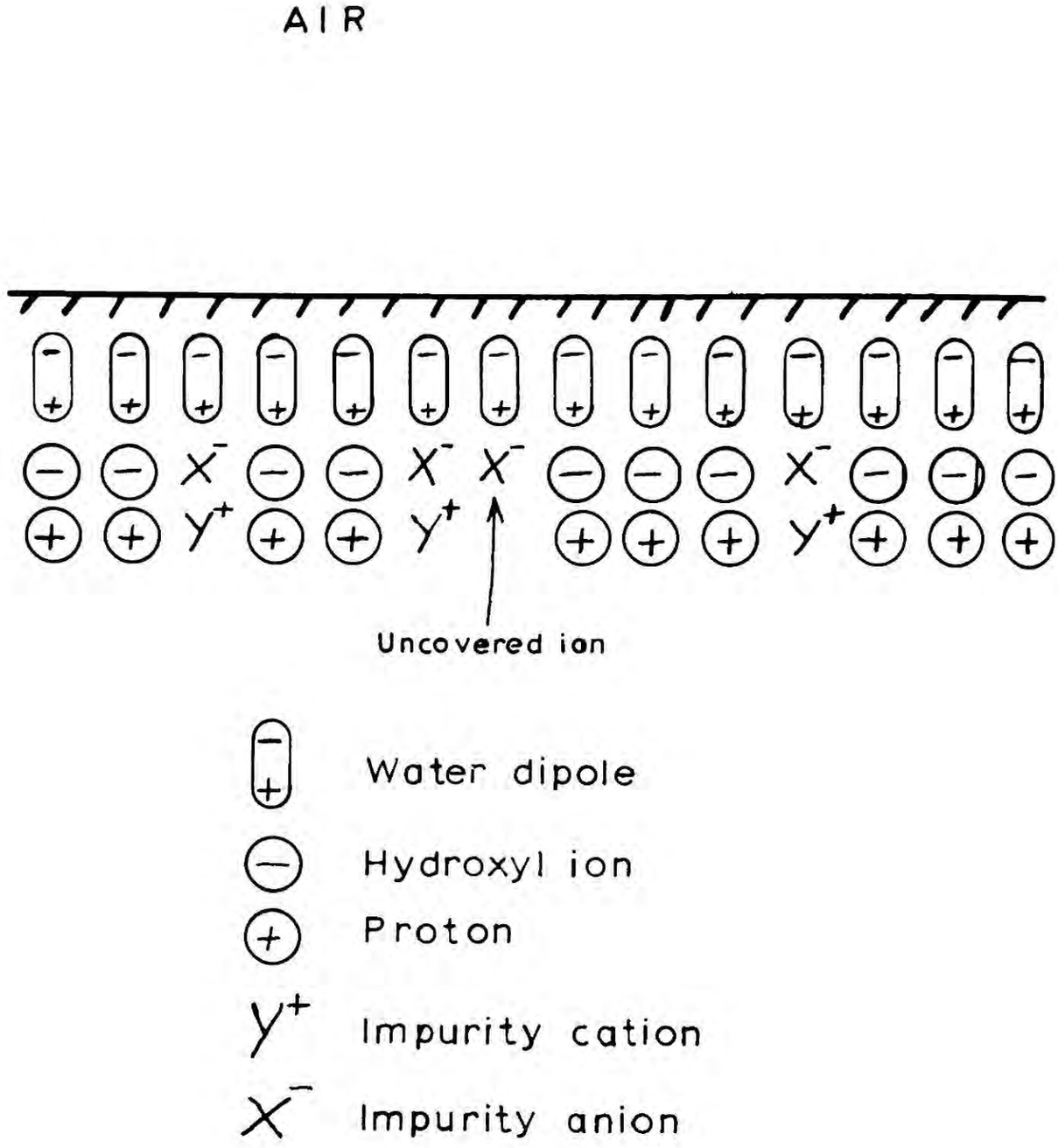

Fig.2.3 Schematic illustration of the double layer (After Alty, 1926)

on an air bubble is not inconsistent with the IRIBARNE and MASON experiments if one assumes the main ionic impurity to be atmospheric carbon dioxide dissolved in the ice.

2.3.2. The Electrical double layer at an air-water interface.

The separation of charge when air bubbles burst at a water surface and when water drops splash or shatter may be explained by the rupture of an electrical double layer of positive and negative charges at the air-water interface. The existence of such a double layer was first suggested by HELMHOLTZ (1879), and its presence confirmed by the work of McTAGGART (1914) and ALTY (1926), who studied the motion of air bubbles in an electric field. By studying the way in which the negative charge on air bubbles in pure water varied with bubble size and purity of the water, ALTY developed a theory describing the form of the charges which made up the double layer (Fig. 2.3).

ALTY said that the polar water molecules were orientated in a preferred direction at the air-water interface, with the positive end of the dipoles pointing into the liquid. These surface molecules electrostatically attracted negative ions and other water molecules. In very pure water with a typical conductivity of 10^{-4} ohm^{-1}m^{-1} impurity ions will be present in concentrations of 1 in 10^7 and ionized water molecules in 1 in 10^8. Most of the surface water dipoles will become covered with a string of water molecules bonded to them by hydrogen bonds. ALTY showed that the impurity negative ions were attracted to the surface in concentrations of about 1 in 10^7 to 10^8. This layer of negative ions then attracted impurity positive ions and protons which formed a diffuse space charge and which were more readily removed by molecular collisions and air escaping from the bubble. The air bubbles in ALTY's experiment were negatively charge because 10% of the negative ions were not covered by positive ions (Fig. 2.3).

CHALMERS and PASQUILL (1937) measured the potential difference across a water-air interface and found that this could be explained by 1 in 25 of the water dipoles being orientated perpendicular to the surface. They

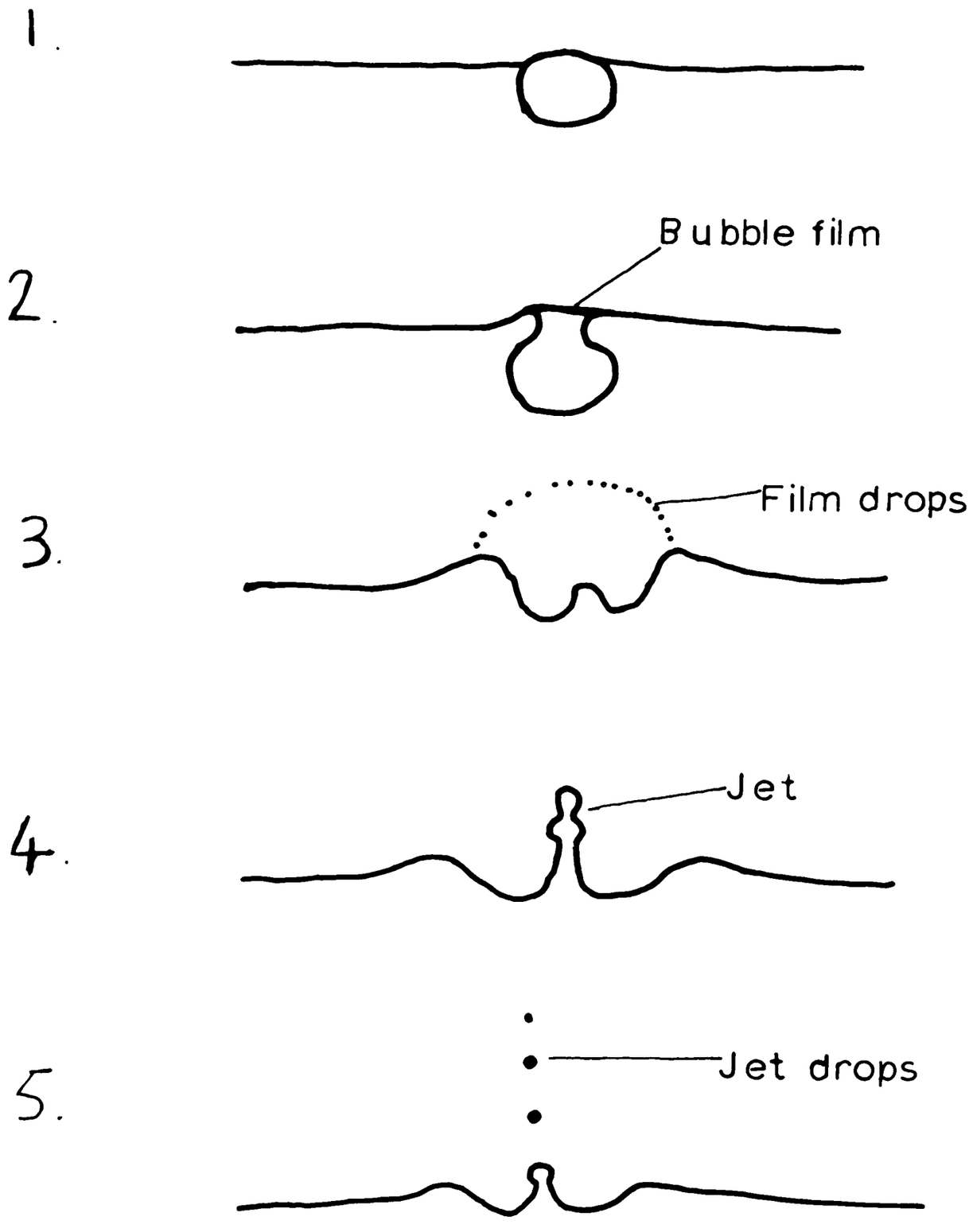

Fig.2.4 The bursting of a 1·5 mm air bubble
(After Woodcock et al. 1953)

suggested that in reality the water molecules are not all orientated in the same direction as ALTY has suggested but on average tend to produce the effect observed.

2.3.3. The mechanism of bubble bursting

The bursting of air bubbles at a water surface has been studied with a high speed cine camera by WOODCOCK et al (1953), who obtained a series of photographs similar to Fig. 2.4. WOODCOCK found that the bursting process was similar for bubbles with diameters ranging from 0.2 to 2 mm. In stage 1 the bubble reaches the surface and then forms a raised cap or film (stage 2). This film bursts and may eject a large number of small droplets called film drops (stage 3). A small jet forms at the base of the depression and grows rapidly as the raised lip subsides (stage 4). The jet becomes unstable and on reaching its maximum height ejects typically five drops called jet drops (stage 5). The total time taken from stages 1 to 5 was of the order of 2 ms. The diameter of the jet drops were found to increase with bubble size from 10 μm for a 100 μm bubble to 100μm for a 1mm diameter bubble.

The time taken for the film droplets to form is generally a few microseconds and MASON (1954) using a microscope slide technique has measured the diameters to range from 0.4 to 1.0 μm. DAY (1964) and BLANCHARD (1963) demonstrated that the number of film drops produced fell off rapidly from 100 for a 2 mm diameter bubble to 10 for a 1mm bubble and less than 1 for a 300 μm bubble. BLANCHARD (1963) estimated the charge carried by a film drop to be 3 electron charges per droplet from a bursting bubble in seawater, which is a factor of 10^3 less than the charge carried by a jet drop from a similar bubble. It can therefore be assumed that the maincharge transfer mechanism associated with air bubbles released in the melting of small precipitation particles will be related to the ejection of jet drops.

2.3.4. Charge separation accompanying the bursting of bubbles.

BLANCHARD (1963) and IRIBARNE and MASON (1967) have found that the droplets ejected from bursting bubbles are generally negatively charged for water with ionic impurity concentrations less than 10^{-4} N and

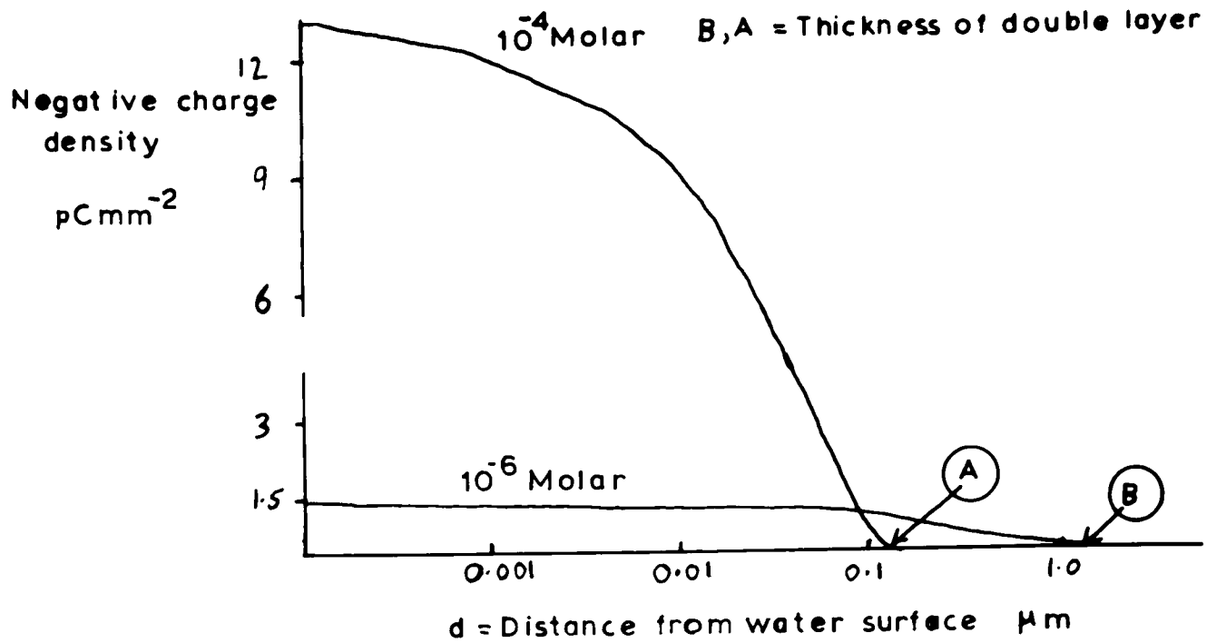

Fig. 2.5 Net charge density between the surface and a depth d

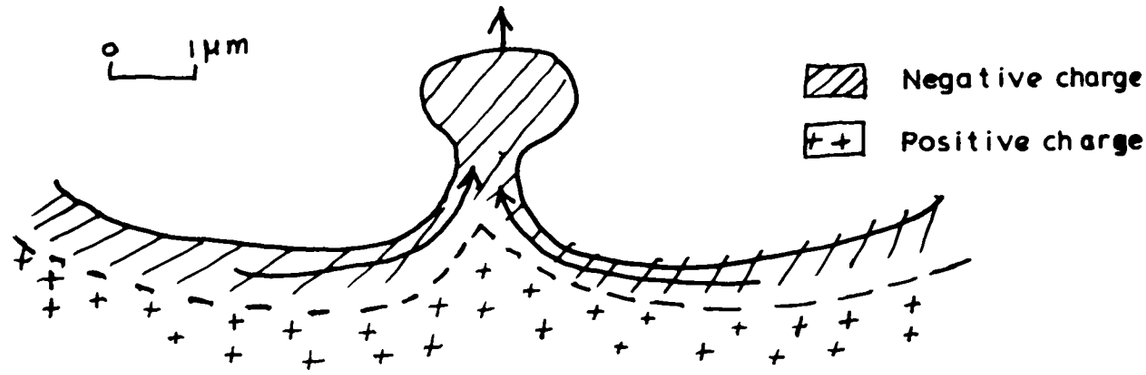

Fig.2.6 a. Formation of a negatively charged jet — Pure water

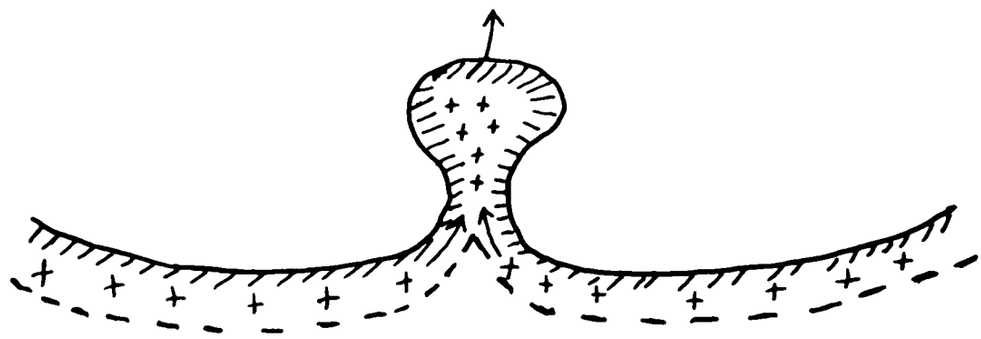

Fig.2.6 b. Formation of a neutral jet — Less pure water

positively charged for less pure water. IRIBARNE and MASON explained these results qualtitatively by studying the behaviour of the double layer during the formation of the jet drops.

IRIBARNE and MASON postulated that the jet was composed of the water nearest the surface of the air bubble, which had slid down the edge of the depression to form a jet at the centre (Fig. 2.4). From photographs of the formation of these jets, taken by WOODCOCK et al (1953) and NEWITT et al (1954), they estimated that the volume of the jet was about 1% of the volume of the bubble. They were then able to calculate the depth d of the surface layer which was needed to make the jet of a bubble of radius R. (Equation 2.1).

$$d = \frac{R}{300} \qquad \text{.....2.1}$$

If the surface layer down to a depth d is mainly the negative half of the double layer then the jet will be negatively charged (Fig. 2.6A). However, should d be greater than the thickness of the complete double layer then the jet will be neutral (Fig. 2.6B). So the thickness of the double layer will govern the charge separation due to bubble bursting and the way this charging varies with bubble size.

2.3.5. The effect of impurities on the thickness of the double layer.

By considering the rate of removal of the ions of the double layer from the electrostatic attraction of the surface water dipoles, GOUY (1910) deduced an expression for the integrated charge density σ over the distance from the surface to a depth x (Equation 2.2).

$$\sigma = (\alpha D T c^{\frac{1}{2}} \exp(-\tfrac{1}{2} \beta c^{\frac{1}{2}} x) \qquad \text{.....2.2}$$

where α and β are constants containing the gas constant and the permittivity of a free space.

D is the dielectric constant of water

T is the absolute temperature

c is the gram molar concentration of ionic impurity.

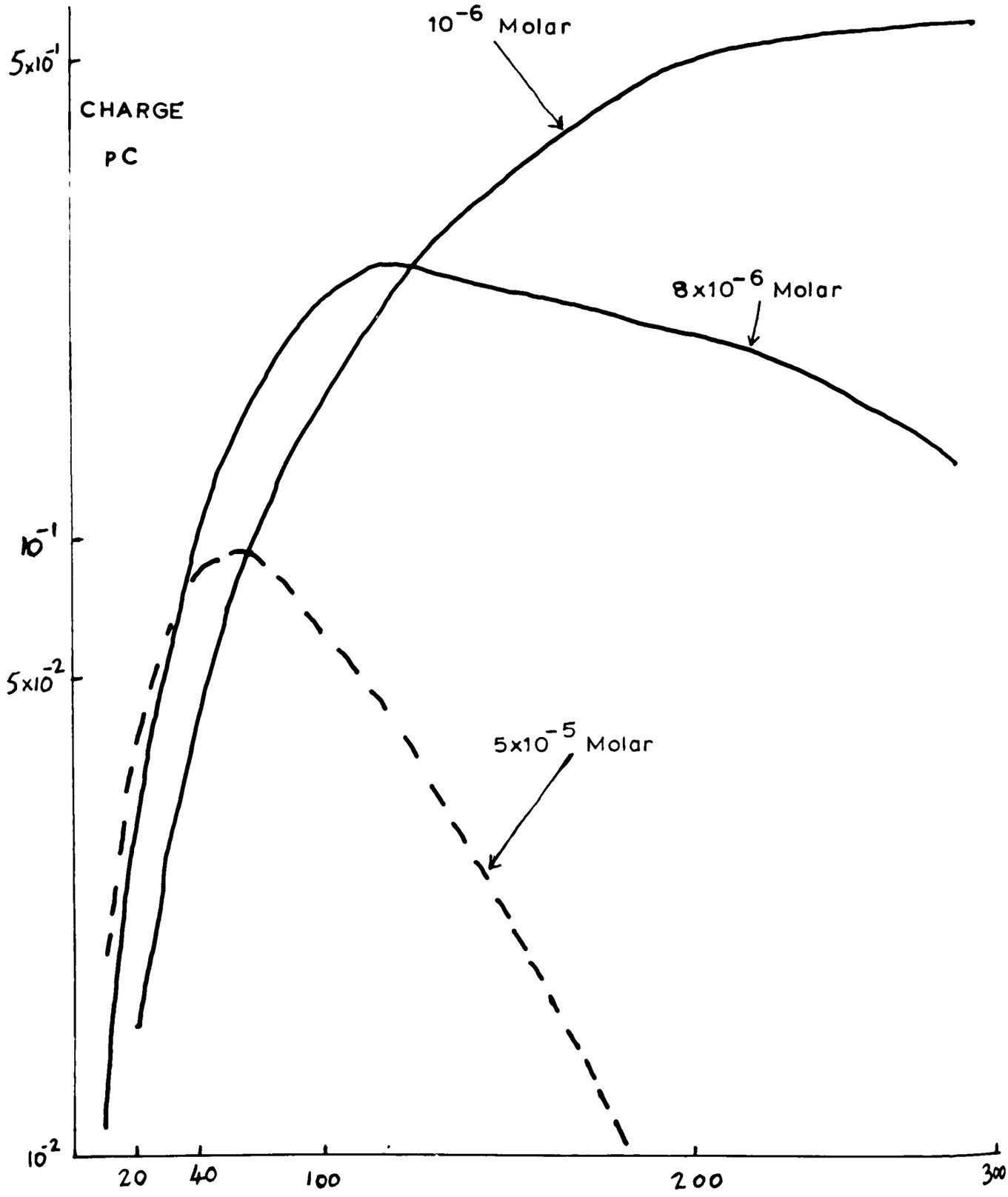

Fig.2.7 Charge separated by the bursting of bubbles
Iribarne and Mason—theory

In fig. 2.5 σ is plotted as a function of x for two concentrations of impurity, 10^{-6} M corresponding to extremely pure deionized water and 10^{-4} M corresponding to a typical cloud water concentration of 6 mgl^{-1} of sodium chloride. The thickness of the double layer is the distance from the water surface at which σ , the integrated charge density below the surface falls to zero. It can be seen from fig. 2.5 that a factor of 100 increase in the ionic impurity concentration causes a factor of 10 decrease in the thickness of the double layer. From equation 2.1, the thickness of the surface layer d which forms the jet of a 200 μm diameter bubble is 0.3 μm and IRIBARNE and MASON observed that bubbles of this diameter eject jet drops of total charge -3×10^{-2} pC for 10^{-5} M solutions and $+ 3 \times 10^{-4}$ pC for 10^{-4} M. These observations agree qualitatively with the above theory.

2.3.6 The dependence of the charge separated by bursting bubbles on the water purity and bubble radius.

By combining equations 2.1 and 2.2, IRIBARNE and MASON deduced a relationship between the total charge on the jet drops (Q) and the water purity and bubble radius. (equation 2.3).

$$Q = 2.9 \times 10^{9} R^{2} C^{\frac{1}{2}} \exp\left(-\tfrac{1}{2} - 1.1 \times 10^{7} C^{\frac{1}{2}} R\right) \quad \ldots 2.3$$

where Q is measured in pC.

Figure 2.7 is a graph of this equation, from which it is clear that for any impurity concentration there should be a bubble diameter at which the charge separated is a maximum. These maxima should also tend to occur at smaller bubble diameters as the water becomes less pure. IRIBARNE and MASON found good agreement with this theory down to 200 μm, the smallest bubbles that they studied. A possible cause for the breakdown of equation 2.3 for bubbles of less than 100 μm diameter may be that the volume of the jet may not be 1% of the volume of the bubble. This behaviour of very small bubbles may be very important in explaining the electrification of melting ice as ice samples often contain many bubbles smaller than 50 μm.

2.3.7 The reversal of the sign of charge separation with very impure water.

If the jet is made up of both components of the double layer then according to the above theory the jet drops should be uncharged. However, IRIBARNE and MASON have suggested a mode of charge separation which will explain their own and BLANCHARD's (1963) observations that with high levels of impurity the jet drops are positively charged with typically 3×10^{-4} pC separated per bubble. As the jet breaks up necks will form between the bulges, which eventually form the drops. Water will tend to flow out of these necks into the drops which are then ejected. Now the positive space charge of the double layer will tend to be distributed along the vertical axis of the jet and so will tend to move out of the necks faster than the negative part of the double layer which is restricted by the surface. IRIBARNE and MASON applied the theory of the flow of water in a capillary tube to the outflow of positive charge from the neck and obtained an upper value for the charge separation of 3×10^{-3} pC, which agrees well with their observations.

2.3.8 The release of air bubbles by melting ice.

When a water drop is frozen virtually all the dissolved air is released as bubbles which are then trapped in the ice. On melting these bubbles are liberated from the ice and are partly absorbed by the meltwater before bursting at the water surface. Because the solubility of air in water rapidly decreases with ~~falling~~ rising temperature, a high proportion of the bubbles will reach the water surface and burst. The amount of air which would be released by the melting of a 4 mm diameter water drop frozen at -10°C would be about 0.45 mm^3. The ice particles melted by DRAKE (1968) and the author contained air bubbles ranging from 10 μm up to 400 μm diameter, however DRAKE did not find any noticeable correlation between bubble spectrum and the degree of charging on melting. He explained this by pointing out that the air bubble structure changed during the melting process as some bubbles coalesced and others dissolved.

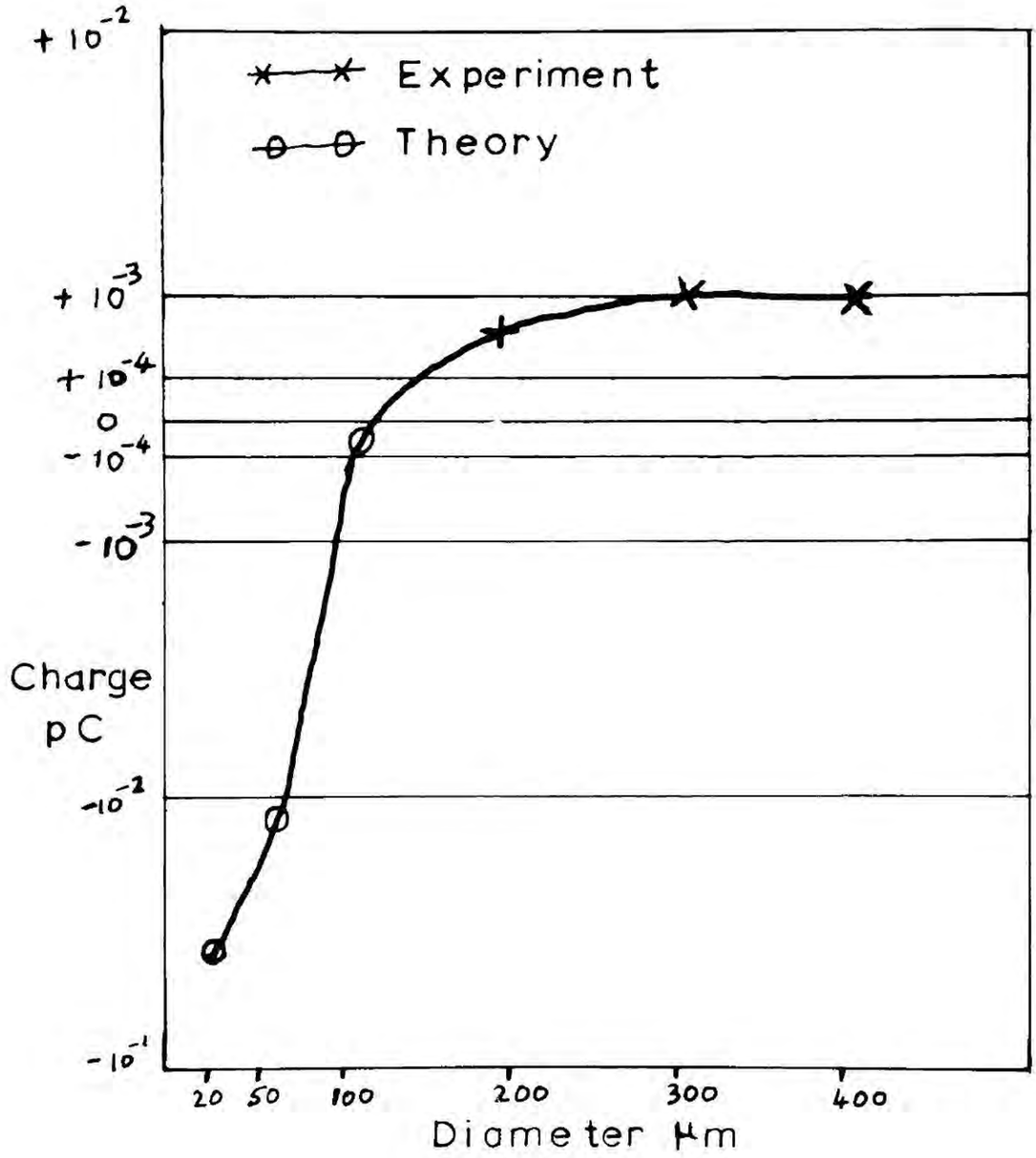

Fig.2.8 The charge separated by the bursting of bubbles in a $3{\cdot}5 \times 10^{-4}$ Molar solution

Iribarne and Mason (1967)

2.3.9 The application of the bubble bursting theory to melting ice electrification.

DRAKE found that the way in which the charge separated by melting ice varied with the concentration of ionic impurities agreed with the IRIBARNE and MASON bubble bursting theory for concentrations less than 10^{-4} M. The less pure the water, the smaller the charge gained by the meltwater. However the theory predicted that the meltwater should become negatively charged for impurity concentrations greater than 10^{-4} M. DRAKE did not find this.

It is suggested by the author that the reason why DRAKE failed to find a reversal in the sign of charge separated was that at high impurity concentrations the charging of small air bubbles is more important than that of the larger bubbles. Figure 2.8 shows the variation in the charge carried by the ejected drops as a function of bubble diameter for water of purity 3.5×10^{-4} M. Below 100 μm diameter the IRIBARNE and MASON theory predicts that the drops ejected will be negative, so in the melting of ice the meltwater would be positively charged.

Further, the negative charge carried by the drops from a 20 μm diameter bubble should be an order of magnitude greater than the positive charges from a 300μ bubble. So even the meltwater from ice of greater than 10^{-4} M concentration of ions may be positively charged, if there are enough bubbles smaller than 50 μm. The range of air bubble diameters in the samples melted by DRAKE was 10 to 400 μm.

Another possible disagreement between experiment and theory was the enhancement of electrification which was found by DRAKE for ice with high concentrations of carbon dioxide. According to the double layer theory the carbon dioxide should have inhibited electrification. It will be suggested later in this thesis that the carbon dioxide probably had escaped from the air bubbles before they burst at the surface of the meltwater.

2.3.10 Melting ice electrification and the spectrum of air bubble sizes.

The range of air bubble diameters trapped in the ice samples of DRAKE and KIKUCHI (1965) was 10 μm to 400 μm. From both the theory and experiments of IRIBARNE and MASON it would be expected that the charge separated by bubbles in different parts of the bubble diameter spectrum would vary considerably with the concentration of impurities. The spectrum probably depends on the rate of freezing of the original water and the size of the water drops. Water drops frozen in an air stream will freeze much faster than in still air. The size distribution of air bubbles in solid precipitation will be highly influenced by the conditions under which the ice particles grow and will be different for opaque and clear hail. Finally, the way in which the ice melts may affect the size of the air bubbles actually bursting at the surface, as the rates at which they dissolve or coalesce may be altered.

2.4 FACTORS INFLUENCING THE CHARGING OF MELTING NATURAL ICE PARTICLES

Laboratory studies of melting ice and bubble bursting electrification have revealed several properties that will decide the amount of charging produced in the real atmosphere by the melting of natural precipitation particles. If one is to predict the amount of electrification produced by this process, not only must their effect on melting ice electrification be known, but the extent to which conditions in clouds will encourage appreciable electrification must also be discovered.

The principle factors influencing melting ice electricication are then

1) Purity of the water
2) Melting rate
3) Air bubble size spectrum
4) Crystal structure of the particle
5) The way in which the melting takes place
   e.g. does convection occur in the meltwater?

CHAPTER 3

THE DESIGN OF A WIND TUNNEL FOR THE FREE FLIGHT OF SMALL ICE SPHERES.

3.1. THE IMPORTANCE OF A FREE SUPPORT SYSTEM

Some of the variables which influence the amount of charging occuring when ice melts were listed in section 2.4. If an attempt is to be made to draw conclusions about the electrification of melting solid precipitation from a laboratory experiment, probably the most important property that must be realistically reproduced is the airflow around the particle. This airflow will not only influence the development of convection in the meltwater, but also the melting process. In the experiment of DRAKE (1968), the ice particles were suspended from a loop of wire 1 mm in diameter and so could be supported when the airflow was greatly different from their terminal velocity. Also the particles were not free to rotate and if they had been free, the onset of convection in the meltwater might not have occurred until much higher temperatures or airflow rates. Furthermore, if the particles could be supported freely in an airstream, then the effect of the electrical contact between the support and the ice particle could be assessed. It was therefore decided to try to develop a method of holding an ice particle in a vertical airstream away from any solid boundaries.

3.2. THE PROBLEM OF TURBULENECE

3.2.1. The effect of turbulence on a supported particle

All methods of freely supporting objects in vertical air-streams are based on the principle that, if air moves upwards with a speed equal to the terminal speed of the object, then the upward drag forces on the suspended object will balance the downward gravitational force. The chief problem in the design of usable air support system is the tendency of the object to drift to the sides of the tunnel. An indication of the difficulty

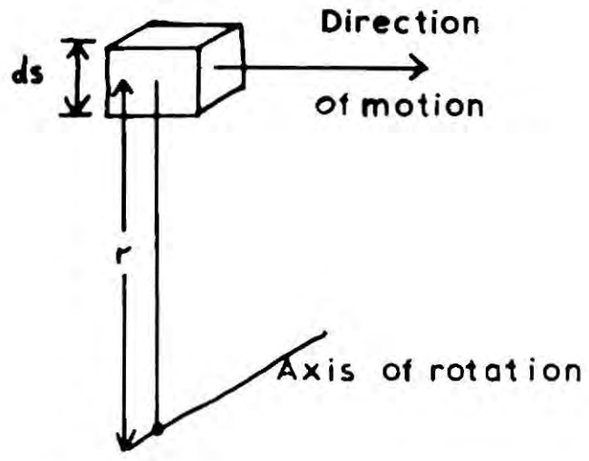

Fig. 3.1 A rotating prism of fluid

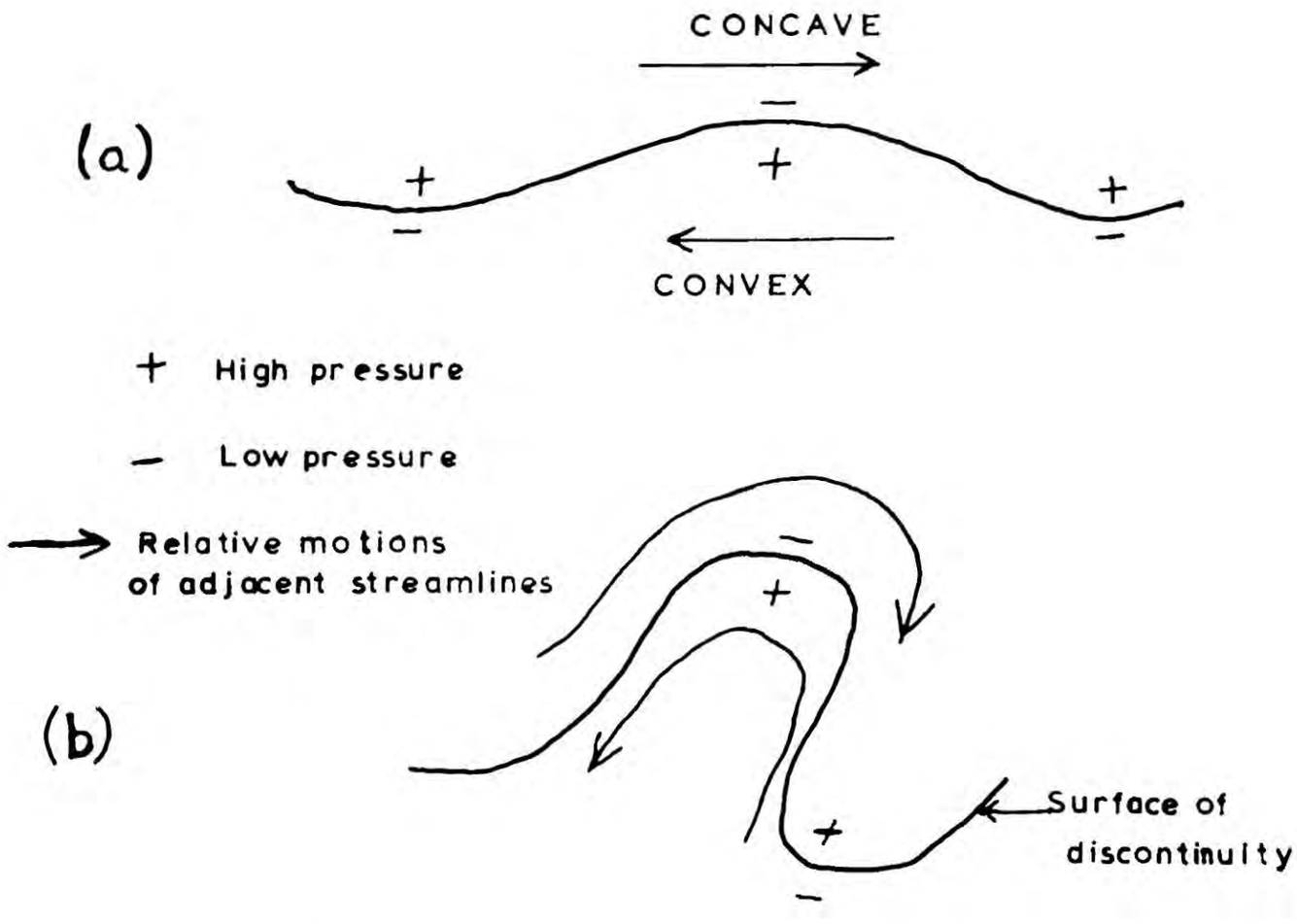

Fig. 3.2 The formation of eddies

is that as the terminal velocity of an ice sphere of 4mm diameter is approximately 10 ms^{-1}, a horizontal drift of only 1% of the terminal velocity will cause the sphere to cross a 150 mm diameter tunnel in 1½ seconds. Even if there is no systematic cause of horizontal motion, any random movement of this magnitude is likely to result in a chance collision with the sides within minutes. It is therefore essential to design a wind tunnel which possesses a very low level of turbulence.

3.2.2. The application of Bernoullis theorum to flow in tunnels

Although strictly concerned with inviscid flow, Bernoullis theorem can be used to describe the conditions which lead to laminar flow becoming turbulent in regions away from the sides of the tunnel, where inertial rather than viscous forces dominate. Bernoulli's theorem can be expressed as

$$p + p^* = \text{constant} \quad \ldots\ldots\ldots\ldots\ldots\ldots\ldots 3.1$$

where p is the static pressure and p^* the dynamic pressure

and $$p^* = \tfrac{1}{2} \rho v^2 \quad \ldots\ldots\ldots\ldots\ldots\ldots\ldots\ldots 3.2$$

where v is the air velocity and ρ the air density.

Equation 3.1 only holds for different points on the same streamline and in general different streamlines will have different values of the constant, corresponding to different energy densities.

3.2.3. Flow along curved streamlines

By considering the transverse acceleration of a curved streamline one can derive a similar expression to equation 3.1. Figure 3.1 shows a prism of fluid rotating with radius r. There will be a pressure gradient due to the motion of the fluid, in order to balance the centrifugal force. This can be expressed as

$$\frac{\rho v^2}{r} = \frac{\partial p^*}{\partial s} \quad \ldots\ldots\ldots\ldots\ldots 3.3$$

where ds is the side of the prism along the principal normal. This is the justification for the principle that if the flow is along parallel streamlines then no pressure gradient can exist across the flow. So a horizontal pressure gradient will cause air to flow to the side of the wind tunnel.

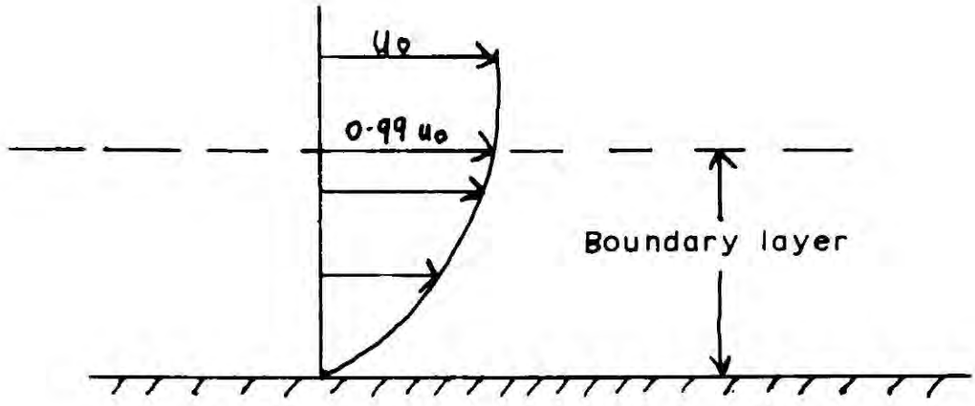

Fig. 3.3 The definition of boundary layer

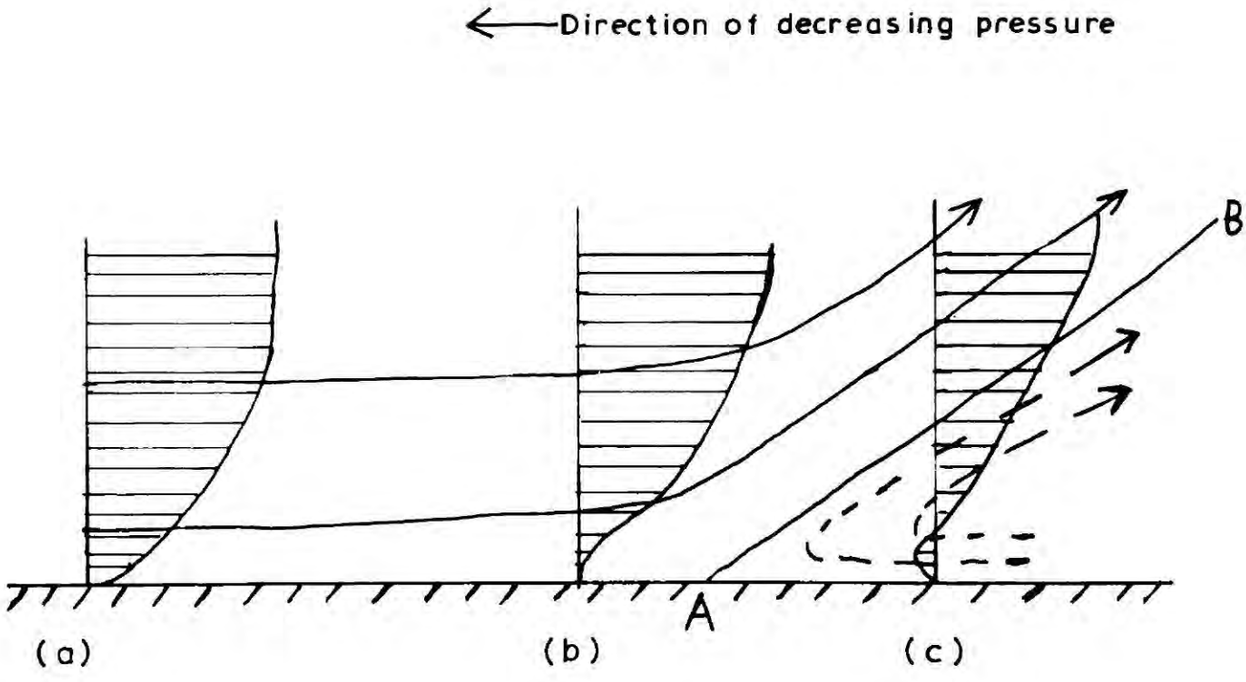

Fig. 3.4 The development of boundary layer separation

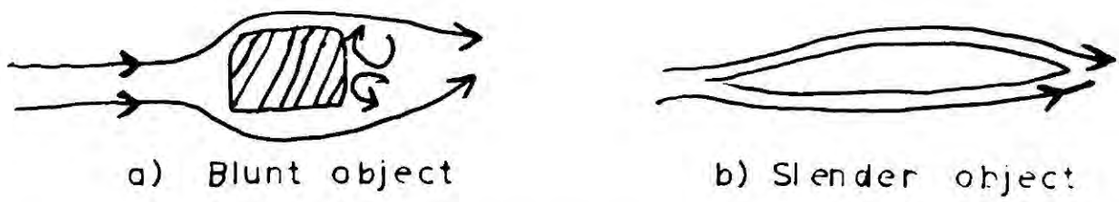

Fig. 3.5 Boundary layer separation at an obstacle

3.2.4 Bernoullis theorum and eddy formation

If one considers a surface of discontinuity or an area bounding regions of fluid with different velocities, then it is possible to chose a frame of reference such that the flow on one side of the boundary is in the opposite direction to the flow on the other (fig. 3.2). If a kink develops in this surface (Fig. 3.2a), then equation 3.3. predicts that the pressure at a convex surface will be higher than at a concave surface. This means that any irregularities which develop in the streamlines adjacent to the boundary will be unstable and will tend to get bigger, causing the production of eddies (Fig. 3.2b). This is the reason why in any low turbulence system the airflow must be as uniform as possible across the section. Two places at which non-uniform flow can arise are at obstructions and bends in the tunnel.

3.2.5. Eddy formation at tunnel walls - Boundary layer separation.

Boundary layer separation is the principal process by which turbulent eddies are introduced into a wind tunnel either from the sides or from objects placed in the airstream. It is possible to take into account the drag of an object, due to a fluid motion over its surface, by assuming that the fluid in contact with the object is moving with the velocity of the surface of the object. There will be a velocity gradient in the region of the obstacle (Fig. 3.3) and the boundary layer is defined as the region of fluid in which the velocity of the fluid is less than 99% of its undisturbed velocity

Fig. 3.4 shows a series of velocity profiles at (a), (b) and (c) near a fluid boundary where there is a pressure gradient opposing the motion of the fluid. As the fluid flows along the boundary it is retarded by the pressure gradient and eventually at A the direction of the flow near the boundary is reversed. This reversed flow piles up against the fluid moving in the original direction and the streamlines associated with these flows leave the boundary. This is called boundary layer separation and it will produce a surface of discontinuity, AB, separating regions of fluid with different velocities and energy densities. This surface will be unstable and will produce a train of eddies by the mechanism described in Fig.3.2.

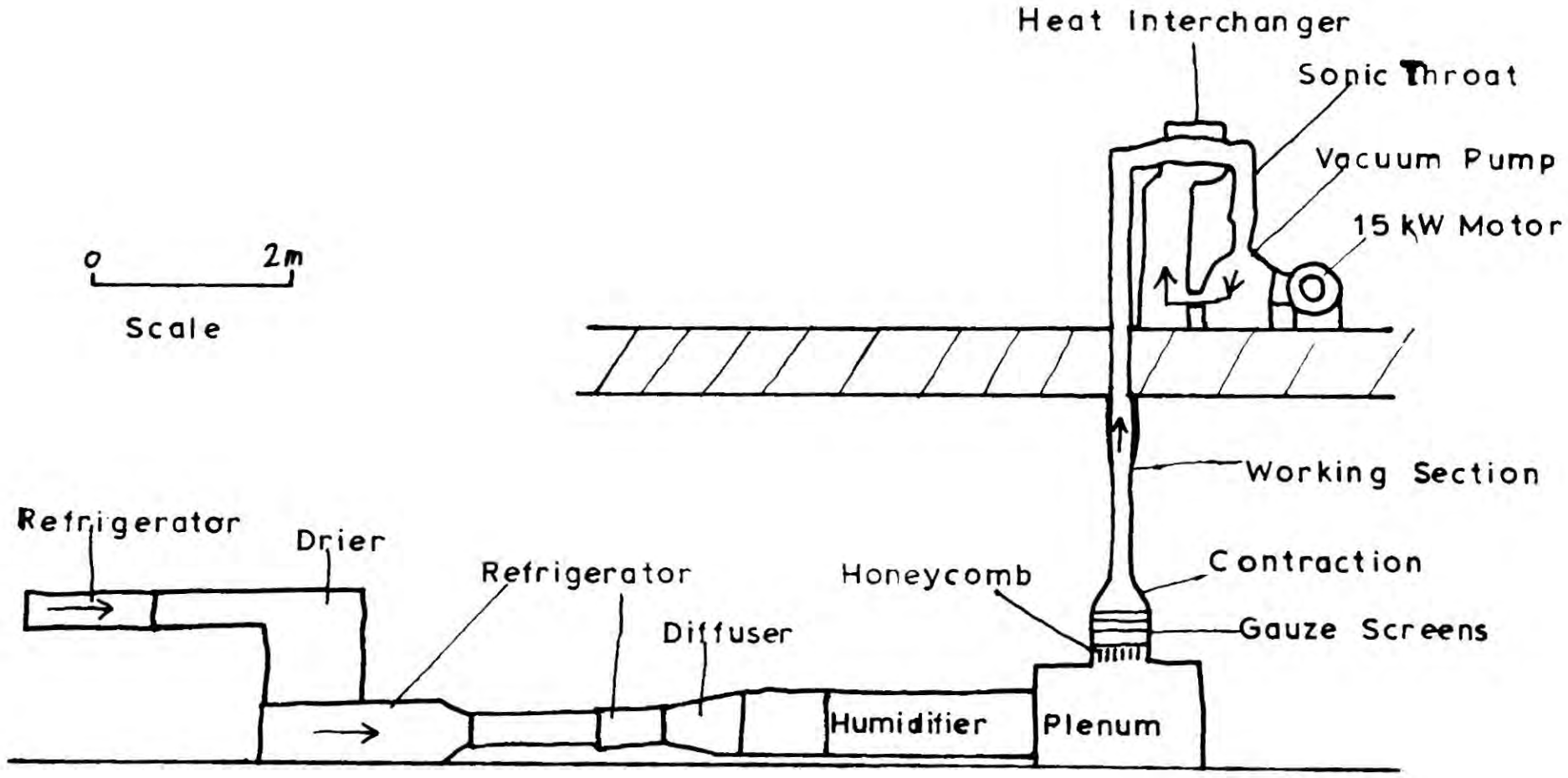

Fig.3.6 The University of California cloud tunnel
(Pruppacher and Neiburger, 1968)

3.2.6. The causes of boundary layer separation

Boundary layer separation will occur wherever there are large enough adverse pressure gradients near a fluid boundary to reverse the flow. In a divergent section of tunnel, the angle of divergence has to be limited to prevent separation occurring at the walls. Another cause is the pressure gradient set up at sharp bends, where equation 3.3 predicts a pressure gradient across the flow due to centrifugal forces, so the fluid at the outside of the bend will be retarded. If objects are placed in the airstream then an adverse pressure gradient will be set up at the rear of the object. The blunter the obstruction, the more likely turbulence will occur (Fig. 3.5 a,b).

3.3. LAMINAR FLOW WIND TUNNELS

3.3.1. Principles of operation

One of the ways of ensuring that the freely supported particle stays away from the walls is to reduce the turbulence to such a level that the particle remains in the position in which it was placed. Tunnels of this type have been described by CHAPMAN (1953), LIST (1959), and PRUPPACHER and NEIBURGER (1968). These tunnels are all larger than 4m in vertical extent and require blowers from 4 to 15 kW power rating. They have wide working sections of about 0.2m in diameter and a great deal of care has been taken to ensure that the airflow in the working section is laminar. This is achieved by the use of honeycombs, gauzes and contractions.

3.3.2. The University of California Cloud Tunnel

The vertical wind tunnel (Fig. 3.6) described by PRUPPACHER and NEIBURGER (1968) was built for the study of freely supported artificial solid and liquid precipitation particles. It is a section tunnel powered by a 15 kW vacuum pump and utilizes several common methods of reducing turbulence. The cooling is provided by three large refrigeration units and the humidity of the airflow can be altered by the humidifier placed upstream of the plenum. Although it was obviously out of the question to build such a system at Durham with the limited finance available some

of the techniques used to smooth the air can be applied to the construction of a smaller wind tunnel.

3.3.3 Methods of reducing turbulence

The first airsmoothing section in Fig. 3.6 is the plenum or stilling chamber, which acts as a capacitance to damp out oscillations. The air then passes into a section containing a honeycomb and a series of gauze screens. Honeycombs reduce eddies by forcing the fluid into pipes which are appreciably narrower than the tunnel; they also help to keep the flow parallel. Screens reduce differences in the longitudinal velocity across the section by providing more resistance to the faster moving regions of the fluid.

The last airsmoothing section in the California tunnel is the contraction where the cross section of the airflow is reduced and consequently the air is accelerated. If the contraction is designed so that the fall in pressure experienced by each volume of air is the same and if the final velocity is appreciably higher than the initial velocity then the main factor governing the outlet velocity will be the pressure drop across the contraction and not the distribution of velocities at the inlet. In the California tunnel the ratio of the inlet area to outlet area was 7:1.

3.3.4 Suction versus blowing

Because the impeller of a blower creates considerable turbulence as well as heating the airstream, it may be preferable to operate the tunnel in the suction mode. In the California tunnel air is sucked through the system by a 15kW vacuum pump delivering 0.2 $m^3 s^{-1}$ of air, with a pressure drop across the pump of the order of 0.9 atmospheres. This large pressure drop appears to have been necessary in order to place a sonic throat upstream of the pump in order to stop disturbances travelling upstream from the impeller. This method of using a sonic throat, which is a region of the pipe where the air flows at supersonic speed, is described by PRANDTL (1952). The chief disadvantage of the suction tunnels is that they have to be carefully sealed in order to prevent air from leaking into the system.

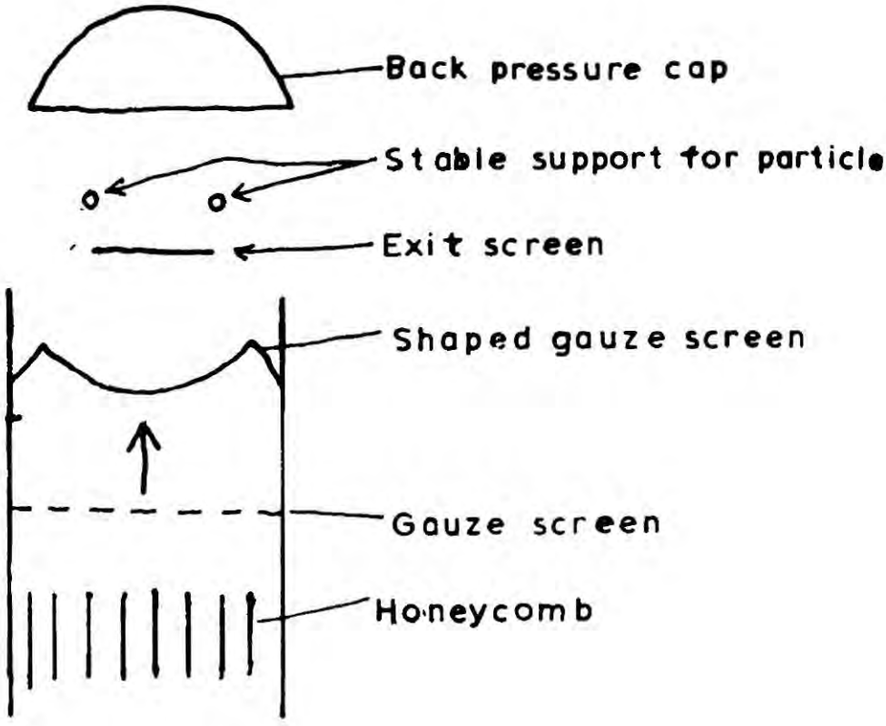

Fig.3.7 A Blanchard-type tunnel

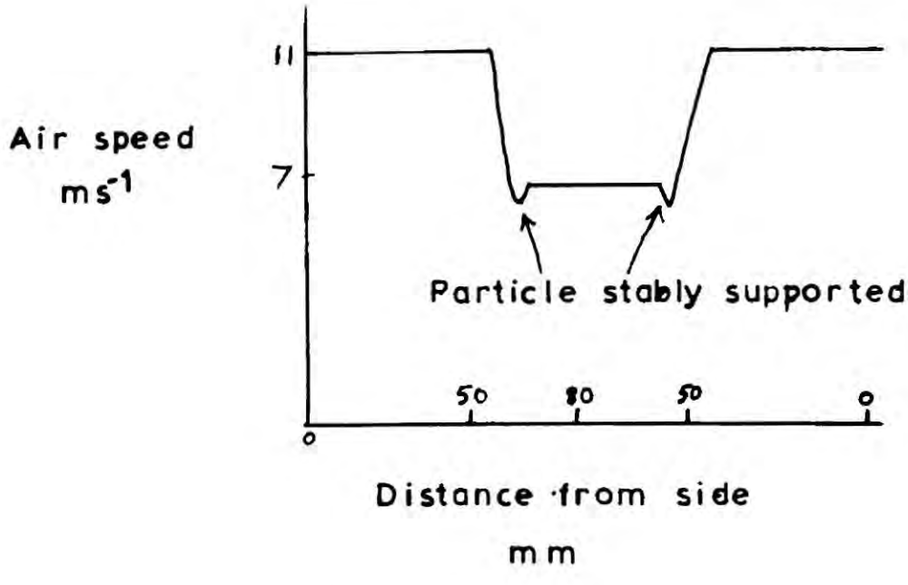

Fig.3.8 Velocity profile for Fig.3.7

(Cotton and Gokhale, 1967)

3.4. VELOCITY WELL SYSTEMS

3.4.1. Principle of operation

Several wind tunnels have been made which support water drops by placing them in a region where the velocity distribution of the airflow is in the form of a well. This gives the drop a position of stable equilibrium. These tunnels fall into two types, either the drop is supported in a divergent section of tunnel e.g. GARNER and KENDRICK (1959) or above the end of the tunnel as in BLANCHARD (1950). These types of support have the advantage that the airflow does not have to be as smooth as in the laminar flow systems.

3.4.2. 'Blanchard-type' tunnels

The essential features of this type of wind tunnel are shown in figure 3.7. Tunnels of this type have been built by BLANCHARD (1950) KINZER and GUNN (1951), KOENIG (1965) and COTTON and GOKHALE (1967). The water drop tends to stay at the edge of the bottom of the velocity well (Fig. 3.8). This well is created by specially shaped screen and the exit screen. The back pressure cap prevents the drop from flying out of the system and also assists the air to spread out on leaving the top of the tunnel. It is essential that the velocity profile does not produce eddies due to the existence of different vertical velocities in adjacent regions of the air. According to Bernoulli's theorum the sides of the wall are unstable unless the airflow from the tunnel tends to spread out. If such a profile were created inside a cylindrical tube eddies would form at the sides of the well.

It is not known to what extent the success of this type of system is due to ability of waterdrops to distort when acted on by shear forces. These systems have never in the author's knowledge been used to support solid objects which could not react in the same way as liquid drops at the boundary of the velocity well. BLANCHARD (1957) found that ice spheres could be supported for only a few seconds. A further advantage of water-drops is that they can be easily placed at the stable position by using a hypodermic syringe.

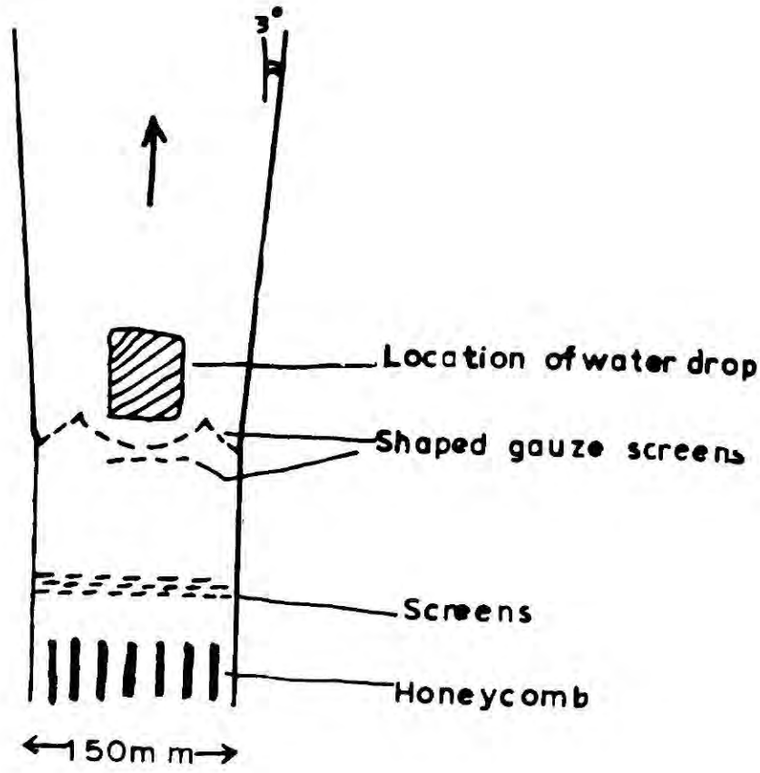

Fig.3.9 Typical divergent tube support

Fig.3.10 The tapered tube
(Kinzer and Gunn)

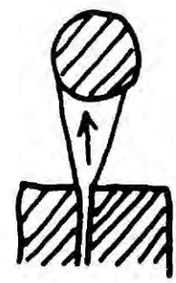

Fig.3.11 The air jet
(Rogers, 1967)

3.4.3 Divergent tube supports

Wind tunnels in which the waterdrop is supported inside a divergent tube (Fig. 3.9), which contains a velocity well, have been built by GARNER and KENDRICK (1959) and IRIBARNE and KLEMES (1970). This method of support has the advantage that the water drop does not have to be carefully placed in the position of stable equilibrium, but can be allowed to fall down the axis of the divergent section and find its own stable position. Both the 'Blanchard-type' and divergent tube supports have tunnel sections of about 150 mm in diameter and supported drops from 2mm up to the maximum drop diameters of about 6mm.

3.4.4 Air jets and tapered tubes

The third type of free support system does not require a highly smoothed airflow and usually consists of an airstream which is of a similar diameter to supported particle. Examples of this method are the tapered tube of KINZER and GUNN (1951) and the air jet used by ROGERS (1967).

The tapered tube (Fig. 3.10) is similar to the rotameter method of measuring airflow rate, the water drop being kept away from the sides by the air rushing past. Great care must be taken to make the tube symmetrical about its axis. ROGERS (1967) found that water drops hit the sides on freezing and it is doubtful if a non-symmetrical particle could be kept away from the sides of the tube.

The principle of the air jet is not well understood, but ROGERS found that the nozzle diameter had to be a factor of 5 smaller than the diameter of the supported ice sphere. The jet can support irregular objects but not water drops and ROGERS found that ice spheres larger than 6mm in diameter could be supported indefinitely. He also suggested that smaller spheres could be supported if the nozzle diameter were reduced. The author tried reducing the size of the nozzle down to 0.5 mm but found that it was nearly impossible to locate the air jet and then place a small ice sphere in it, without a sophisticated alignment system.

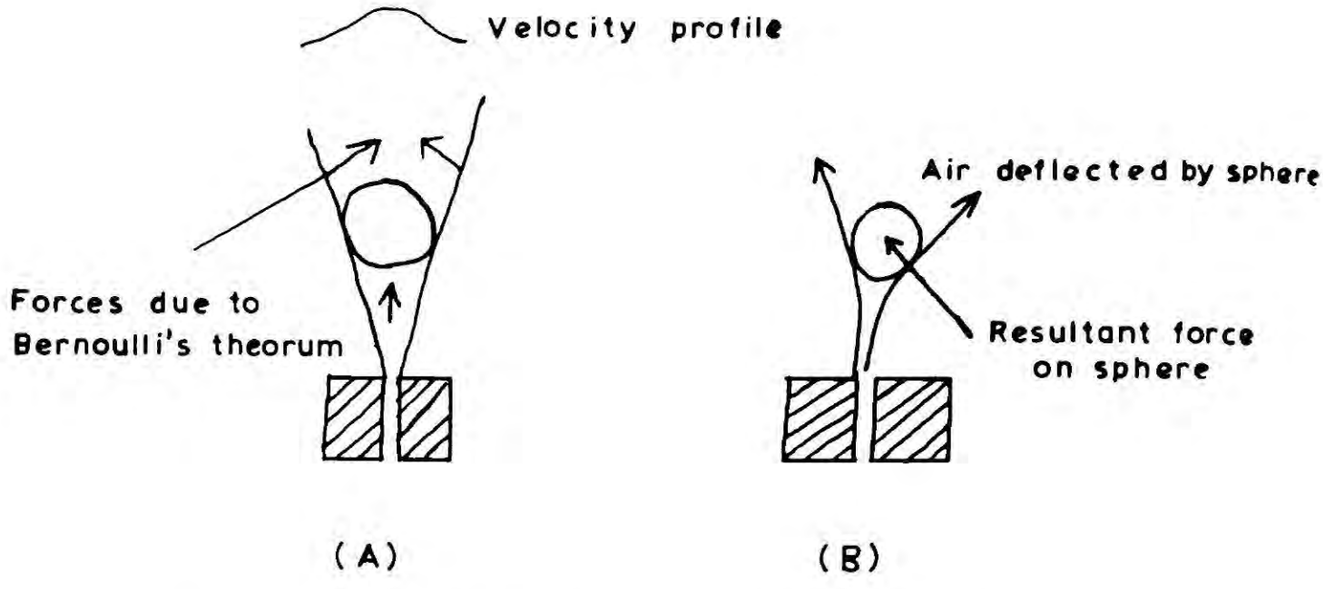

Fig.3.12 Possible mechanisms for the air jet system

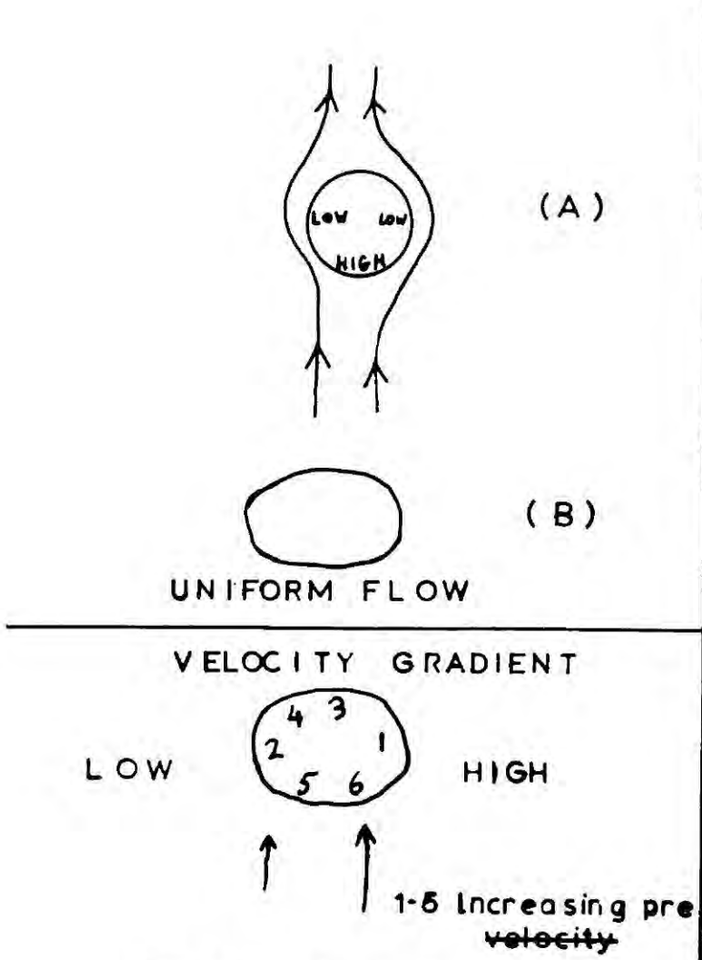

Fig.3.13 Deformation of water drops

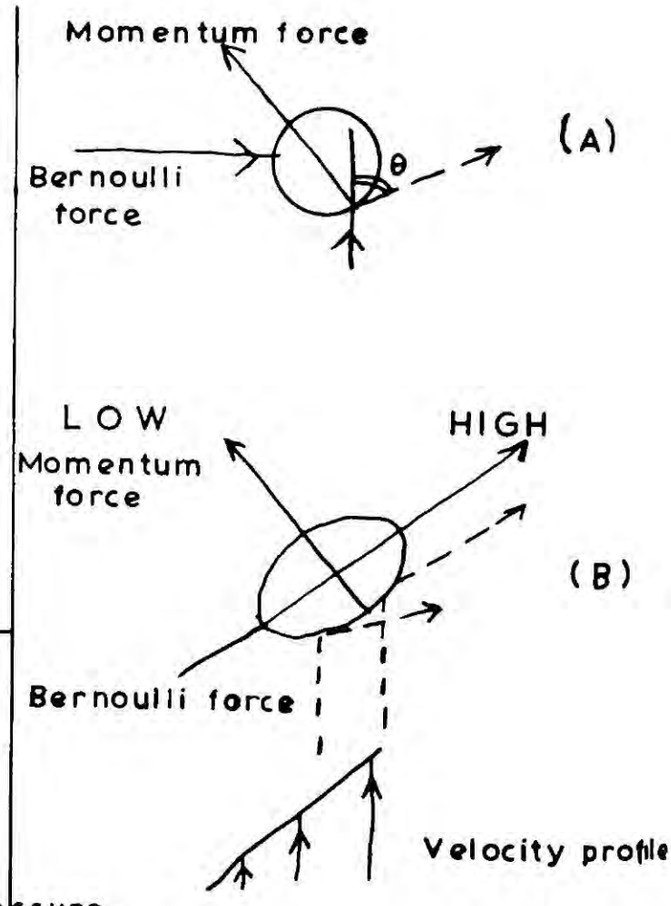

Fig. 3.14 Water drops in a velocity well

3.5. THE DESIGN OF THE SUPPORT TUBE

3.5.1. The choice of the type of support

In the preceding section three types of free support system were discussed, namely the laminar flow, velocity well and the air jet methods. The choice of a system is restricted by the volume of air in the cold room and the limited cooling capacity available. During any sensitive electrical measurements the refrigerating compressor would have to be switched off as it caused the cold room to vibrate. The operation of the wind tunnel would cause appreciable heating due to the compression of air at the blower and the heating of the air in the working system. So if the temperature of the air in the region of the particle is to be kept constant over a 10 minutes period the equivalent of cold room volume should not be circulated faster than about every three minutes. Previous laminar flow wind tunnels have had a diameter of at least 150 mm which would mean that air equivalent to the volume of the cold room woould be circulated every 18 s if the air speed in the working section was 10 m s^{-1}. KINZER and GUNN (1951) built a velocity well system with a diameter of 30 mm which suggests that such systems can be more readily designed with small diameters than the low turbulence tunnels. Although air jets provide more stable support for ice spheres larger than 6 mm, it is clear that the flow round real hailstones is far closer to that in velocity well systems. In the circumstances this last system seems to be the best compromise.

3.5.2. Problems of supporting solid particles.

All the velocity well systems have been designed to support water drops rather than ice spheres. BLANCHARD (1957) found that ice spheres could be supported in his wind tunnel for only few seconds, whereas waterdrops could be supported indefinitely provided that there was no evaporation. The airjet will however support solid particles.

The mechanism of the air jet is sometimes explained by Bernoulli's theorem by saying that because the velocity at the axis of the jet is greater than at the edges, the air pressure is least at the centre (Fig.3.12) This neglects the fact that the particle is of similar size to the jet and

the vertical velocity in the centre beneath it is probably zero. An alternative explanation is described in Fig. 3.12B, in which the air jet is deflected by the sphere and the change in momentum of theair causes a force to push the particle towards the centre of the jet.

A simple application of Bernoulli's theorem cannot be used to explain the velocity well systems as the force on the supported water drop should be directed towards the walls of the well, where the air velocity is higher. However it is possible to explain why liquid drops can be supported while solid objects cannot, by assuming that the drop may be deformed by the forces acting on it. In a uniform airflow a water drop will tend to be deformed by the difference in pressures at the side and the bottom (SPILHAUS, 1947), see figure 3.13 A,B. According to MASON (1957) this deformation is very small for diameters less than 1mm. If the drop is in a region where the vertical air speed increases across the drop, then the pressure distribution will be more complex, but if one applies Bernoulli's theorem to the air flowing over the surface the distribution is probably similar to Fig. 3.13C. This pressure distribution will tend to cause a deformation which will be inclined to the vertical (Fig. 3.14). This will have the effect of increasing the force due to the deflection of the air (Fig. 14) and should help the water drop to be kept away from the boundary of the air flow. A solid particle will not deform and so will be ejected from the well by the Bernoulli forces (Fig. 3.14A).

3.5.3. Preliminary design considerations

In order to limit the rate at which the cold room was heated up, the diameter of the tunnel in the region where the particle would be supported (the working section), was restricted to 40 mm. Assuming a maximum velocity in this section of 10 ms^{-1} a volume of air corresponding to the cold room volume would be circulated every 5 minutes. As the blower available heated the air by about 10°C, the air had to be sucked through the tunnel rather than blown. This limited the possible designs to a divergent tube similar to that built by GARNER and LANE (1959) rather than the open top type used

Fig. 3.15 The divergent tube working section

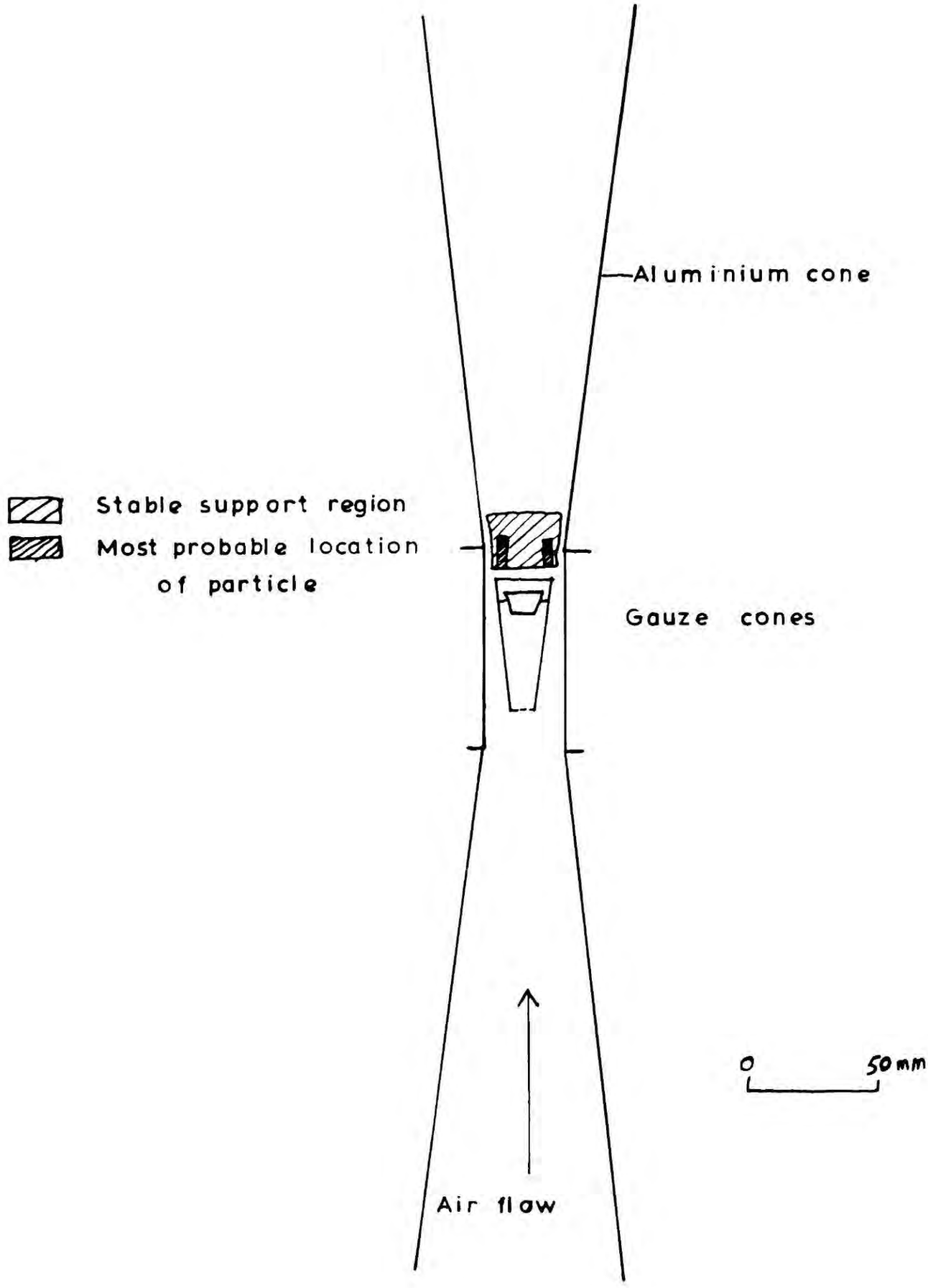

BLANCHARD (1950). In fact at this stage of the design the author was unaware of GARNER and LANE's work.

3.5.4. Stability in the vertical direction

In a divergent tube wind tunnel the air speed falls off towards the top of the tube so at some height in the tube the particle is supported by air flowing at its terminal speed. The degree of stability is governed by the restoring force on the particle which increases with the angle of divergence. However a limit to this angle is set by the possibility of the formation of eddies due to boundary layer separation at the divergent walls. POPE and HARPER (1966) quoted the largest angle between the two walls for laminar flow as 8°, but say that angles up to 45° can be tolerated provided the flow is carefully guided round the corner. It was decided to make the angle between the walls 12° in order to increase the damping and to study methods of guiding the air into the divergent section. After experiments with various flow-shaping devices it was found that two concentric gauze conelets seemed to stabilize the motion of small plasticine spheres. The gauze used was brass 'minimesh' made by the Expanded Metal Company and had an open area of 75% and a strand thickness of 0.13 mm. This design was very similar to the working section that was finally used (Fig. 3.15).

3.5.5 Stability in a horizontal plane

The divergent tube was installed above a smoothing section consisting of a honeycomb and a gauze screen and was connected to a small 150 W blower. Initially this pilot tunnel was operated at room temperature and plasticine balls were used to test various modifications aimed at increasing the stability of the particle. The problem of keeping the particle away from the walls was only partly solved and attempts to create a velocity well in the centre of the tube by placing screens below the gauze flow-shaping cones did not stop the balls from rattling around the bottom of the support tube. However, it was found that if the gauze cones were aligned so that their sides were parallel to the upper aluminium cone, then the balls tended to hover around the top of the gauze cones. The ball could be dropped from the

top of the aluminium cone and would stay in the shaded region of Fig. 3.16. The particle showed a definite preference for staying in the heavily shaded region shown in the diagram. At this stage the main difficulty in improving the system was that the airflow entering the working section was probably not very smooth. So it was decided to build a more permanent wind tunnel inside the cold room.

3.5.6. Air smoothing in the main wind tunnel

The air was first passed through a 150 mm long honeycomb with a 10 mm grid. The next stage was a mesh screen with holes 1.5 mm x 1.0 mm and finally the tunnel was contracted from a diameter of 75 mm to 30 mm. The blower was also operated in the sucking mode. Ideally several screens should have been placed between the honeycomb and the final screen but there was not enough space. Unfortunately the tunnel had 2 right-angle bends just upstream of the honeycomb and these should have been replaced with a settling chamber if the turbulence in the working section were to be reduced further.

3.5.7 The performance of the support system

Ice spheres from 2 to 5 mm diameter were supported in a very similar way to the plasticine balls. After about 10 to 30 minutes flight they would crash into the wires which supported the gauze cones and so get caught. They would go very near the sides every 2 to 3 minutes and it is probable that they made contact with the walls in the 5 seconds that elapsed before they moved away. The motion was distinctly different from that in the early attempts at keeping the balls away from the sides of the tunnel and there was a very marked tendency to hover around the top of the gauze cones.

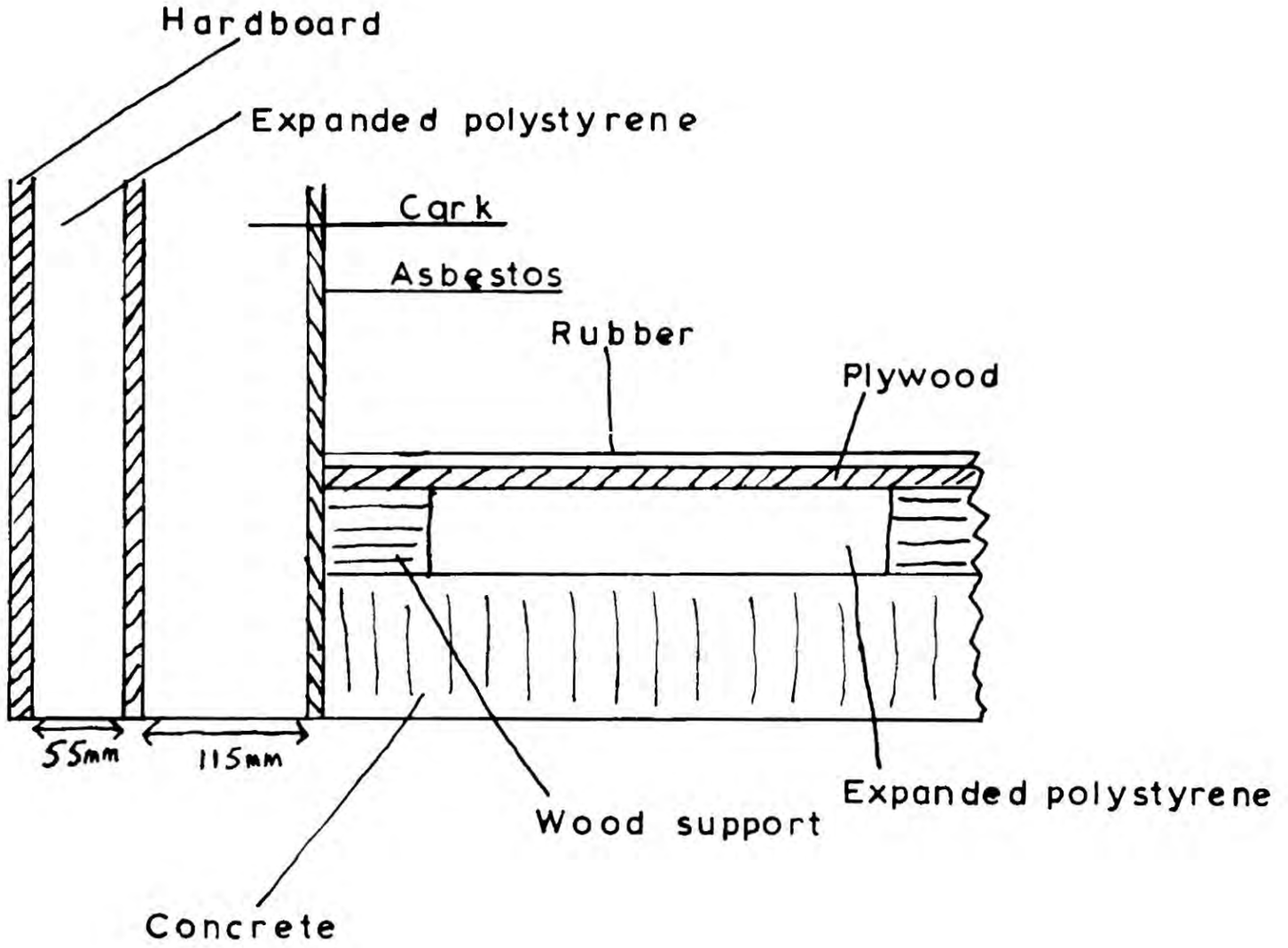

Fig.4.1 Cross section of floor and walls of cold room

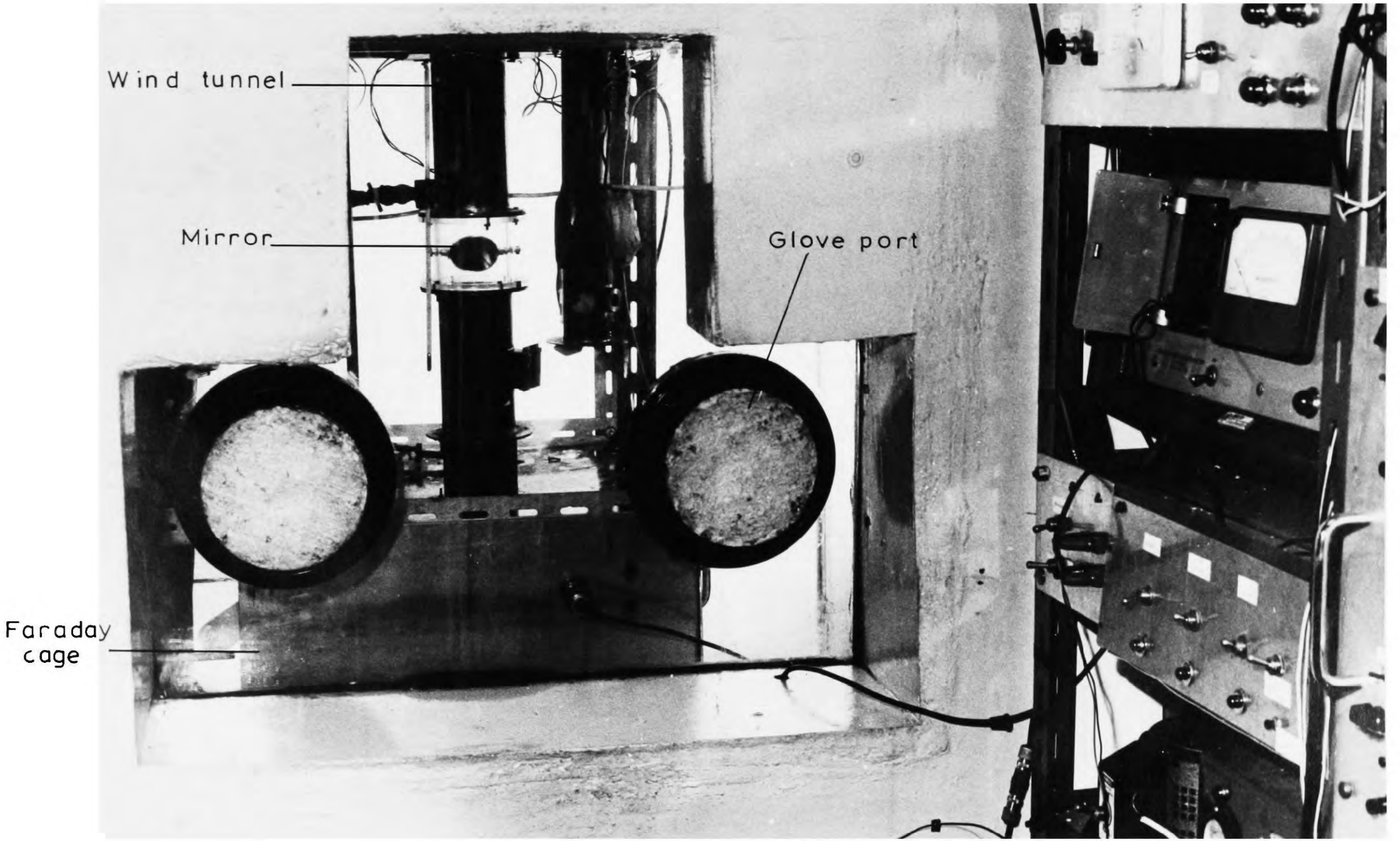

Fig.4.2 View through the double-glazed window

CHAPTER 4

THE CONSTRUCTION AND INSTRUMENTATION OF THE WIND TUNNEL

4.1. THE ADAPTATION OF THE COLD ROOM

4.1.1 The preparation of the cold room

To study the support of ice spheres, the tunnel was placed inside a cold room. The cold room available was formerly a butcher's cold store, powered by a 300 W compressor, which was capable of holding a temperature of 30°C below the ambient temperature. The total volume of the cold room was $4m^3$ and the insulation consisted of 113 mm of cork and 55 mm of expanded polystyrene (Fig. 4.1). The walls and floor were heavily engrained with dirt so the room was extensively refitted. A new concrete floor was laid and used as a foundation for a false floor made of 15 mm plywood lying on a wooden frame which was filled with expanded polystyrene (Fig. 4.1). The plywood floor was then covered with a 6 mm rubber sheet which made a water-tight joint with the walls to prevent water seepage during defrosting. The surfaces of the inside walls and roof were removed with sandpaper and were finally cleaned with detergent to remove all traces of grease and fat. Finally the inside of the cold room was covered with 3 coats of polyurethane paint which formed an inert seal to the walls. A new defrosting tray capable of holding about 20 litres of water was fitted below the cooling coils.

4.1.2 The window

Because of the limited space avilable inside the cold room the experiments were performed from the outside, using a double glazed window fitted with glove ports. As the window would be an important source of heat loss it was made as small as possible. The window was placed on the inside walls to enable the operator to reach as far into the cold room as possible (Fig. 4.2). PROBERT and HUB (1968) suggest that 12 mm is the optimum thickness of a double glazed window for a temperature difference of about 30°C. If the gap is greater convection tends to build up, reducing the advantage of the extra thickness. The two panes were made of 12.5 mm perspex with a similar thickness of air gap. The windows were

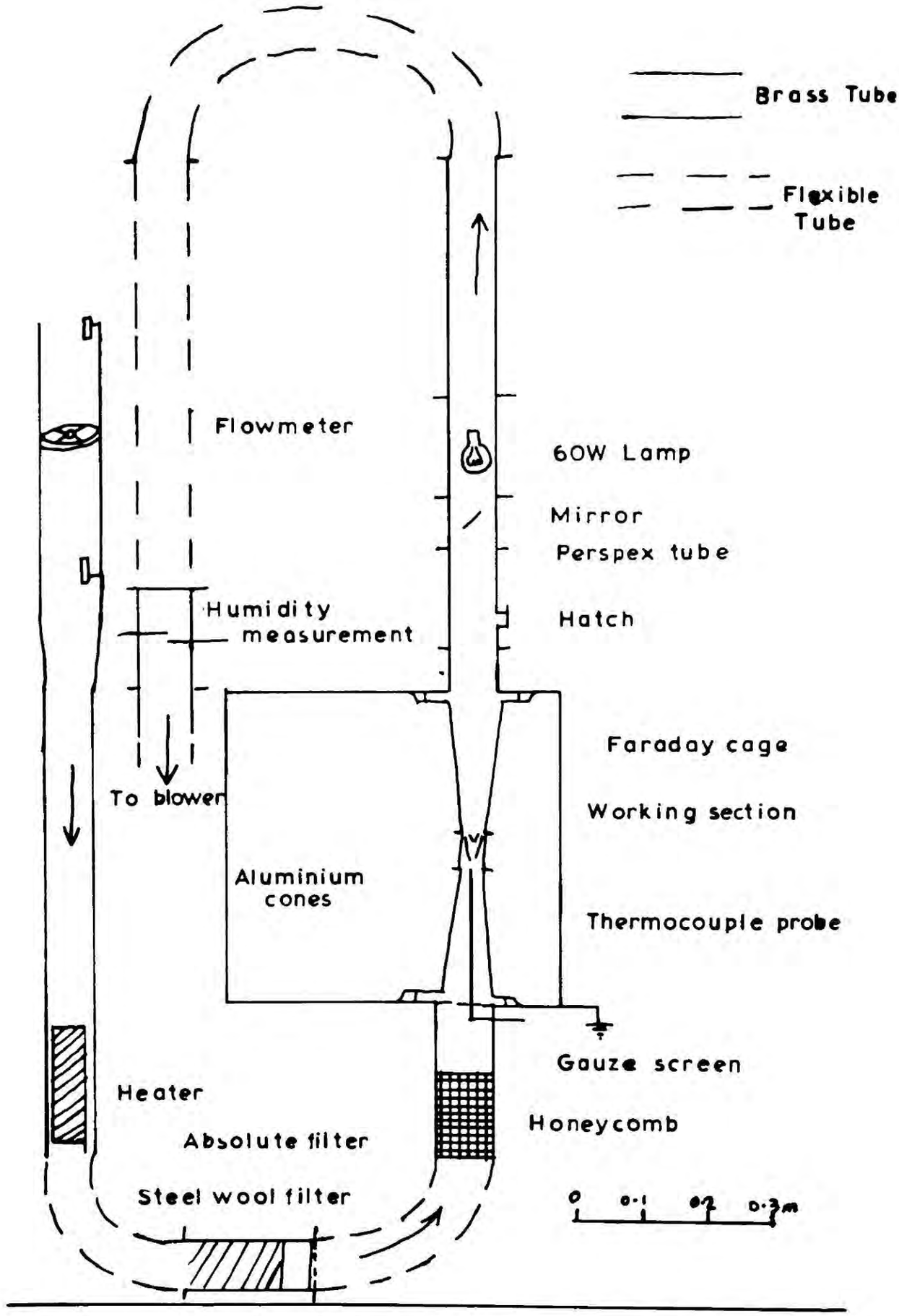

Fig.4.3 Vertical section of wind tunnel

sealed with perspex cement and paint and never misted upon the inside, although on very cold days condensation sometimes formed on the outer pane. The glove ports were never fitted with gloves as these would restrict the operator's ease of movement and as most operations only took a few seconds no appreciable heat loss was caused. When not in use the glove ports were filled with expanded polystyrene stoppers.

4.1.3 Electrical connections to the cold room

It soom became apparent that a large number of wires would have to pass into the cold room to enable the wind tunnel to be instrumented. In the early stages of experiments when the circuitry would have to be constantly modified there was an obvious need for interconnecting plugboards on the inside and outside of the cold room. These were built and fitted with sixteen 4 mm sockets. The inside board was also equipped with mains sockets. Two 12-way cables and several mains and coaxial leads were run through the walls; these were all used in the next two years.

4.2. THE WIND TUNNEL

4.2.1. Limitations on design due to the cold room

Unfortunately the window was fitted to the cold room before the wind tunnel was designed and it soom became apparent that the window was mounted too low. Ideally as large a length of straight piping as possible was required upstream of the working section, but this was limited to about 0.6 m by the height of the cold room floor and windows. This straight section contained a honeycomb, a gauze screen and a contraction but a bend had to be made in the tunnel to enable a heater to be placed in the air-stream. The blower had to be mounted at ground level to minimize vibrations so another bend was required downstream of the working section. The wind tunnel as finally built was about 7 m in total length and included two 180° bends (Fig. 4.3).

4.2.2 The blower

The blower used was a Siemens 0.7 kW 3-phase blower capable of a maximum volume flow rate of $35\,\ell\,s^{-1}$ and a maximum pressure drop across he blower equivalent to 1.1m of water. The blower was used to suck

Fig.4.4 Plan view of wind tunnel

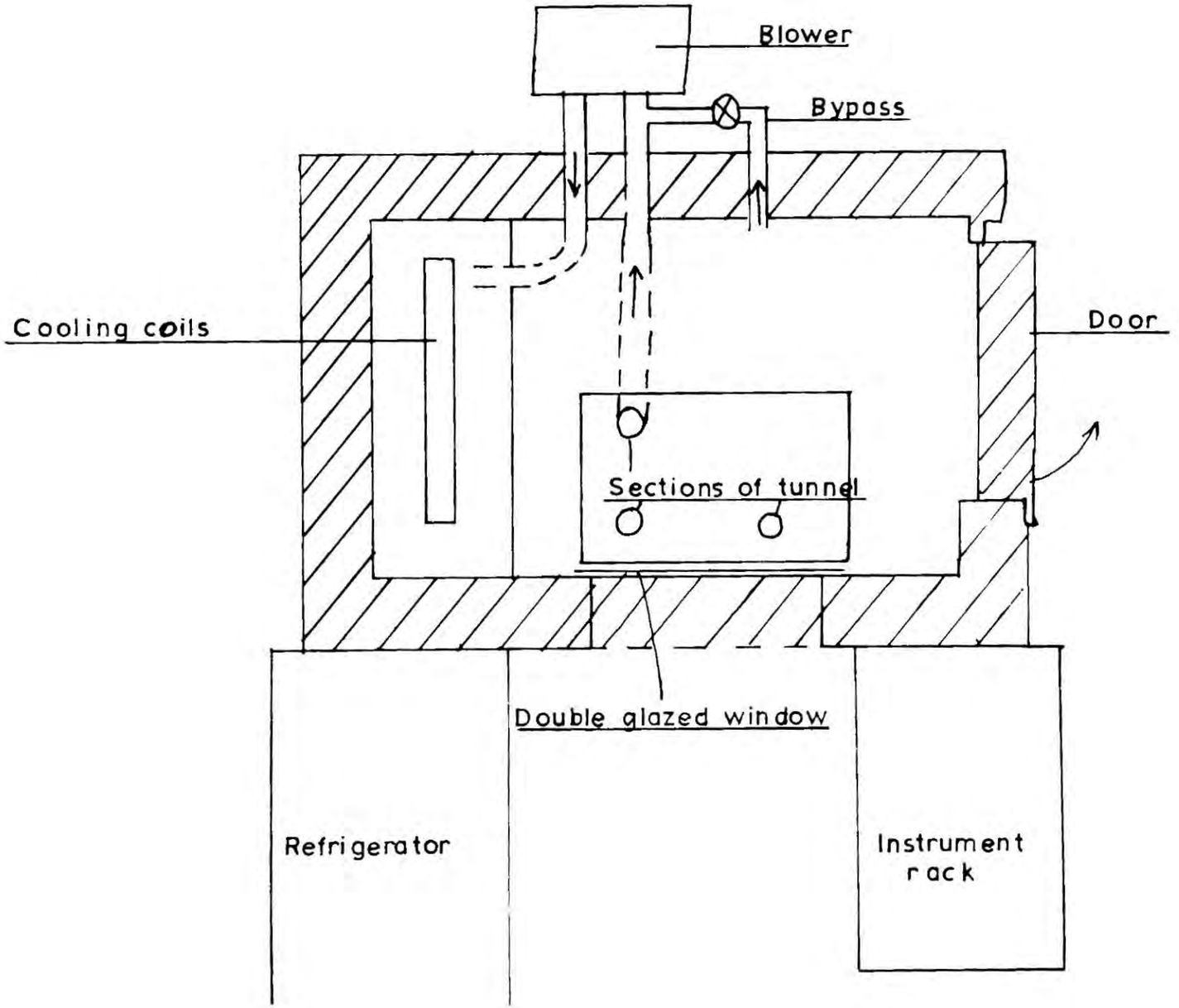

air through the working section at a maximum air velocity of 20 ms^{-1} in the 31 mm diameter section, which corresponds to 20 ℓs^{-1} of air. The air leaving the blower was heated by about 10°C depending on the airflow rate, so the outlet from the blower was directed over the cooling coils to help maintain the temperature of the cold room. The blower was bolted to the concrete cap of a brick pillar and the vibration produced was negligible. For safety reasons the blower was located outside the cold room but it was found that provided the pipes were well lagged the heat losses were small compared to the compression heating of the blower.

4.2.3 Airflow control.

The airflow was regulated by a butterfly valve located in a bypass pipe which met the main tunnel at the inlet to the blower (Fig. 4.4) The valve was connected to an electric motor and could be operated from the main control panel or at the valve itself. This method proved adequate and the air velocity could be regulated to better than 0.5 ms^{-1}.

4.2.4. The wind tunnel layout

The layout of the wind tunnel is shown in figures 4.3 and 4.4. There was only space for two airflow smoothing stages, the honeycomb which consisted of square tubes of 10 mm side and a total length of 150 mm, and a 'minimesh' screen. It was not possible to place any screens downwind of the working section. The heater, which was a heating element from a water boiler, could be operated at up to 200 watts. All the brass sections between the heater and the working section were lagged with a 50 W heating tape, which reduced the thermal time constant of the system. The air in the working section could then be raised from -8°C to + 10°C in about 4 minutes.

The particle in the working section was viewed by the use of a 50 mm diameter mirror which also served to shield the ice from the direct radiation of the 60 W lamp which was used to illuminate the working section. The heating effect of the lamp was found to be less than 0.2°C. The ice spheres used in the free flight experiment were inserted into the tunnel through the hatchway which was placed just below the mirror.

4.2.5. Construction details

To enable as many as possible of the parts to be interchangeable most of the sections were made from 75 mm diameter tubing fitted with 110 mm flanges with standard holes for the securing bolts. The whole tunnel was built around a 'Handyangle' frame which was bolted to the floor of the cold room. The tunnel sections were connected to the frame by means of sheets of aluminium fitted with a 75 mm hole and boltholes to match the flanges. The Faraday cage was made from sheets of aluminium. The flexible tubing was manufactured from neoprene impregnated fibreglass on top of a galvanized screen spring and the maximum leakage quoted by the manufactuers was 0.1% of the volume flow rate per metre of pipe under conditions typical of its use in the wind tunnel. The flexible tubing was carefully sealed to the brass flanges by means of P.V.C. tape and adhesive and some sections were fitted with rubber gaskets to reduce the leakage.

4.3. MEASUREMENT OF ELECTRIC CHARGE

4.3.1 The principle of measurement.

The two aluminium cones (Fig. 4.3) inside the Faraday cage were insulated from earth at both ends and were connected by means of a low noise coaxial cable to a vibrating reed electrometer (V.R.E). If there is a charge separation process inside the upper cone with one sign being retained on an ice particle in the cone and the opposite sign being carried away in the airstream, the Cones will act as a Faraday pail and a charge equal to that carried by the ice particle willbe induced onto the outside of the cones and will flow to earth through the 10^{12} ohm input resistor of the electrometer. The electrometer will therefore measure the charge separation current if the value of the imput resistor is known. The main amplifier of the V.R.E. was calibrated by applying an accurately known voltage to its input stage. The input resistor was checked to $\pm$ 10% by passing a known current through it and noting the voltage indicated by the output meter on the V.R.E. The background noise level was found to depend largely on the design of the insulation and the space charge carried by the air in the wind tunnel.

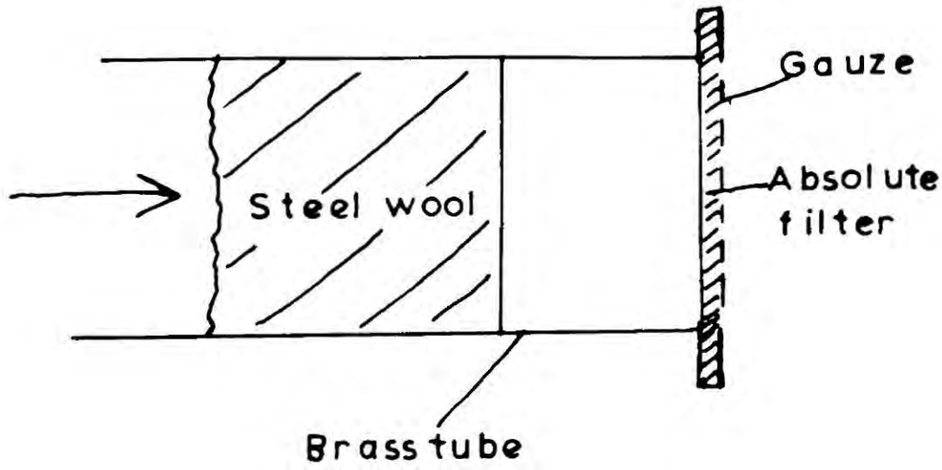

Fig.4.6 The space charge filter

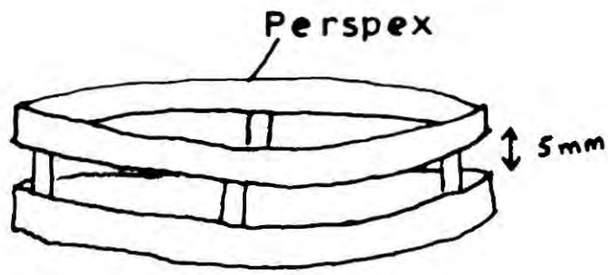

A) An early form of insulator

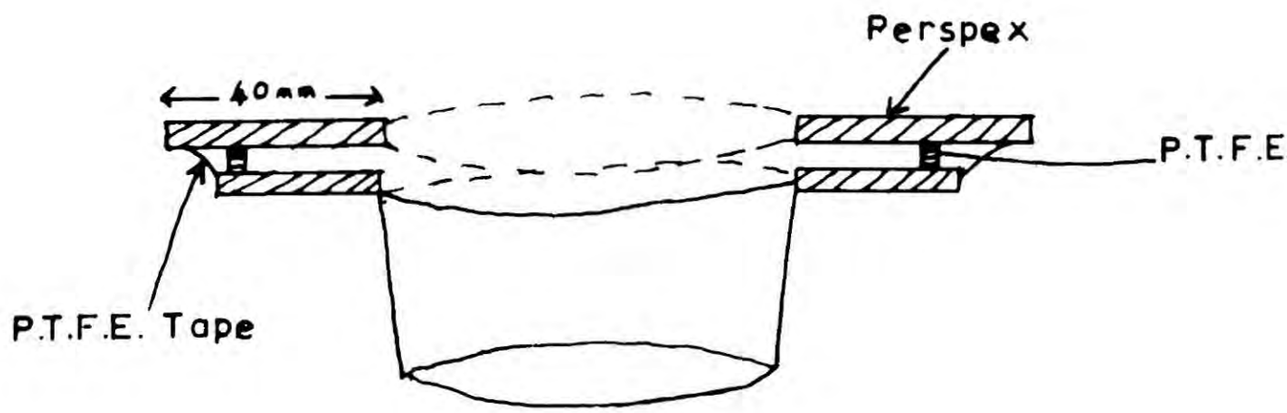

B) The final design

Fig 4.5 The design of insulators

4.3.2. The performance of different types of insulators

The insulators were developed by studying their performance in the pilot wind tunnel in which the air was blown through the tunnel. The first design (Fig. 4.5A) consisted of two perspex rings separated by four 4 mm diameter perspex spacers. When the airstream was heated or allowed to cool after heating, the V.R.E. would record a noise level of up to 0.2 pA which was suspected to be due to the insulators. A later design (Fig. 4.5B) eliminated these noisy periods of record. The chief modification was to move the spacers away from the airstream and replace the perspex with P.T.F.E. It was thought at the time that the noise may have been caused by water condensing on the metal sides of the tunnel and being forced over the insulating air gap. This seems an unlikely explanation as the dew point of the air was usually lower than the probable temperature of the tunnel walls.

When used in the main tunnel the insulators were sealed with P.T.F.E. tape and silicone rubber to prevent air leaks due to suction through the air gap. All the surfaces of the insulators were carefully cleaned with detergent and hexane before use to remove any grease.

4.3.3. Noise due to space charge

Because approximately 0.01 $m^3 s^{-1}$ of air passed through the tunnel one might expect that the working section may behave as a crude space charge collector despite the earthed gauze screen upwind. Before a space charge filter was place in the airstream, the current measured by the V.R.E. could on some occasions be attributed to space charge, e.g. the noise that occurred when the heater was used after a long period of not being used. The most dramatic evidence for the effect of space charge occurred when a nearby building was being demolished and clouds of dust entered the laboratory. When the cold room door was opened and the dust allowed to enter the wind tunnel, the V.R.E. registered a maximum current of 0.4pA which fell back to zero about 10 minutes after the door was shut. A space charge filter (Fig. 4.3) was then installed permanently in the wind

tunnel. This consisted (Fig. 4.6) of a steel wool filter followed by a fibreglass absolute filter of the type used by BENT (1964) as a ⥤filter for a space charge collector. With this filter installed there was no significant V.R.E. deflection when the door of the cold room was left open, so it was assumed that the filter would be completely effective under normal operating conditions.

4.3.4. Noise due to aerial effects

Another source of noise was associated with the probes used to measure the temperature of the working section. As shown in figure 4.3, the probe, which is a piece of stiff wire supporting either a thermocouple or thermistor lead, runs up the centre of the lower cone without making contact with the walls. This lead penetrates the Faraday cage and may act as an aerial as it is about 4m long. Noise due to this source reached up to 0.1pA when thermistors were used but later with thermocouples as the sensing device the noise was negligible. This was probably because of the high resistance of the thermistor circuit, which was typically 3 kΩ as opposed to the 5 to 10 Ω of the thermocouples, It was also found necessary to carefully screen the light bulb that was used in the Faraday cage with a later modification of the tunnel.

4.3.5. Additional sources of noise

One further cause of noise was the failure to remove the semiconducting layer surrounding the dielectric in low noise coaxial cable. This layer has a small resistance compared to the $10^{12}\Omega$ input resistor of the V.R.E. and resulted in an intermittent short circuit when the cable was vibrated, e.g. when the blower was switched on. If the spacers in the insulator were not securely fixed, their movement when the air was passing through the tunnel tended to cause an appreciable nose level.

When all the sources of noise mentioned above had been reduced successfully the background noise level was 0.002 pA throughout a complete heating and cooling cycle lasting 30 minutes.

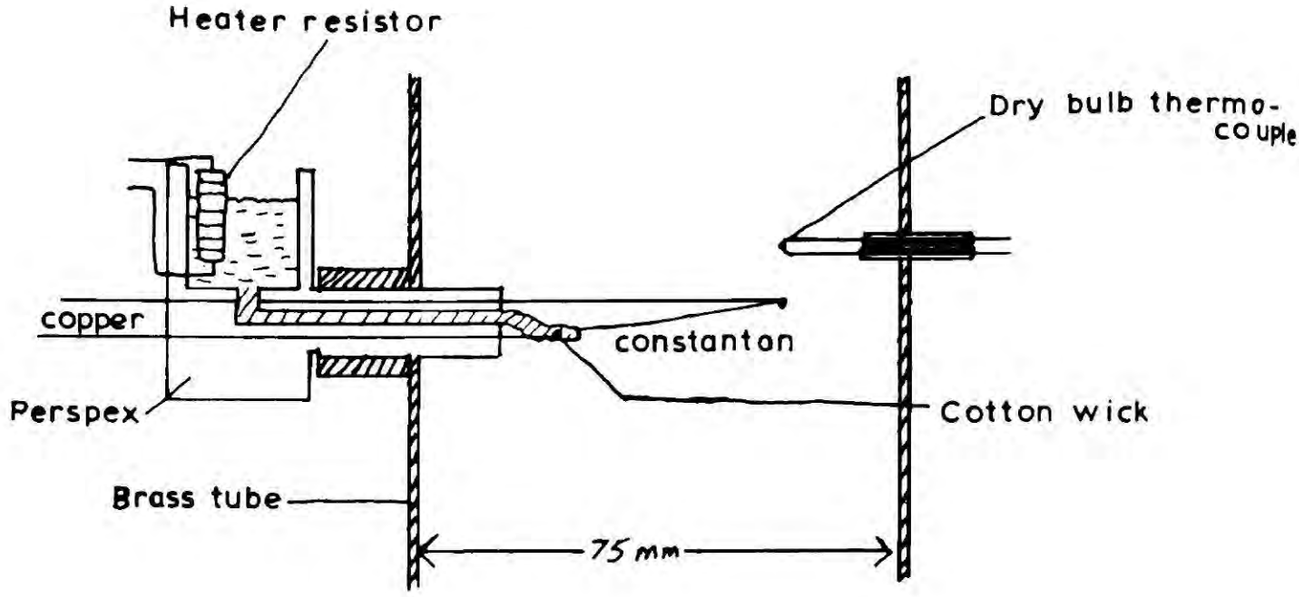

Elg.4.7 Humidity measuring section

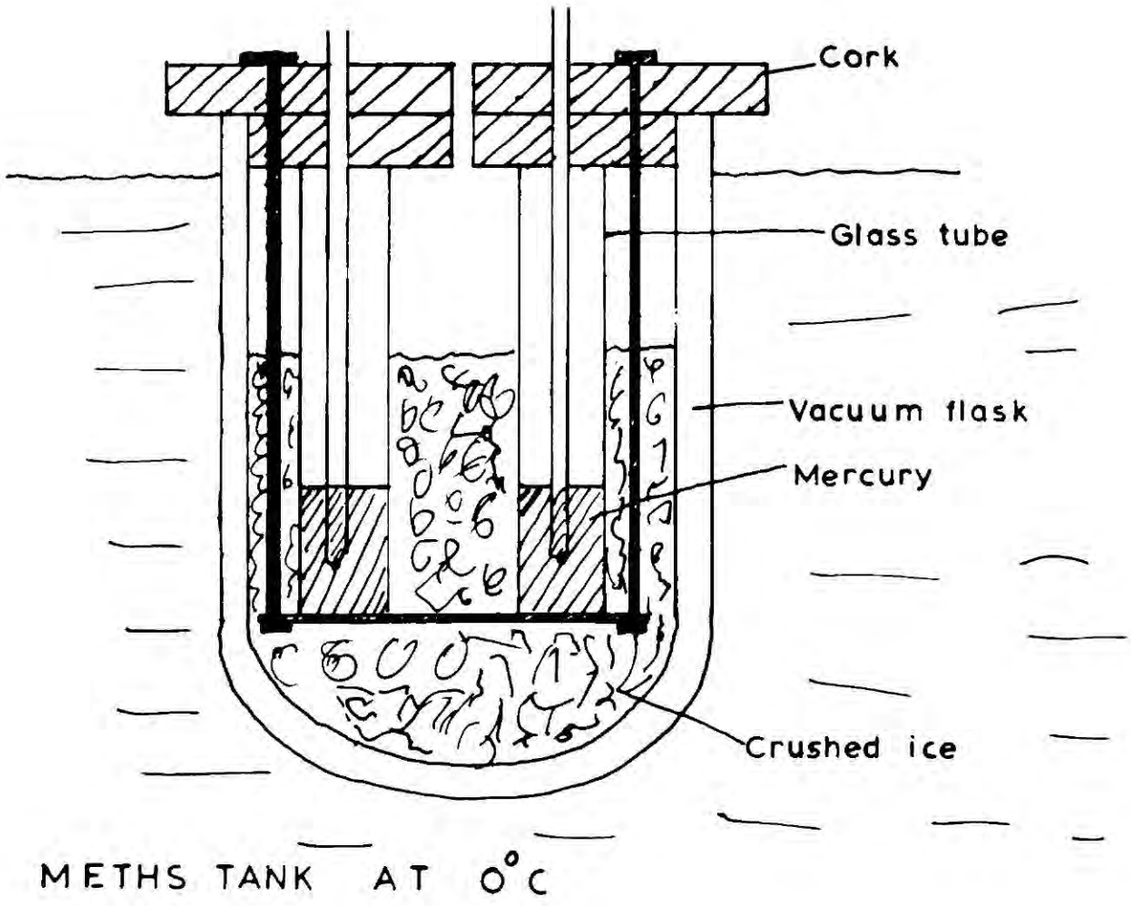

Fig.4.8 Thermocouple reference junction unit

4.4. THE MEASUREMENT OF TEMPERATURE AND HUMIDITY

4.4.1. Temperature measurement

In the pilot wind tunnel, temperature was measured by observing the variation in current passing through a thermistor when a constant voltage was applied across it. To avoid heating the thermistor, the current had to be kept to a minimum which made it difficult to use this method to produce a signal suitable for recording on a chart recorder. As mentioned in section 4.3.4 the relatively high resistance of the thermistor tended to cause noise on the V.R.E. output when the temperature measuring probe was inserted into the working section of the wind tunnel. So low resistance copper-constantan thermocouples were used which gave an E.M.F. of approximately $40 \mu V\ ^{o}C^{-1}$ and the signal was amplified with an integrated circuit D.C. amplifer. The temperatures of the cold room, the outlet from the blower, and 2 other points in the wind tunnel were also measured.

4.4.2. Measurement of humidity

The humidity measuring section was placed downwind of the working section (Fig. 4.3) and care was taken to ensure that there were no leaks in the tunnel between the 2 points. Dry bulb and wet bulb depression were measured using copper-constantan thermocouples as in figure 4.7. The water held in the perspex container could be melted by the heater resistance and allowed to wet the cotton wick which covered one junction of a differential thermocouple. The value of relative humidity was read off the tables for an aspirated psychrometer in KAYE and LABY (1970). This was presumed to be justified as increasing the airflow did not cause any increase of wet bulb depression for the range of wind speeds used. The probable error in the relative humidity was $\pm$ 3%.

4.4.3 The thermocouple reference junction

Four separate thermocouple reference junctions were required and these were contained in one unit (Fig. 4.8). A vacuum flask, containing crushed ice and the junctions, was placed inside a tank containing about 20 litres of methylated spirits which was held about $0^{o}C$. This ensured

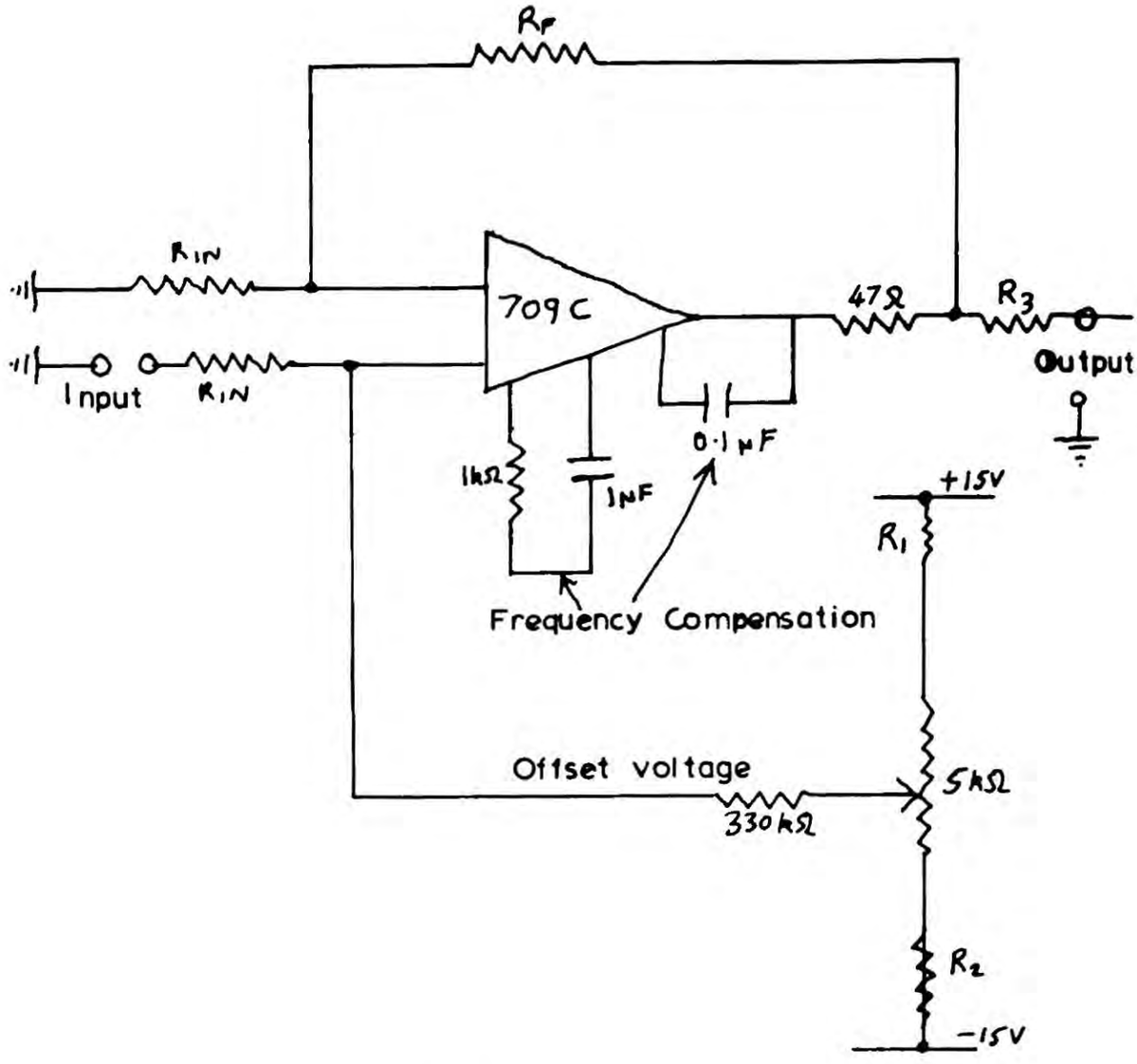

Fig.4.9 Basic d.c. amplifier circuit

Amplifier	R_{IN}	R_F	Amplification	R_2	R_3	R_1
1	47Ω	56kΩ	1,200	4·7kΩ	620Ω	1kΩ
2	56Ω	68kΩ	1,200	1kΩ	620Ω	1·8kΩ
3	56Ω	68kΩ	1,200	5·6kΩ	620Ω	1kΩ
4	56Ω	33kΩ	600	1kΩ	620Ω	1kΩ
5	120Ω	133kΩ	1,100	—	820Ω	1kΩ

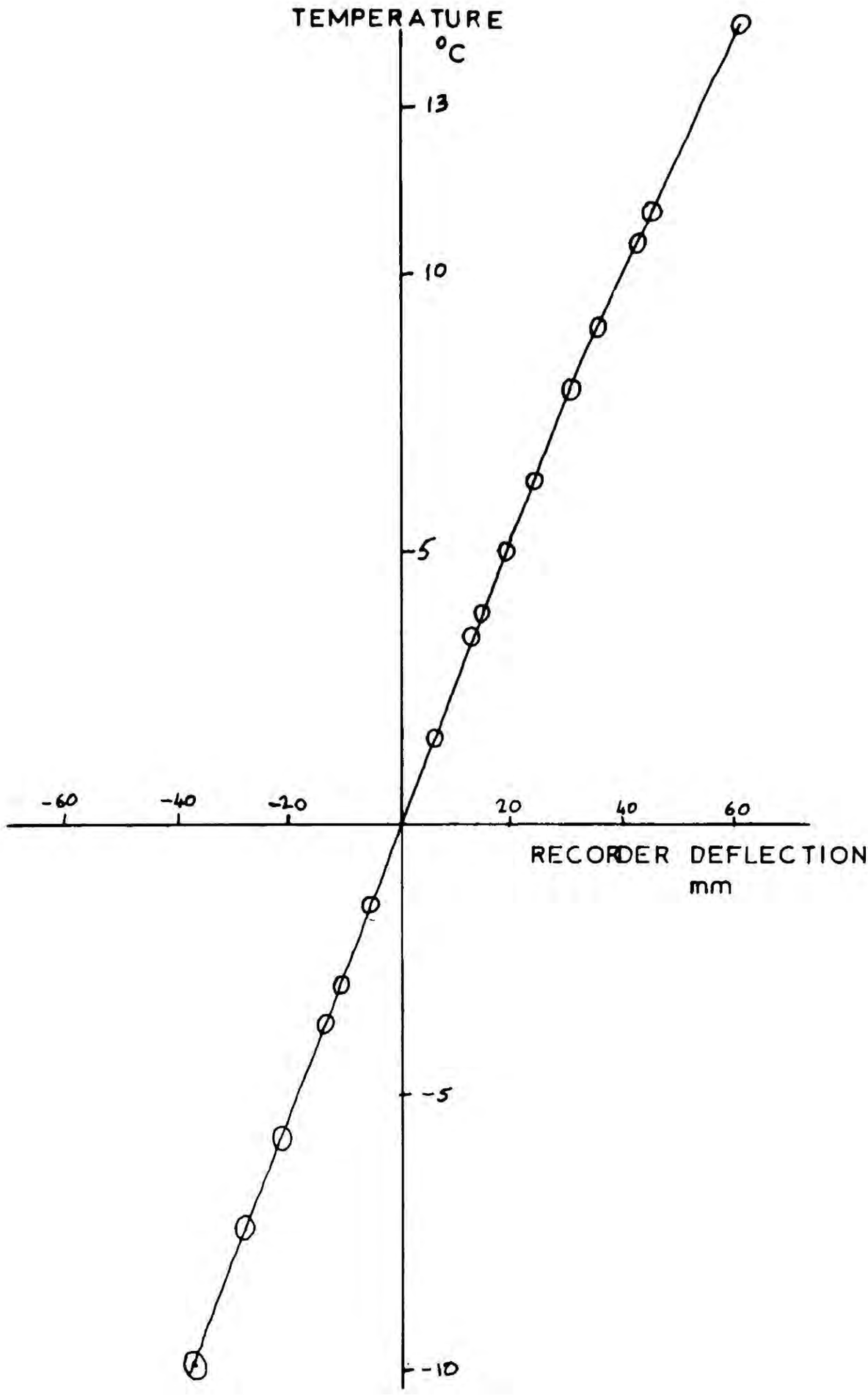

FIG. 4.10 TYPICAL AMPLIFIER CALIBRATION
(Working temperature)

that the ice only had to be replaced weekly. The mercury acted as both a heat sink and a good thermal contact with the ice.

4.4.4. The thermocouple amplifiers.

The 5 D.C. amplifiers all used similar 'Radiospares' Integrated circuits (709-OPA) which were powered by a ± 15 V stabilised power supply. The amplification could be varied by altering the value of the feedback resistor R_F and the input resistor R_{IN} (Fig. 4.9). The offset voltage had to be applied to the input to ensure that there was zero output for zero input current. Large values of frequency compensation capacitors were used to prevent instability caused by the amplification of unwanted high frequency noise. The biggest difficulty in building the 5 circuits into one rack mounted panel was theelimination of earth loops which caused the amplifiers to go offscale. This was solved by connecting every earth point of the circuit to a common earth and by screening as much of the thermocouple leads as possible.

4.4.5. Calibration of the thermocouples.

A calibration junction consisting of a copper-constantan junction in a vacuum flask filled with paraffin was permanently available for calibrating the temperature measuring circuits. The junction could be readily heated through the full range of temperatures that were measured in the wind tunnel. One important source of error in this calibration was that caused by the calibrating thermocouple having a different resistance than the measuring thermocouple. As the amplifers were set to zero by shorting out the thermocouple, this could cause different zero readings for the two thermocouples, which would not be readily detected. A preset resistor was placed in series with the calibrating thermocouple and before calibration the resistance of the reference thermocouple junction was adjusted. A typical calibration curve is shown in Fig. 4.10 . These curves were reproduceable over the period of measurements to ± 0.2°C.

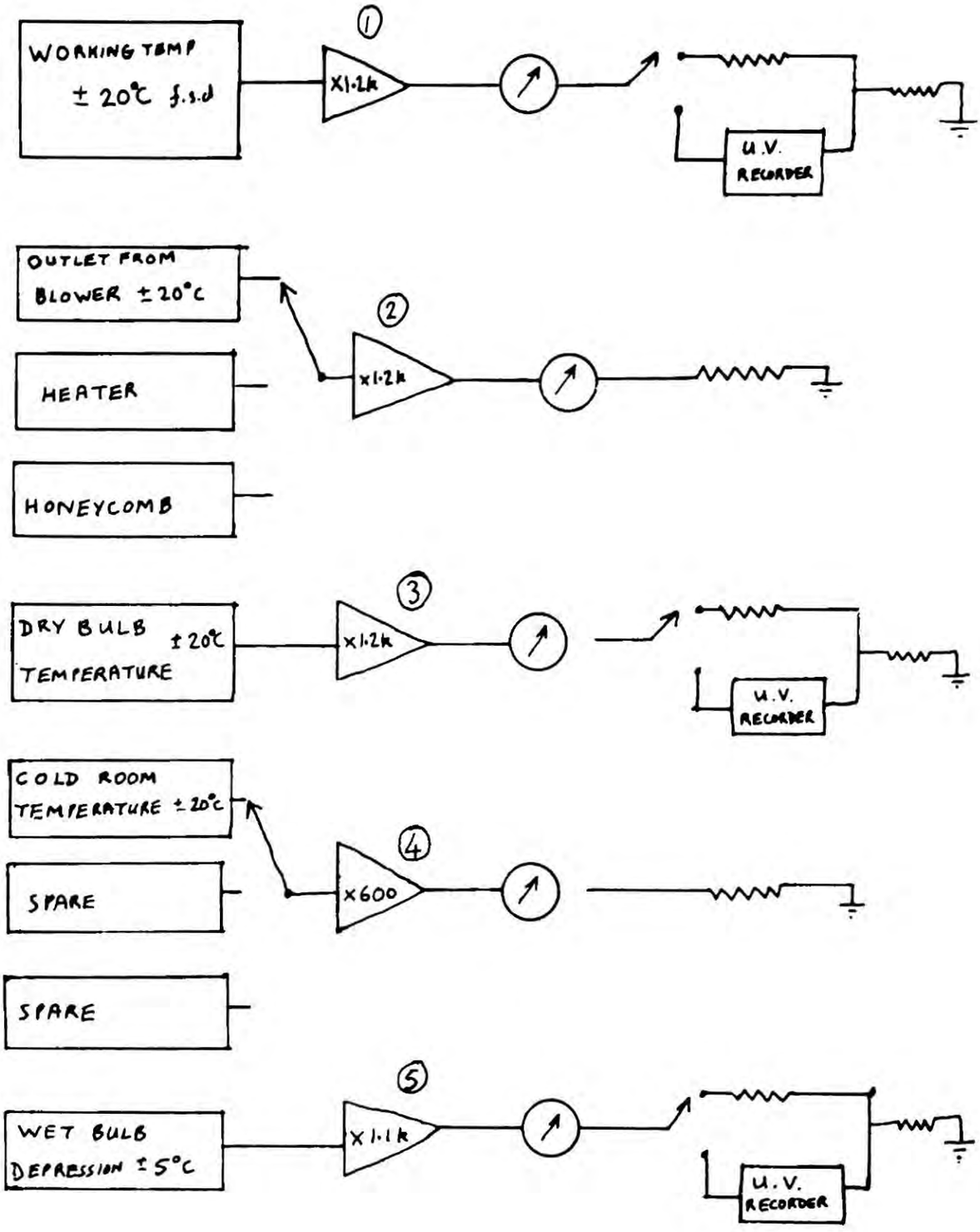

Fig. 4.11 Block diagram of temperature measuring circuits

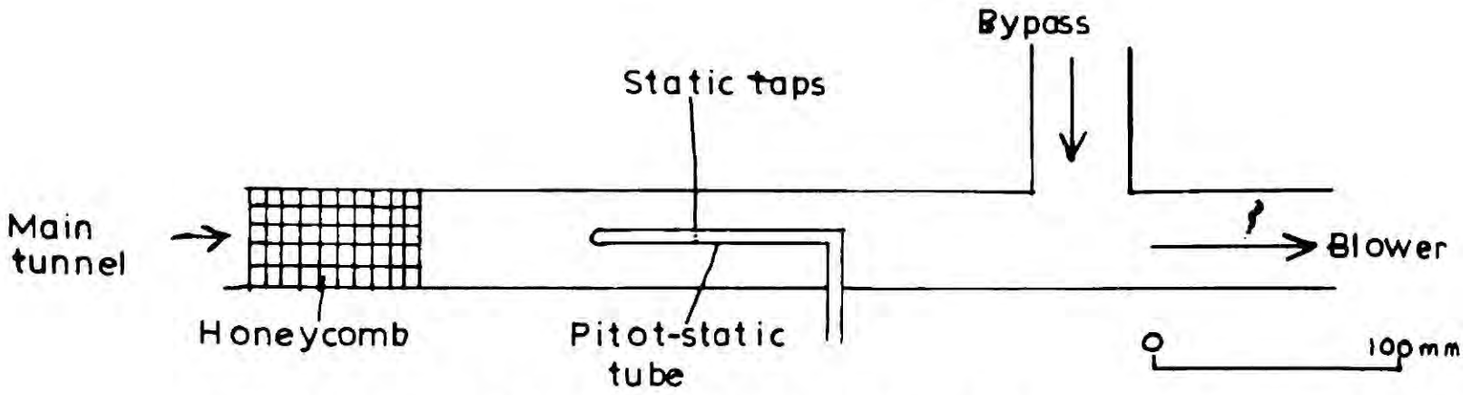

Fig.4.12 Location of pitot-static tube

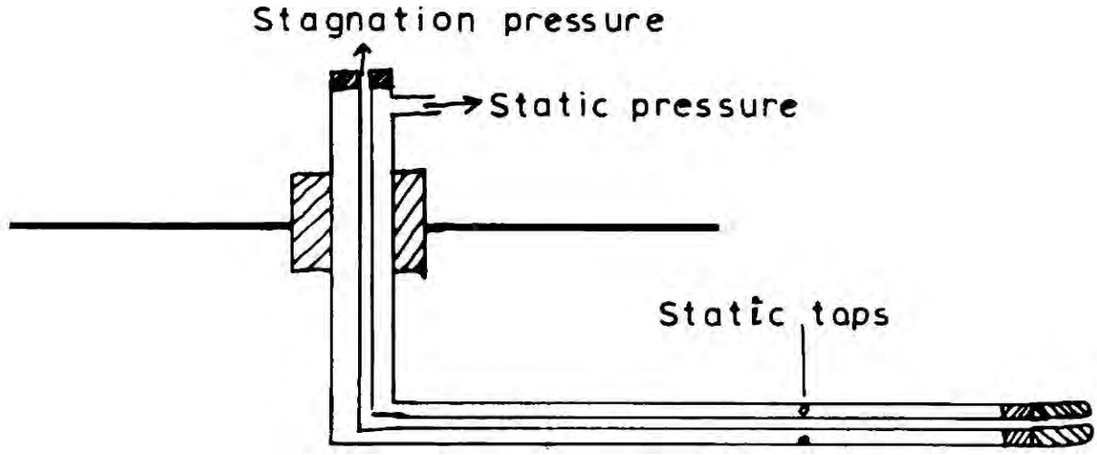

Fig.4.13 The pitot static head unit

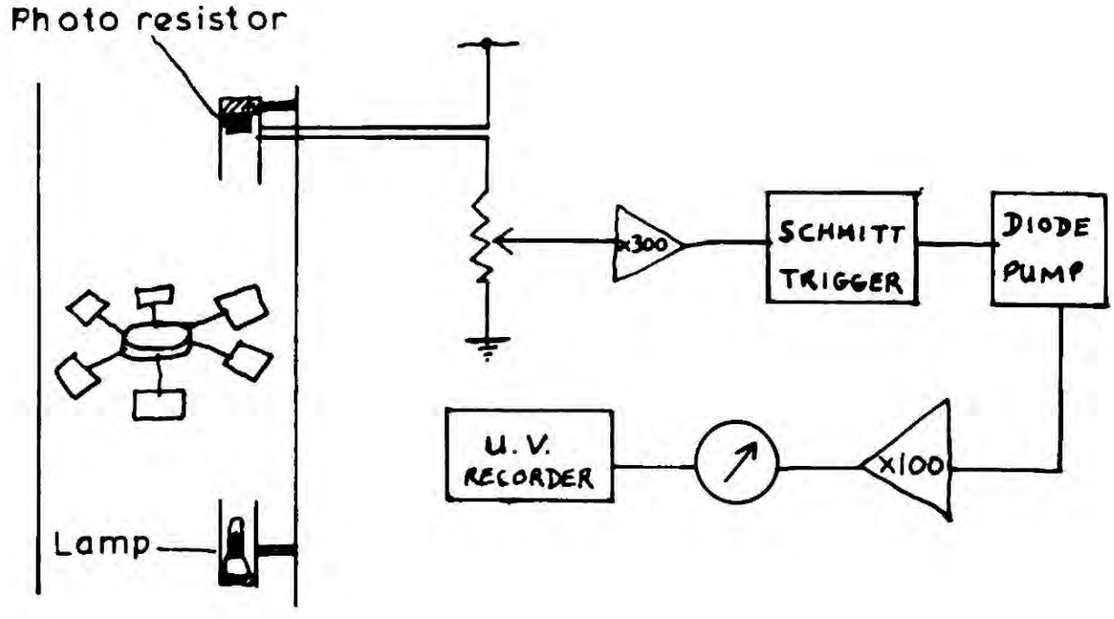

Fig.4.14 The run of wind device as a flowmeter

4.4.6 The automatic recording of temperature and humidity.

Five thermocouple amplifiers were built of which two were capable of monitoring three thermocouples each but gave only a meter output. These were very useful in the early stages of the experiment and also for checking that the heating elements had cooled down. The amplifiers used for the two humidity temperature measurements and the working section temperature were connected to both meters and ultra violet recorder channels. The recorder galvanometers could be switched into the output circuit of the amplifiers by means of a bypass switch (Fig. 4.11). This switch could replace the galvanometer with an equivalent resistor. The recorder galvanometers were protected against both positive and negative overloading by Zener diodes placed back to back with a suitable load resistor. The recorder was used on the 50 mm min^{-1} speed throughout most of the experiments. Other channels were used to record air flow velocity and the electric current measured by the V.R.E.

4.6. THE MEASUREMENT OF AIR SPEED

4.6.1. The pitot-static tube

A pitot-static tube was constructed (Fig. 4.13) and carefully positioned parallel to the wind tunnel at a point upstream from the junction of the bypass pipe and the main wind tunnel (Figs. 4.3, 4.12). The pressure difference between the static and stagnation pressures was measured by an inclined water manometer. According to the theory of the pitot-static tube this difference in pressures should have been proportional to the square of the air velocity. However, when this instrument was calibrated against a calibrated run of wind machine the pressure difference was found to be directly proportional to the velocity. Further, the calibration changed if the flow was restricted by placing a sleeve valve in the main tunnel. The pressure difference was also an order of magnitude greater than expected.

A probable explanation for this failure is that there was a static pressure gradient down the tube in which the pitot-static probe was placed

and this caused an appreciable static pressure difference between the static and stagnation taps. This was greater than the difference between the static and stagnation pressures at any point on the probe. According to the Hagan-Poisseuille law the flow rate is directly proportional to the pressure gradient down a tube for laminar flow, so one would expect the measured static pressure difference between the two taps to be proportional to the air velocity.

4.6.2. The run of wind machine as a flowmeter.

A run of wind machine with vanes was fitted into the wind tunnel near the entry point (Fig. 4.3) The vanes chopped a light beam (Fig. 4.14) which fell on a photoresistor producing a series of pulses which were fed into an amplifier and a Schmitt trigger which was used to produce square pulses of a regular height. By using a diode pump circuit to produce an output proportional to the pulse repetition frequency, the air velocity could be recorded on a meter and ultra violet recorder. This device worked very well at room temperature, but the run of wind machine tended to be unreliable at low temperatures. This flowmeter was used in alteringthe airflow to the required value but was of little use for accurate measurements. As the airspeed in the working section could be judged to $\pm$ 0.5 ms^{-1} by noting the movement of water drops near terminal velocity it was decided not to attempt to remedy the fault.

CHAPTER 5

THE PREPARATION OF ARTICIFICAL CLOUD WATER

5.1. THE SOURCE OF IMPURITIES IN HAIL

5.1.1 Impurities and hail growth

The concentration of impurities in hail is likely to be the same as in the cloud droplets from which it was formed. If the hail grew by accretion onto a frozen water drop then throughout its growth it will have been formed from cloud droplets. According to LUDLAM (1950) even if the kernel of the hail was formed by the direct condensation of the vapour, growth from 1mm diameter will be mainly by the accretion of supercooled water drops.

5.1.2 The contamination of cloud water.

True aerosols are not readily captured by falling waterdrops or hail, but according to BYERS (1965) are carried around in the airstream. Particles larger than a few microns are adsorbed at the surface of falling precipitation. GREENFIELD (1957) showed that particles smaller than 1 μm enter cloudwater by coagulating with small cloud droplets. Droplets which have grown from condensation nuclei will be contaminated by the original condensation nucleus.

5.1.3 Condensation nuclei and cloud water purity

Condensation nuclei may be classified by size into

Giant radius $> 1\mu$m

Large radius between 0.2 and 1.0 μm

Aitken radius $< 0.2\mu$m.

JUNGE (1953) measured the nucleus content of the air both near Frankfurt and on the Zugspitze and found the number of large nuclei varied from 5×10^7 to 4×10^8 m^{-3}, with a mean of 1.3×10^8 m^{-3}. As WEICKMANN and AUFM KAMPE (1953) estimated the concentration of droplets in Florida thunderstorms to be 10^8 m^{-3} it appears that large nuclei are probably the main form of active condensation nuclei in thunderstorms as they are effective at lower supersaturations than Aitken nuclei. Since the concentration of nuclei increases rapidly with decreasing radius it would

seem that the most common size of active nucleus in thunderclouds lies at the lower end of the large nucleus range i.e. 0.2 - 0.3 μ m radius.

The actual concentration of the condensation nucleus substance in the cloud water depends on the size to which the droplets grow by condensation of water vapour, because above a certain size they are likely to grow faster by coalescence, which will not greatly alter the impurity concentration. MASON (1957) considered that droplets will grow to a radius of about 20 μm by condensation; however this estimate was based on purely hydrodynamical considerations. SARTOR (1970) has deduced theoretically that the mass growth rates of droplets of 10 μm radius will be increased by an order of magnitude, even without charges being present on the droplets, if the potential gradient exceeds 30 kVm^{-1}. Should charges of 3×10^{-3} pC be present on each 10 μ droplet in a potential gradient 300 kVm^{-1} then the growth rates should be enhanced by 3 orders of magnitude. As the values of charge and potential gradient in the extreme case are slightly smaller than the maximum values found by GUNN (1950) it seems likely that this process provides an explanation of why precipitation can develop so rapidly in a cumulonimbus cloud. In a thunderstorm cell 5km thick with an updraught of 10 ms^{-1} cloud droplets at the base have only 10 minutes to develop into precipitation, while the time, calculated by BEST (1951) to reach 10μ m radius by purely condensation from the vapour is of the order of one hour for a supersaturation of 0.05%.

It would therefore seem that an upper limit to the radius of droplets formed by condensation from the vapour in thunderclouds is probably 10μ m.

5.1.4 The chemical nature of condensation nuclei.

The most effective condensation nuclei are soluble in water and generally hygroscopic. The composition of large nuclei is not well known but the most likely substances are sodium chloride from the oceans and ammonium sulphate, which is formed from sulphur dioxide and ammonia from the decomposition of organic matter.

5.1.5 Estimation of the impurity concentration in cloud water due to condensation nuclei.

If the most important nuclei have radii between 0.1 and 0.3μ m and the cloud droplets grow from the vapour phase up to 10μ m radius, it is possible to estimate (~~Fig.~~ Table 5.1) the concentration of impurities, assuming a specific gravity of 2.0 for the condensation nucleus. (S.G. of sodium chloride is 2.2, of ammonium sulphate 1.8).

Cloud droplet radius produced by growth from the vapour	Radius of condensation nucleus	Concentration of impurity
μ m	μ m	mg ℓ^{-1}
10	0.1	2.0
10	0.2	16.0
10	0.3	54.0
20	0.1	0.3
20	0.2	2.0
20	0.3	6.8

TABLE 5.1. Impurity concentrations in cloud water due to condensation nuclei.

As can be seen from table 5.1 the actual concentration of impurity is very sensitive to the radii of both nucleus and droplet, neither of which is known accurately. It would seem likely that the range of concentration of impurities is about 2 to 20 mg ℓ^{-1}. This, it will be seen later, agrees well with the range of the purest cloud water samples. It is clear from this analysis that if electric fields do greatly enhance the coalescence of cloud droplets of less than 10 μ radius, then thunderstorm rain should contain a higher level of impurities than non thundery rain. The only relevant observation by FISHER and GAMBELL (1964) does not confirm this. Furthermore possible absorption of sulphur dioxide and nitrogen peroxide by precipitation has not been considered. This calculation has also neglected the effect of the washout of nuclei which will probably be less in cumulonimbus than in stratiform clouds.

TABLE 5.2 IONIC IMPURITY CONCENTRATIONS IN CLOUD AND RAINWATER AT LOW POLLUTION SITES

REFERENCE	LOCATION	AIR (A) GROUND (G)	Na	Cl	SO_4	NO_3	NH_4	Mg	Ca	K	HCO_3	TOTAL	ELECTRIC CONDUCTIVITY	REMARKS
ODDIE 1962	S.E. England	A	2.2	3.3	3.9	1.2	0.3	0.3	1.3	0.5	-	13.0	-	All types of weather
			0.6	0.5	0.3	0.4	0.1	0.1	0.2	0.2	-	2.4	-	Thermally stable air from S.W. -3 flights
DROZDOVA PETRENCHUK 1966	North Russia	A	2.4	6.3	0.6	0	0.6	-	0.4	-	-	10.3	30	All types of weather
PETRENCHUK SELEZNEVA 1970	North Russia	A	0.2	0.8	2.4	0.2	0.5	0.3	0.8	0.3	0.6	6.2	14	Frontal precipitation
	Ukraine	A	0.3	1.0	2.4	0.2	0.8	0.3	0.2	0.2	0.9	6.3	12	Frontal precipitation
KOMBAYASI ISONO 1967	Hawaii	A	-	-	-	-	-	-	-	-	-	-	3 - 120	3 flights conductivity high at low levels.
BROCAS DELWICHE 1963	Antartica 300ml fron coast.	G	1.1	0.4	-	-	-	-	-	0.3	-	71.8	-	Analysis of snow and ice
FETH WHITEHEAD 1964	50 ml S.E of San Fransisco	G	2.2	3.8	1.8	0.2	-	0.4	0.8	0.4	5.0	12.0		Collection of rain in clean funnel
			0.8	1.2	0.7	0.1	-	0	0.4	0.4	3.0	8.0	3.5	
WILSON 1958	New Zealand	G	0.2	0.4	2.0	0.4	0.1	0.1	0.7	0.1	-	4.0		Collection of rain in clean funnel
FISHER GAMBELL 1964	50 km South of Washington D.C.	G	0.2	0.3	3.0	2.0	0.5	0.1	0.3	0.1	-	6.5	-	Thunderstorm Rain - towards end of rainfall clean funnel

Concentrations in mg l^{-1} Conductivity in μmho cm^{-1}

5.2 MEASUREMENTS OF IMPURITIES IN CLOUD AND RAIN-WATER

5.2.1 Types of measurement

There are three methods of collecting precipitation for chemical analysis namely 1) cloud collection

2) collection at the ground where the funnel used also collects fallout between periods of precipitation.

3) collection at the ground of rainfall only.

Unfortunately most measurements are of type 2 and there are very few measurements made in clouds.

5.2.2 The effects of the geographical location of the sampling site.

High levels of impurities in precipitation both in and below clouds will arise near a source of nuclei. This may be an industrial centre, where sulphur and ammonium impurities predominate, or near the sea, where sea salt is present in abnormally large concentrations. Generally the impurity concentrations found in clouds are likely to be a more reliable guide to the levels found in thunderstorms, but if the samples are taken in slowly moving stratus clouds over an industrial area the concentration is likely to be much higher than in a cumulonimbus.

5.2.3 The effects of washout on measurements at the ground.

PETRENCHUK and SELEZNEVA (1970) have compared cloud measurements with ground measurements of impurity concentrations in precipitation, for various parts of the Soviet Union, and deduced the amount of contamination occurring during the fall of the precipitation from cloud base. This ranges from 45% in the north of Russia to 80% in industrial Ukraine.

5.2.4. The purity of thundercloud water.

A number of recent measurements of the concentration of dissolved impurities in precipitation both at the ground and in clouds are contained in Table 5.2. It can be seen that there is a wide range from 2 to 13 mg ℓ^{-1} even for measurements which were selected for being either in cloud or collected at the ground under conditions where washout was small. The

most common impurities are sulphate (SO_4), chloride (Cl) and soldium (Na). Concentrations which have been obtained in various types of weather are liable to be heavily biased by a few periods of rainfall during inversion conditions, where the total ionic concentration can be as high as 100 mgℓ^{-1}. (DROZDOVA and PETRENCHUK, 1966).

From Table 5.2 the minimum concentration of ionic substances in cloudwater probably lies around the 2.0 mgℓ^{-1} value found by ODDIE (1962) from airborne measurements in a clean airmass and BROCAS and DELWICHE (1963) from snow in Antarctica. An upper limit to the concentration for thunderstorms is hard to estimate but is probably about 10 mgℓ^{-1} which is the average value for all weather conditions in a fairly low-polluted area such as Northern Russia (DROZDOVA and PETRENCHUK, 1970) and a little less than the average of the airborne measurements made over southern England by ODDIE(1962).

5.2.5 The lower positive charge and the purity of cloudwater.

The concentration of dissolved substances in the cloudwater of a thunderstorm will depend on the level of air pollution near the storm and the nearness of other sources of aerosols such as the sea. Many of the cloud droplets will form near cloud base in an updraught that has come from the lowest 2 km of the atmosphere, where the air is probably well mixed. The lower positive charge has been observed several times by SIMPSON and SCRASE (1937) and SIMPSON and ROBINSON (1941) at Kew, which is not in an area of low pollution. If the lower positive charge were found to be present in most thunderclouds then any mechanism explaining its origin must not be highly sensitive to the concentration of impurities. Therefore, from considering both the theory of the formation of impurities in cloud water and recent measurements it seems that the mechanism of the lower positive charge must be effective in the impurity range 2 to 10 mgℓ^{-1}.

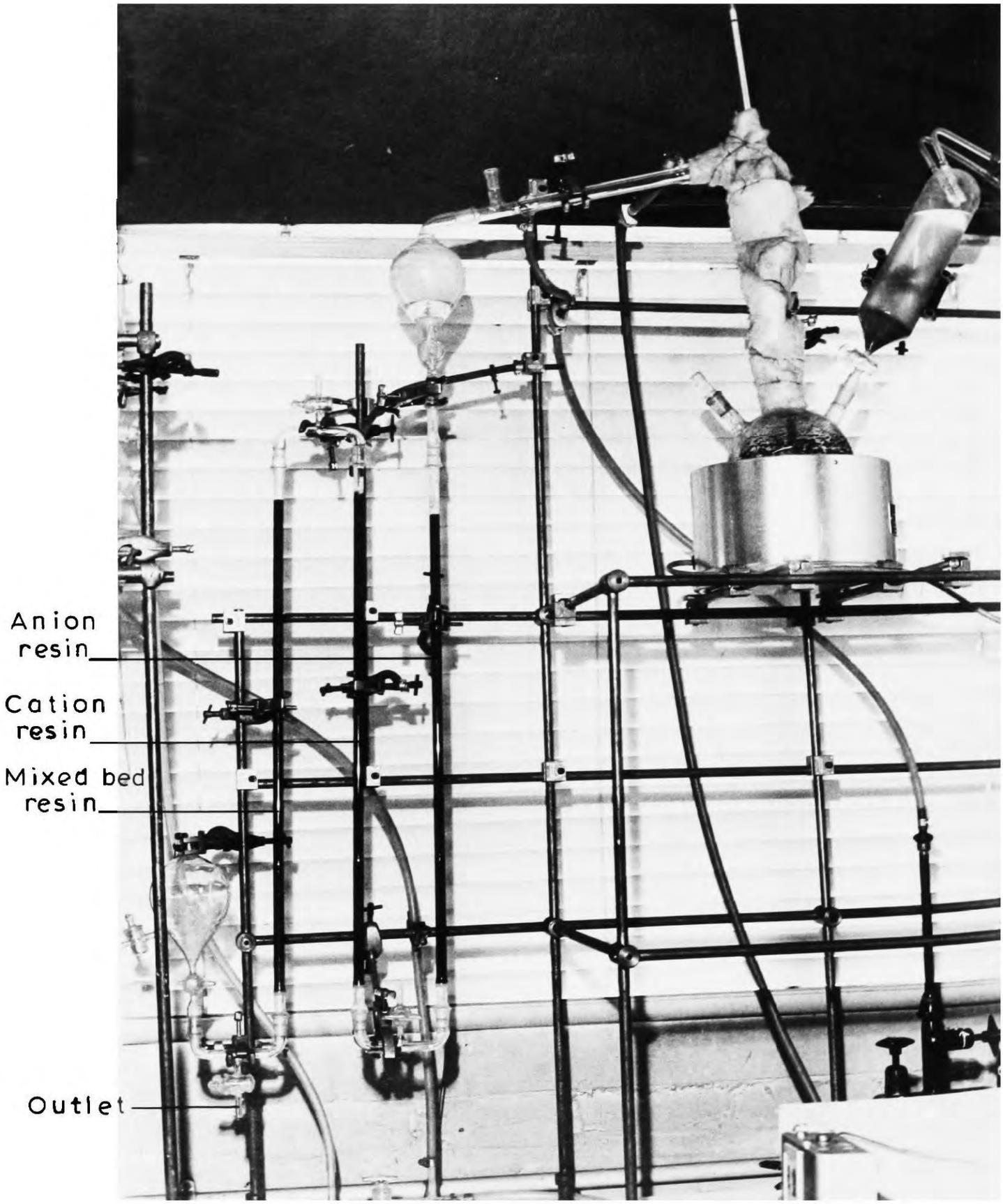

Fig. 5.1 The deionizing apparatus

5.3. THE PREPARATION OF ARTIFICIAL CLOUD WATER

5.3.1. Outline of the method.

The artificial cloudwater was made by adding known quantities of pure chemicals to water which was at least a factor of 30 purer than the final solution. The impurities in ordinary tap water consist mainly of dissolved ions such as calcium, copper and sodium, and also grease and microorganisms. These were reduced to a low level by a distillation and deionizing unit.

5.3.2. The deionization of water.

Ion exchange resins consist of porous beads of an inert material such as polystyrene containing functional groups which tend to absorb ions. The resins fall into two broad classes, cation and anion exchanges, depending on the type of ion removed from the surrounding solution. The process of removal of an ion of one sign and its replacement by another ion is reversible and can be expressed as:

CATION RESIN

$$R - SO_3H + Na\,Cl \rightleftharpoons R - SO_3\,Na + N\,Cl$$

ANION RESIN

$$R - N\,H_3^+\,OH^- + H\,Cl \rightleftharpoons R - NH_3^+\,Cl + H_2O$$

where R is the base and SO_3H and NH_3^+ OH are the functional groups of the resins. If one runs a weak solution of sodium chloride through a cation resin then the resultant outflow will contain hydrochloric acid and if this is run into an anion resin the acid will tend to be turned into pure water.

All ions are not removed equally and the selectivity of the resin can be expressed in terms of an exchange potential for a particular ion. In general multivalent ions are more easily removed from dilute solutions because they have higher exchange potentials, namely,

$$Th^{4+} > Fe^{3+} > Ba^{2+} > Zn^{2+} > NH_4^+ > K^+$$

Another type of deionisation uses mixed bed resins which are an intimate mixture of cation and anion resins. These have the advantage of working at effectively neutral pH and are highly efficient.

5.3.3 The water purification system.

Figure 5.1 shows the complete unit, which was capable of producing appoximately 1 litre of pure water every hour with very little attention needed. The layout of the distilling apparatus was recommended by Dr. R. Dawson and consisted of a 2 litre flask fitted with a fractionating column to prevent splashing, and the steam was condensed in the Liebig condenser. Water could be continuously run into the flask from the reservoir which was refilled every half hour. The flask contained an alkaline solution of potassium permanganate which was used to oxidise any organic matter to carbon dioxide and water.

The deionising columns were 0.7m long and 10 mm internal diameter. The resins was held in place by sintered glass plugs at the bottom and pyrex chippings at the top. The water ran through the system under the head of water from the small reservoir. The flow rate for optimum deionization depends on the volume of resin and using the manufacturers specification this worked out at 900 ml per hour.

The cation resin used was marketed by B.D.H. as Amberlite IR-120 and the anion resin was Amberlite IRA-400. The latter resin was supplied in the chloride form and had to be converted to the hydroxyl form before use by washing with a measured volume of 1 N sodium hydroxide. This was done in the apparatus on the left of figure 5.1. The treated resin could then be thoroughly mixed with deionized water to remove all traces of the alkali. The mixed bed resin was called MB-1 and was a mixture of IRA-400 and IR-120.

5.3.4 Purity of the deionized water.

The most abundant impurity in the deionized water was carbon dioxide which was in equilibrium with atmospheric carbon dioxide. When this was removed by bubbling with nitrogen the conductivity of the water fell from 0.8 to 0.15μ mho cm^{-1}. This lower value corresponds to an ionic concentration of slightly less than 0.1 mgℓ^{-1}.

5.3.5 The artificial cloudwater.

Electrical effects involving the rupture of the double layer at a water surface have been found by DRAKE (1968) and IRIBARNE and MASON (1967) to be independent of the species of ion present, and to depend only the actual ionic concentration. It would appear from the measurements of impurity concentrations in cloudwater (Table 5.3) that the principal constituents are sodium, chloride and ammonium ions. So it was decided to make up artifical cloudwater consisting of only sodium chloride impurities. Later, if time permitted, other impurities such as sodium sulphate and ammonium sulphate could be used. The concentration used was 4.5 mg ℓ^{-1} giving a conductivity of 8.1 μmho cm^{-1}, which falls well within the probable range of impurity concentrations in thunderstorm precipitation (2 to 10mg ℓ^{-1}).

The chemicals used were a special highly pure grade. manufactured by B.D.H called 'analar' with a maximum impurity level of 0.1%. Approximately 2g of sodium chloride was weighed out and dissolved in 250 ml of deionized water. This was then diluted further by taking out 10 ml samples with a pipette. Finally the water was stored during the experiments in a 1 litre Pyrex bottle. All the glassware used in the preparation of the water was carefully cleaned with propanol, detergent and thoroughly rinsed in running tap water and finally rinsed and left to stand in deionized water.

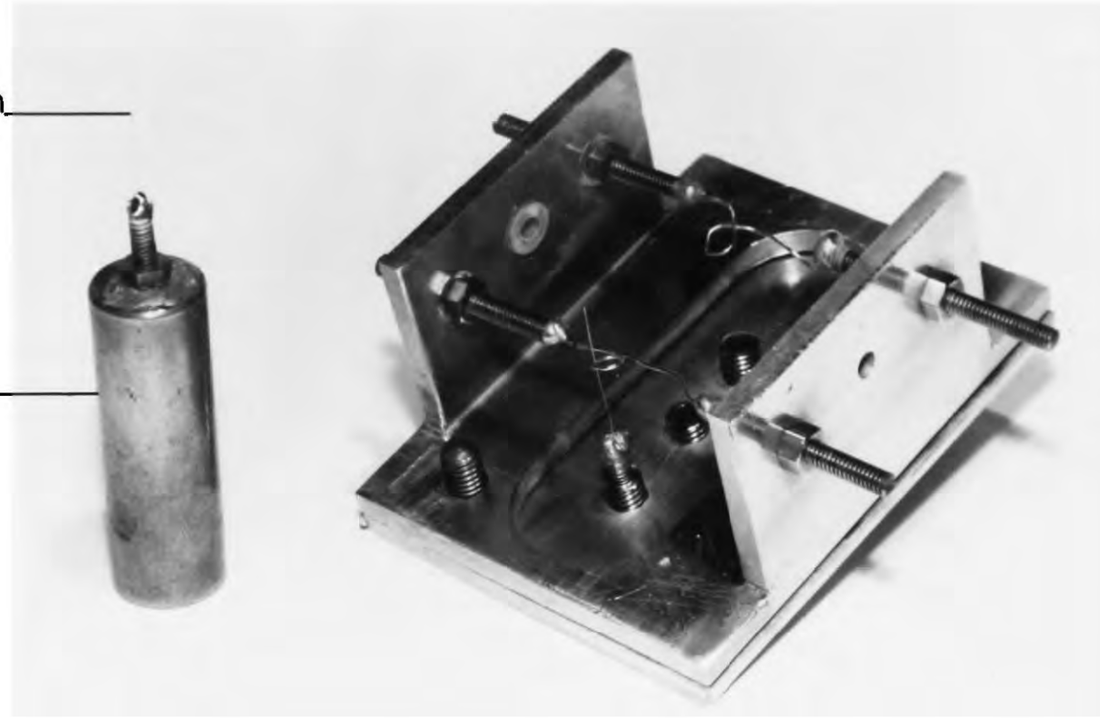

Mould for freezing water drops onto a 120 µm wire

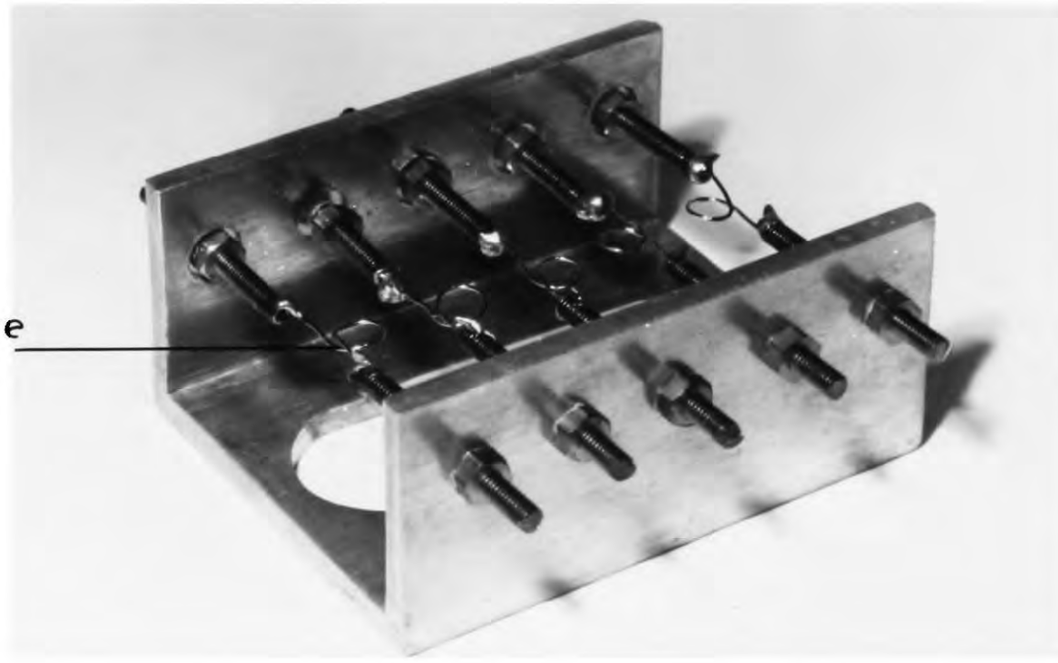

Mould used in the free flight experiments

Fig.6.1 Moulds for freezing water drops

CHAPTER 6

FREE FLIGHT EXPERIMENTS ON MELTING AND EVAPORATING ICE PARTICLES

6.1. EXPERIMENTAL PROCEDURE

6.1.1 Preparation of the ice particles.

The ice particles were made by freezing water drops suspended in ice moulds (Fig. 6.1). These moulds consisted of 3 to 5- mm diameter loops of platinum wire from which drops were hung. Each hoop was connected to an aluminium frame by 2 brass rods, one of which was insulated from the frame by a perspex bush. The wire could be cleaned by heating to white heat by an electric current from an accumulator.

The water drops were left in a refrigerator to freeze at about -15°C, Nucleation would often not occur for several hours, but in these early experiments no attempt was made to control the time of nucleation or measure the freezing temperature. When required, the ice particles were rapidly removed from the refrigerator and placed in the cold room. The ice samples were then either knocked out of their hoops with a tapered pyrex tube or released by electrically heating the hoop. The frame was designed to enable the ice particles to fall clear into a clean evaporating basin.

The ice particle was put into the wind tunnel through the hatch (Fig. 4.3) and allowed to fall into the working section, where it seen moved into its position of equilibrium. The particle was carried from the basin to the tunnel in the end of a pyrex tube and was sucked out as soon as the tube was placed in the partially open hatch. Care had to be taken to ensure that all the surfaces in contact with the ice were below 0°C as the particle tended to stick in the tube if it started melting.

The ice particles were shaped in a similar way to the drops hanging from the hoops. They tended to be somewhat ellipsoidal, with a definite tendency to be wider at the end which was in contact with the support. In these experiments the only dimension measured was the maximum width.

6.1.2 Precautions to avoid contamination of the ice.

All the glassware used in storing the pure water and manipulating the ice spheres was carefully cleaned in propanol and detergent, and then rinsed with tapwater and deionized water for several hours. All the glassware was made from borosilicate glass rather than soda glass to ensure that the water would not dissolve silicates from the walls of the containers. The evaporating basins and tapered tubes were kept under deionized water when not in use and were carefully dried with warm air from a hair drier before use. If there was any doubt as to the cleanliness of a container, deionized water was allowed to stand in it for a few hours; any contamination was shown by an increase in the electrical conductivity of the water. The aluminium working section and the brass gauzes were also cleaned with metal polish, detergent and running water, but could not be considered clean in the present investigation.

6.2. THE BEHAVIOUR OF THE SUPPORT SYSTEM.

6.2.1. Solid ice spheres.

The wind tunnel was capable of supporting an ice particle for about 30 minutes but eventually the particle would crash onto the airflow shaping gauzes. This was likely to occur at any time but probably after 30 minutes in the tunnel the particle had lost so much mass by evaporation that it tended to move up the working section into a region where the flow was less uniform, and as a result be liable to crash down onto the gauzes. Every 2 or 3 minutes the ice particle would tend to come near the walls and probably touched for a few seconds before moving away to hover somewhere else.

6.2.2. Melting ice spheres

It was impossible to support an ice particle in the wind tunnel throughout its melting process. During the melting experiments the air temperature rose from about $-5^{\circ}C$ to $+7^{\circ}C$ at a rate of about $2.5^{\circ}C\ min^{-1}$.

However, because the wet bulb depression would be of this order, the actual temperature of the ice surface was probably between 0 and $+2^{o}C$ on impact. The reason for the particle sticking to the sides soon after reaching $0^{o}C$ is probably that there was a water film, over the ice surface which assisted adhesion. Whether the ice particles touched the sides every few seconds, or the presence of the water film made the particles unstable, is not known. A disadvantage of the experimental layout was the difficulty of judging the position of a particle merely by looking down into the tunnel and so 2 black rings were painted round the core to help judge the perspective.

6.2.3 Suggestions for improving the support system

The probable reason for the failure of the wind tunnel to keep melting particles away from the sides was that the level of turbulence was too high. The flow shaping gauzes at the bottom of the working section were certainly an improvement in helping the ice spheres to keep away from the walls. However the air velocity seems to gust both in the vertical and horizontal directions. If the height of the working section (Fig. 4.3) could have been increased to eliminate the need for 2 right angle bends in the tunnel then the turbulence could have been reduced. A large settling chamber could then have been placed at the entrance of the tunnel and connected to the working section by means of a specially shaped contraction. The effect of the impeller blades of the blower, travelling upstream as pressure waves, was not appreciated and no screens were placed downwind of the working section. It is clear that the restrictions made on the design of the tunnel by the need to avoid contamination of the ice samples and to measure very small currents make the design of a viable support system nearly impossible. It may have been better to have concentrated on producing a workable wind tunnel rather than allow the design to be compromised by too many preconditions.

6.2.4 Conclusions on the study of melting electrification using wind tunnels

At present there does not appear to be a wind tunnel design which will freely support small ice particles apart from the laminar flow tunnel described by PRUPPACHER and NEIBURGER (1968). If a small tunnel were built which could perform this task then this would be a useful tool in the laboratory study of Cloud Physics. However, a tunnel that will support a melting ice particle throughout the transformation from solid to liquid would probably have to be more sophisticated than a tunnel which merely supports solid particles. During the melting process the terminal speed of the particle will change which will mean that the air speed will have to be changed. As the forces on a solid particle have different effects than on molten drops, which can be deformed, it is quite possible that a system that will support an ice sphere will not support a water drop.

6.3. THE ELECTRIFICATION OF MELTING ICE

6.3.1 Electrification in free flight.

Electrical measurements were made on 9 ice spheres of 3 to 5 mm diameter which were freely supported away from the sides during the early stages of melting. The average dry bulb temperature at which they crashed to the sides was $+4^{o}C$. Wet bulb depression was not measured, but from later measurements the air at the surface of the spheres was probably less than $2.5^{o}C$ on impact (Table 6.1). There was no electrification above the $\pm$ 0.003 pA background level for any of the samples. This is in agreement with later observations with ice spheres melting on platinum wires, when the electrification did not commence until the melting was well advanced. The ice was made from water of electric conductivity 0.75 μ mho cm^{-1} in equilibrium with laboratory carbon dioxide.

6.3.2. The melting of ice particles on the sides of the tunnel.

After the melting ice particles had crashed on the sides of the tunnel, melting proceeded rapidly and the ice usually was fully melted within 90 to 120 s. The ice core circulated in the meltwater during the later stages

of melting. Although the sides of the tunnel had been carefully cleaned, impurities would certainly have entered the meltwater during melting. The charge produced during the melting of the 9 ice particles made from water of conductivity 0.75 $\mu mho\ cm^{-1}$ is contained in Table 6.1. The rate of charging reached a maximum in the last stages of melting and tended to persist for about 15 seconds after the last traces of ice had vanished.

TABLE 6.1 The charge produced by ice particles melting on the side of the wind tunnel.

Charge +pC	Diameter mm	Temperature of Air ^{o}C	Wet Bulb Depression ^{o}C
5.0	3	2.2	1.5
4.3	$3\frac{1}{2}$	3.5	2.5
3.3	$4\frac{1}{2}$	4.3	2.0
4.0	4	5.2	2.0
3.1	$4\frac{1}{2}$	4.1	4.0
1.4	5	4.2	2.0
2.9	4	4.5	2.5
0.8	3	3.0	1.7
2.1	4	3.0	1.8

There is no significant relation between the diameters or the temperatures of crashing, and the charge produced. The mean charge was 3.0pC with a standard deviation about the mean of 0.5pC. For an average diameter of 4mm this corresponds to a ratio of charge to mass of 0.1pC mg^{-1} (0.3 esu g^{-1}). All ice samples produced positively charged meltwater

Fig. 7.1 Wire loop supports used by Drake (1968)

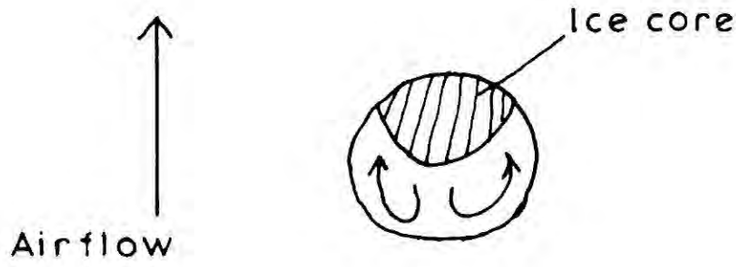

Fig. 7.2 Convective currents in a melting ice sphere
Drake and Mason (1966)

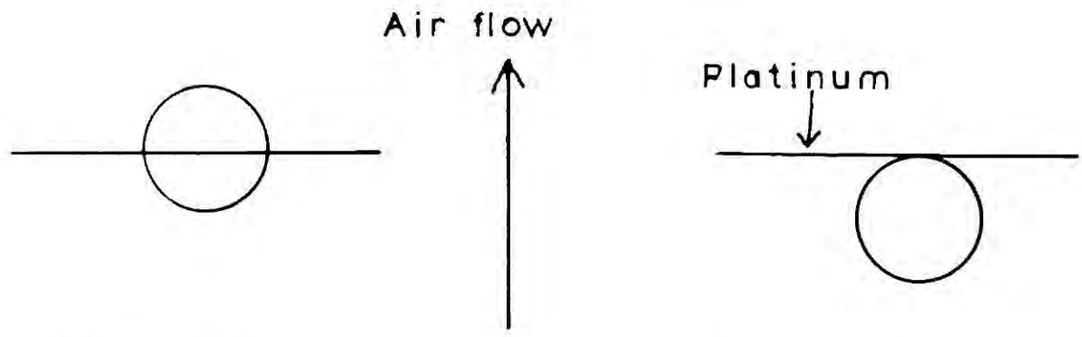

a) Ice sphere b) Partially molten

Fig. 7.3 Straight wire support

CHAPTER 7

EXPERIMENTS WITH MELTING ICE SPHERES HANGING ON PLATINUM WIRES

7.1. THE SUPPORT OF MELTING ICE SPHERES

7.1.1 Previous methods of support.

DRAKE (1968) has shown that the way in which the melting ice particles are ventilated can affect the amount of charge separated by an order of magnitude. In terms of the air bubble theory, ventilation aids the removal of the negatively charged jet drops formed by the bursting bubbles. A high rate of ventilation also assists the formation of convection in the meltwater, thus helping the bubbles to burst at a surface free from contamination. Convection in the meltwater will also alter the spectrum of sizes of the bubbles bursting at the surface by reducing the clustering of bubbles at the ice-water interface. Clearly the airflow around the particle and the way in which it reacts to the airstream greatly influence the amount of charging produced by the melting ice.

DINGER and GUNN (1946) and MAC CREADY and PROUDFIT (1965) melted blocks of ice in containers in an airstream. They found a charge separation which was an order of magnitude less than that measured by DRAKE (Fig. 7.1) using 2 to 6 mm diameter ice spheres hanging from 1 mm loops of constantan. The difference between these results was attributed by DRAKE to the onset of convection in the meltwater. This convection has been described by DRAKE and MASON (1966) who melted frozen water drops suspended from a mesh of 10 μm fibres. These convection currents sometimes randomly rotated the ice core (Fig. 7.2), and their velocity increased with increasing melting rate and wind speed but never exceeded a few cm s^{-1}.

The wire loop support did not permit the melting particle to rotate and this may increase the motion of the ice core. This type of support also allows a particle to be held in an airstream which is moving considerably faster or slower than its terminal speed. If the airspeed is higher than the terminal speed, the melting water surface will tend

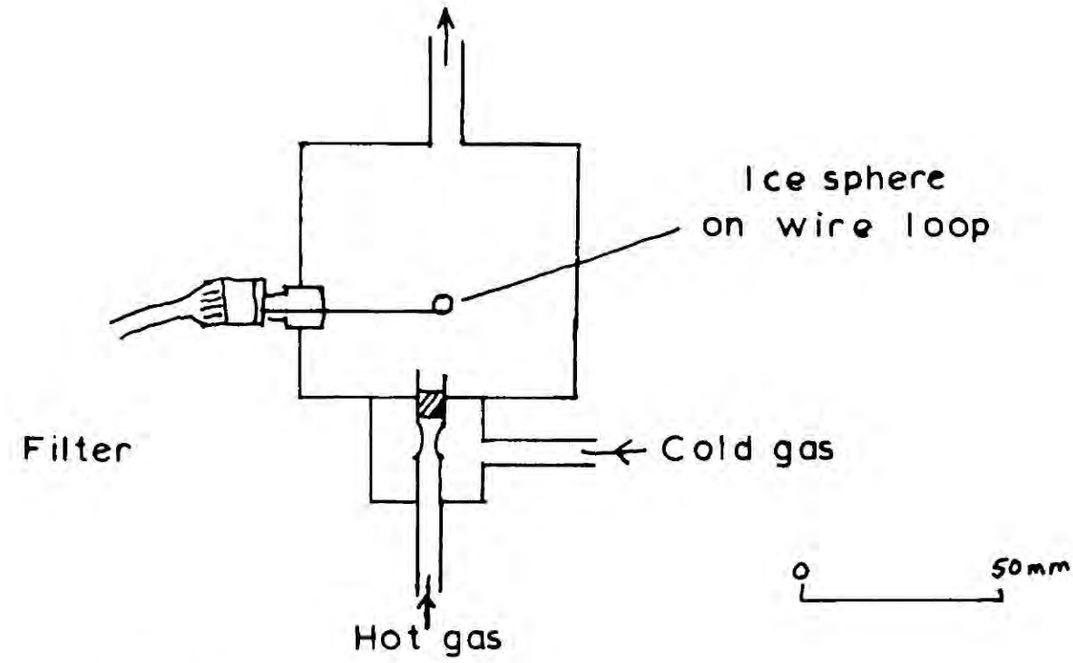

Fig.7.4 Melting chamber used by Drake(1968)

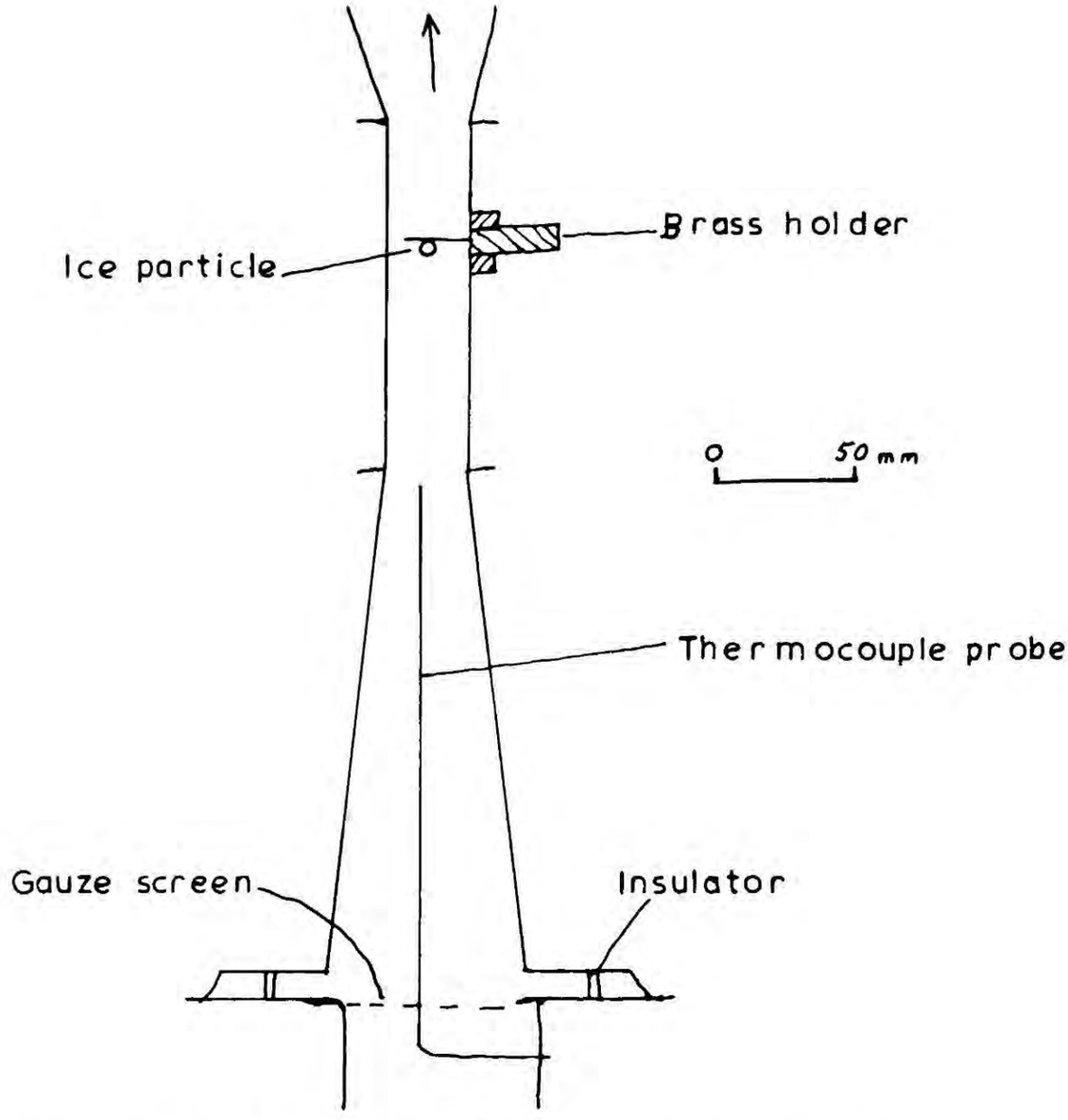

Fig.7.5 Modified tunnel section used with wire support

to vibrate and ripple more than in nature, possibly enhancing charging. Therefore it was decided to try to develop a more realistic method of support.

7.1.2 A straight wire support

Water drops were frozen onto a 130 μm platinum wire (Fig. 7.3a) and placed in the wind tunnel. During the melting process the wire moved through the melting drop until it was tangential to the water surface (Fig. 7.3b). If the airspeed was nearly equal to the terminal speed of the drop then it would continue to hang on the wire finally falling or flying off between 30 and 60s after melting was complete. Judging by the speed with which the particle left the wire, the airspeed was generally within 1 ms^{-1} of the terminal speed of the drop. During the melting process the particle sometimes rotated about a vertical axis, and always vibrated like a jelly in the later stages of melting.

7.1.3. Comparison of the wire support with Drake's experiment.

In the experiment of DRAKE (1968), the melting particle is supported in a jet of air (Fig. 7.4) which is of approximately the same width as the particle. As it is likely that this jet is mixing with the environmental air, the turbulence in the region of the particle was probably greater than in the present investigation (Fig. 7.5), where the airflow has been smoothed by a honeycomb, gauze and contraction section. Because the surface of the meltwater is not constrained by the support the whole particle is free to rotate in a more natural manner. While it might be argued that microturbulence is probably present in thunderclouds, this low turbulence system has the advantage of giving the particle more degrees of freedom than previous methods of support.

7.2. THE EXPERIMENTAL PROCEDURE

7.2.1 Preparation of the ice particles.

The ice particles were prepared in special moulds (Fig. 6.1) which could easily be cleaned. The platinum wire was soldered to the end of a short length of brass rod which could be placed in a holder fixed to the

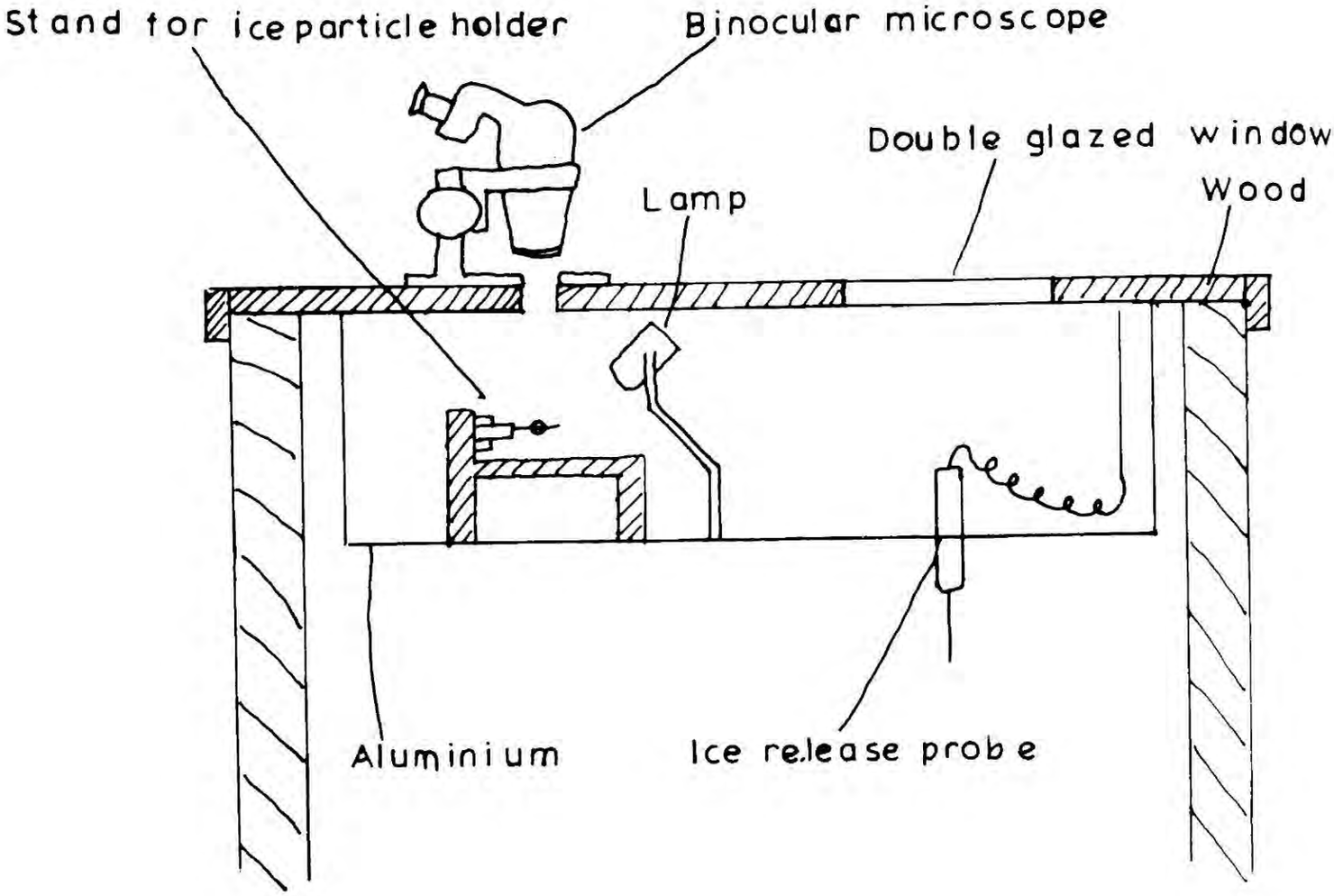

Fig. 7.7 The refrigerator

baseplate of the mould. The wire then passed through the centre of the water drop which was suspended from the platinum wire loop. The drop was nucleated either by ice crystals produced by liquid nitrogen, or by small crystals on the end of clean platinum wire. After nucleation the drop was allowed to freeze completely before being released from the mould by heating the wire loop with an electric current. The brass rod with the wire and ice particle attached could then be removed from its mould with tweezers and screwed into the holder (Fig. 6.1). The ice particles were frozen in a refrigerator and transferred to the cold room in a perspex box to prevent melting.

7.2.2. Examination of the ice particles.

A refrigerator was modified to enable the ice particles to be studied under a microscope before melting (Fig. 7.7). This refrigerator was capable of maintaining temperatures down to -13°C and on cool days could reach - 15°C and so was used to freeze the water drops. An Olympus Zoom - Stereo microscope was placed on the wooden top of the refrigerator and focused on the ice sample which was held in the stand. The advantages of this microscope were the large working distance, and the wide field of view which enabled the whole particle to be studied simultaneously, even at the maximum magnification of 40x. The microscope could also be fitted with a camera but in order to speed up the experiments only brief notes of bubble size spectrum, degree of opacity and the presence of cracks were made. The dimensions of the particles in 3 mutually perpendicular directions were measured with a ruler. As the particles were not regular a more accurate method of assessing the mass was difficult without risk of contamination.

7.2.3. The melting stage.

In order to increase the melting rate an attempt was made to build a humidifying unit which would reduce the wet bulb depression in the working section. Early experiments with passing steam into the tunnel failed

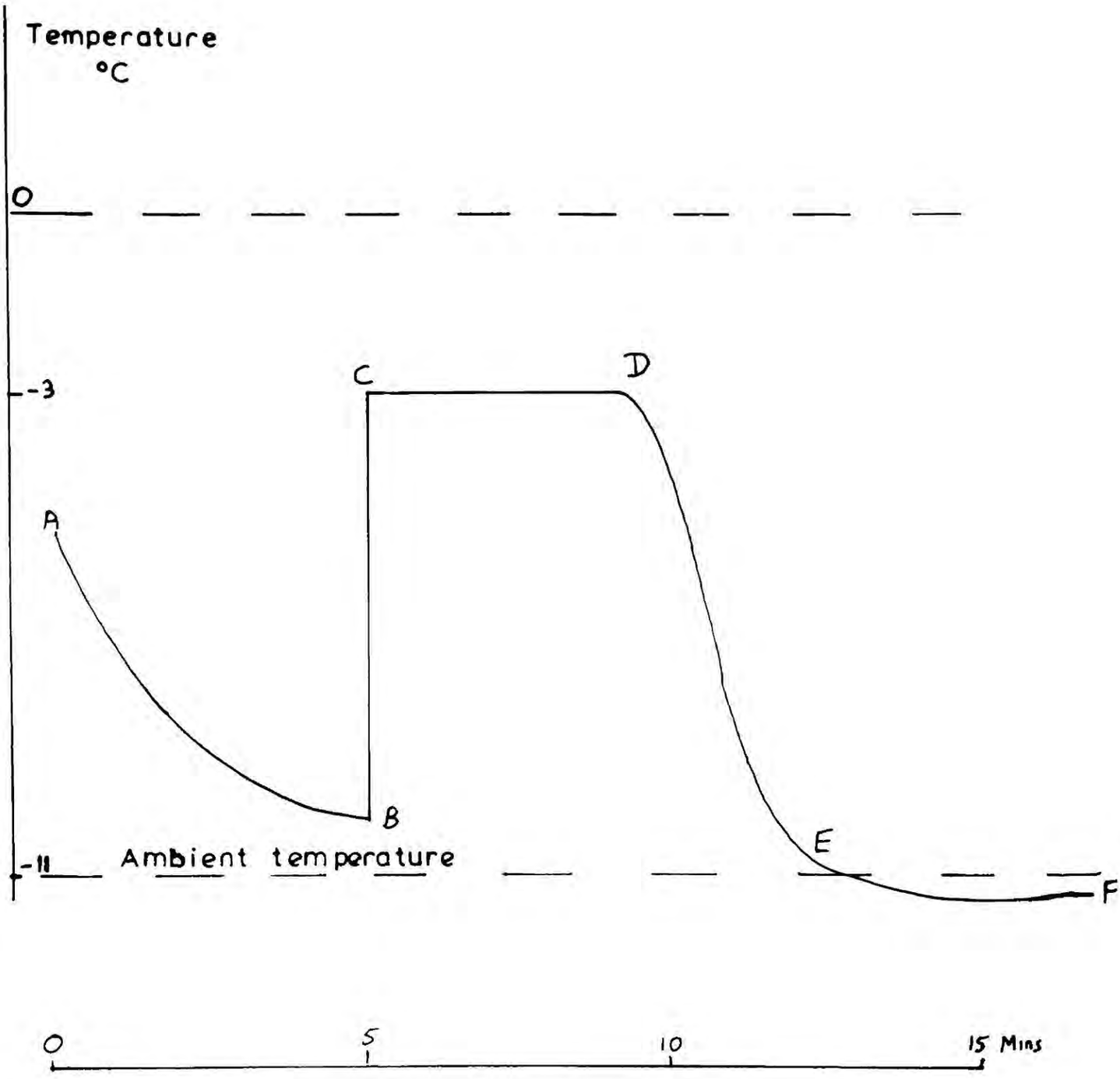

Fig. 7.8 The surface temperature of an ice sphere during freezing

because of condensation and subsequent blockage due to water freezing in the pipes leading into the cold room. A humidifier consisting of a deep tray of water and a 100 W lamp bulb did increase the humidity slightly but with the high flowrate of air in the tunnel a more sophisticated device would be needed to bring the relative humidity up to 90%. The extra heating capacity did enable the melting rates to be increased despite the increased wet bulb depression. At the maximum melting rate attainable a 4 mm ice sphere melted in 2.5 minutes. MASON (1956) calculated that a 4 mm solid ice sphere would melt in 3 minutes while falling from the $0^{o}C$ level in a cloud, assuming a saturated adiabatic lapse rate.

During melting the particle could be viewed through the mirror in the wind tunnel and notes were made of the state and manner of melting. These could be synchronised with the records of temperature and charging current by using the event marker on the ultra violet recorder. An idea of the airspeed was obtained by noting the path of the drop after it left the wire. After the melting run was completed any water left in the working section was removed with tissue paper fixed to the end of a piece of wire.

7.2.4. Precautions to prevent contamination of the ice particles.

The wire loops in the ice moulds and the platinum wire supports were cleaned before use by electrically heating to white heat. Between experiments the wire supports were stored in deionized water. The pipettes and the other glassware were cleaned in the same manner as described in Chapter 6. The tweezers were washed in deionized water after use. All the equipment used to manipulate the water and ice specimens was stored in a glove box to prevent contamination by dust.

7.3. THE ICE PARTICLES

7.3.1. Description

The particles were usually misshapen spheres due to the distortion of the original drop under gravity while hanging in the mould. Their masses ranged from 25 to 60 mg but typical dimensions were 4.5mm x 4.5mm x 4mm and a mass of 36 - 40 mg. Usually the centre of the particle looked opaque. After being examined under the microscope the particles were

classified into 2 groups, namely milky and bubbly. In bubbly ice the bubbles were generally distinguishable with clear ice visible between them. Milky ice contained patches where the bubbles could not be easily resolved and the ice looked opaque because of a mass of tiny bubbles less than 20 μm in diameter. In general the lower the freezing temperature the more likely the ice was to be milky and the bubbles small. In the range -6 to -9°C the ice was rarely milky and usually very clear outside the central bubbly area. In the range -13 to -15°C the ice usually contained a milky central region, or at least a very opaque are made up of a mass of bubbles. Large bubbles were less common in such ice, but it was evident that more air was trapped than in ice frozen at higher temperatures. This is consistent with the increase of gas solubility in water as the temperature falls.

7.3.2 The freezing process

The behaviour of the water drops during freezing was studied by replacing one of the ice moulds with a constantan loop and making a copper constantan thermocouple junction on the loop in contact with the surface of the water drop. (Fig. 7.8) shows the variation in surface temperature during the freezing process for a $3\frac{1}{2}$ mm diameter water drop freezing in an environment at -11°C. During the period AB the temperature of the drop falls towards the ambient temperature of the cold room. At B the drop is nucleated by an ice crystal and the surface temperature rapidly rises to about -3°C and remains constant for about 5 minutes. This may be explained by assuming that initially an ice shell rapidly forms and the latent heat released heats the drop until the ice-water interface is at 0°C. Hereafter the rate of freezing is governed by the conduction of the latent heat through the ice shell and its release to the environment. Hence the surface temperatures of the particle will be below 0°C. At a time D the freezing is complete and the particle cools to the ambient temperature E and finally to the wet bulb temperature F.

This experiment confirmed that little error was introduced into the measurement of the freezing temperature, provided that nucleation did not occur until the drop had been in the refrigerator for 5 minutes at -11°C

and longer for higher temperatures. At this time the rate of cooling had dropped to $0.2^{o}C\ min^{-1}$.

As only 10 - 15% of the water freezes during the initial rapid ice growth phase (Equation 7.2), the air bubbles structure is probably greatly influenced by the rate of loss of heat during the slow growth period. This heat loss can be calculated from the duration of the slow growth phase and the supercooling of the drop T. The mass m of the water frozen during the fast phase is related to the total mass M of the drop, the specific heat s of water and the latent heat L of water by equation 7.1.

$$M\ s\ \Delta T = mL \qquad \ldots\ldots\ldots\ldots\ 7.1$$

$$\therefore \quad \frac{m}{M} = \frac{s\Delta T}{L} = \text{Fraction of drop frozen (f)} \ldots\ldots\ 7.2$$

The rate of heat loss H during the slow growth phase is related to the duration t of this phase by equation 7.3

$$H = \frac{M(1 - f)\ L}{t} \qquad \ldots\ldots\ldots\ldots\ 7.3$$

For the $3\frac{1}{2}$ mm drop in Fig. 7.8 the heat loss as given by equation 7.3 is 21 mW. This is nearly an order of magnitude less than from a comparable drop falling at its terminal speed in a saturated atmosphere at the same temperature (cf. section 8.4).

7.4. THE ANALYSIS OF THE MELTING EXPERIMENTS

7.4.1 The control of the important parameters.

As has been described in section 2.4, the electrification of melting ice is highly dependent not only on the melting conditions, but also on the chemical composition of the water and the way in which the particle was frozen. DRAKE (1968) has suggested that melting rate and water purity have the greatest effect on melting electrification, but early in the present investigation it became apparent that the temperature at which the water was frozen was also important.

The chief difficulty experienced in analysing the data was that the experimental conditions could not be regulated at will. For most of the time the thermostat on the cold room was not operational so the temperature of the cold room depended to a large extent on the laboratory temperature.

Fig.7.9 A typical melting electrification record

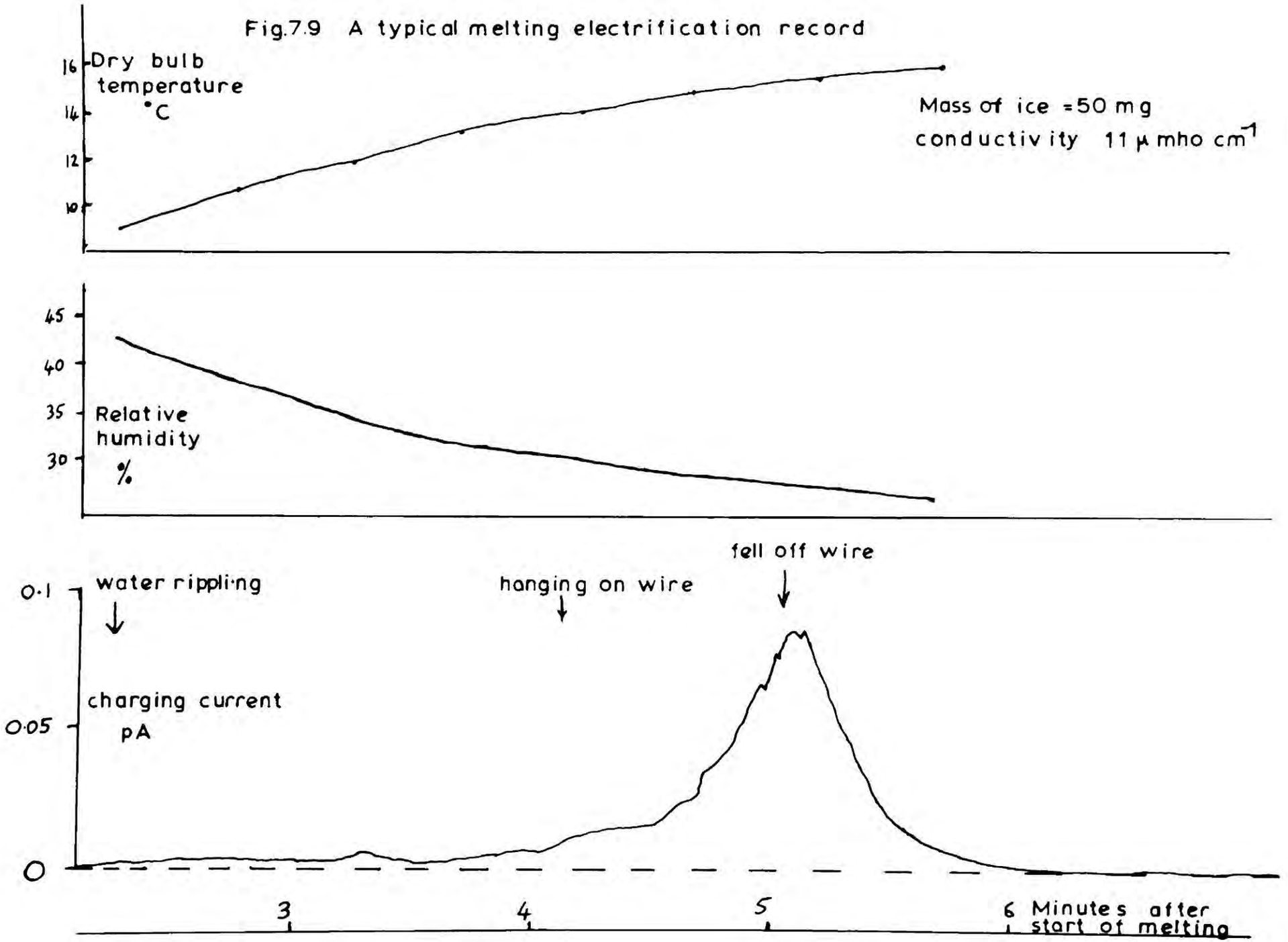

This was of importance because the melting rate of the particles depended largely on the relative humidity of the air. This fell off rapidly with increase of the temperature through which the air in the wind tunnel was heated. The freezing temperature of the particles could be controlled to $\pm$ 2°C and care was taken to nucleate the drops when they were within 1°C of the environmental temperature.

The mass of the ice particles could be measured to $\pm$ 25%, a more accurate measurement was made difficult by the need to avoid contamination, and their irregular shape. The same purity of the water was used for each set of measurements. The carbon dioxide concentration in the water would probably depend on the temperature at which the ice was melted (c.f Chapter 9) and so did not have to be controlled.

The maximum rate of performing the melting experiments was 3 per day of which only about 2 out of 3 could be successful, the others being rejected usually because the ice particle was dropped or the platinum wire did not pass through the centre of the particle. This limited the number of particles studied and therefore made the analysis of melting electrification in terms of all the important variables difficult. This limitation was accepted in designing the experiment in order to attempt to obtain a more realistic support system. However, because of the difficulty of regulating all the variables the conclusions are limited in a way which is often found in outdoor studies in atmospheric electricity.

7.4.2. The electric charge produced by melting ice.

All the 150 ice particles melted on platinum wires gained a positive charge and on no occasion was negative charging observed. The typical pattern of electrification is shown in Fig. 7.9. For over half the melting period no charging was measured and the advent of water rippling over the ice surface was usually accompanied by a small positive current of a few fA. When the particle started to hang on the wire and became free to move, the rate of charging increased rapidly to a definite maximum. Usually the particle would then leave the wire and stick to the

Fig 7.10 Charge separated by melting 4 mm diameter ice particles

Pilot investigation

Freezing temperature -11 → -13 °C

Conductivity of water = 75 μmhos cm^{-1}

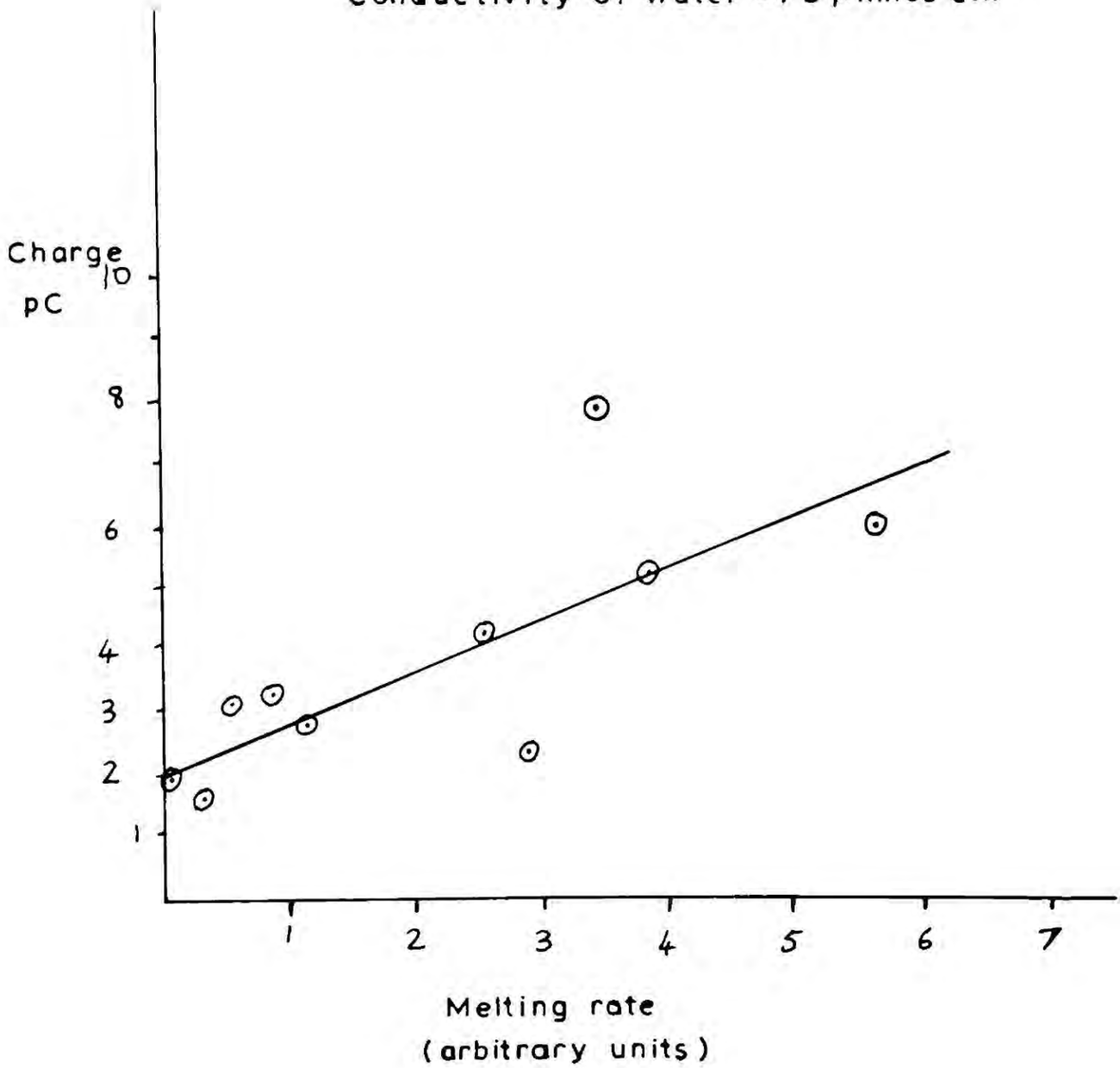

sides of the wind tunnel. If the charging continued on the sides for more than a few seconds it was concluded that the electrification process was not complete at the moment the particle left the wire and the observation was rejected. This pattern of electrification is very similar to that observed by DRAKE (1968), but no negative charge was observed early in the melting process.

The value of the charge produced was estimated by summing the average charge produced in 1 minute intervals up to the time at which the current decayed with the time constant of the V.R.E. Values of the dry bulb and wet bulb depression as well as the temperature of the air near the ice particle were read off the recorder chart and used to calculate the average melting rate during the last minute of melting.

7.4.3 Analysis of early melting experiments with deionized water.

15 ice particles of about 4 mm equivalent diameter, made from deionized water with conductivity 0.75 μ mho cm^{-1}, were melted. The average charge produced was + 3.5 $\pm$ 0.5 pC, which corresponds to a charge/mass ratio of + 0.11 $\pm$ 0.03 pC mg^{-1} (0.37 esu g^{-1}); the errors quoted are standard deviations about the mean. This compares with 0.4 pC mg^{-1} measured by DINGER and GUNN (1946) at melting rates nearly 200 times greater. DRAKE found electrification of + 0.2 pC mg^{-1} for ice spheres of similar water purity when vigorous convection did not develop in the meltwater, but this increased to + 1.0 pc mg^{-1} with the onset of convection.

Unfortunately during these experiments the humidity measurements were subject to a systematic error, and it was not possible to quote an absolute value for the melting rate. In Fig. 7.10 the charge separated is plotted against melting rate for ice frozen between -11 and -13°C. There is a definite tendency for the charging to increase with melting rate. DRAKE did not measure the melting rate in absolute terms but it is probably that these data correspond to the lowest

melting rates that he studied, as the total time for the ice to melt was on average 8 minutes compared with 90 seconds to 2 minutes shown in the 'typical records' in DRAKE'S paper.

Fig. 8.1 The melting of an ice sphere falling in saturated air from the 0°C, 700 mb level (Mason, 1956)

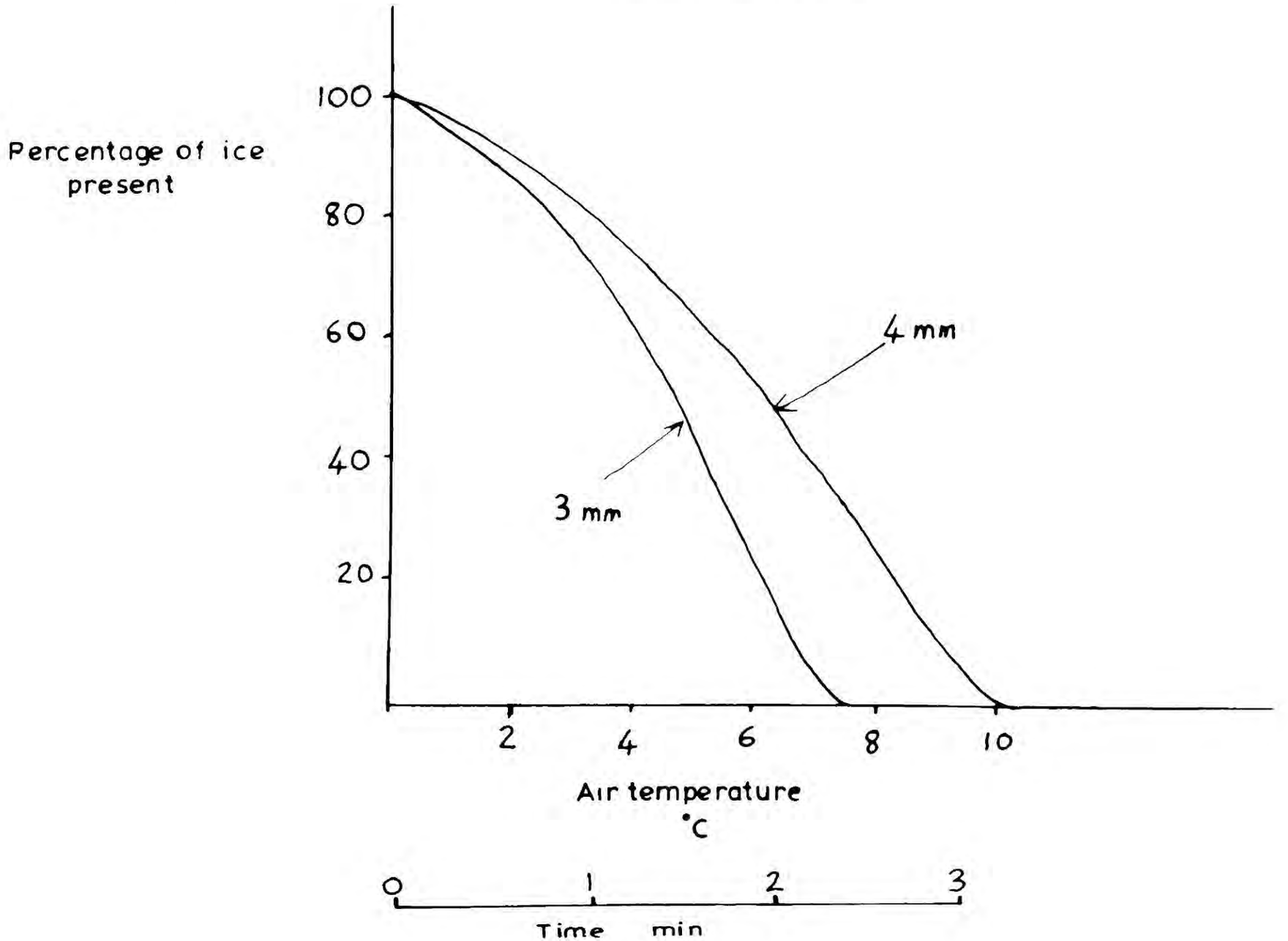

CHAPTER 8

THE EFFECT OF MELTING RATE AND FREEZING TEMPERATURE ON MELTING ELECTRIFICATION.

8.1. MELTING RATE AND THE ENVIRONMENT.

8.1.1 The melting of falling natural small hail.

MASON (1956) has solved the heat transfer equations for ice spheres falling from the 0°C level in a cloud, assuming a wet adiabatic lapse rate. This calculation shows (Fig. 8.1) that a 4 mm diameter ice sphere of specific gravity 0.9 will have completely melted by the time it reaches the +10°C level, approximately 3 minutes after the melting started. The average melting rate during the last minute of melting is 14 mg min^{-1} for a 4 mm particle and 9 mg min^{-1} for a 3 mm particle. If the melting hail were to fall out of the cloud then the melting rate would be reduced because the heat gained by condensation of water vapour would be decreased. MASON also showed that ice particles of lower density would melt more slowly because of their lower fall speeds.

An upper limit to the melting rates of ice particles of 4 mm diameter and less can be set at 14 mg min^{-1}. As the air in the wind tunnel was not saturated it was intended to try to alter the air temperature and relative humidity so that the ice particles could be melted at realistic melting rates.

8.1.2 The melting of ice particles in the wind tunnel.

The rate of heat flow to a melting ice sphere has been given by LUDLAM (1950) as

$$\text{Heat Flow} = 4\pi b \left[\epsilon_h K_a (T - T_s) + C_m L_v D (P - P_{sat}(T_s)) \right] \quad \ldots\ldots 8.1$$

where b is the radius of the particle, T_s its surface temperature, T the dry bulb temperature of the air away from the particle, P, $P_{sat}(T_s)$ are the concentrations of water vapour in the remote environment and at the water surface respectively. The latent heat of vaporization, L_v = 2.56×10^6 J kg^{-1}, the diffusion coefficient of water vapour, D = 2.4×10^{-5} $m^2 s^{-1}$, the conductivity of air, K_a = 2.5×10^{-2} Wm^{-1} $^oK^{-1}$.

The coefficients C_h and C_m take into account the effect of ventilation on the heat and vapour flow and are given by

$$C_h = 1.6 + 0.3\ (Re)^{\frac{1}{2}} \qquad \text{(KRAMERS, 1946)}$$

$$C_m = 1.0 + 0.23\ (Re)^{\frac{1}{2}} \qquad \text{(FRÖSSLING, 1938)}$$

For a 4 mm sphere at terminal speed, Reynolds number Re = 2400, C_h = 16.3 and C_m = 12.2.

The density of water vapour P is equal to the saturation density of the air at the dew point $P_{sat}(T_{dew})$. The surface temperature of the melting sphere may be taken as 0°C as this introduces a maximum error of 3% into the final value of the heat flow.

For values of dew point between 0 and -10°C the data given by KAYE and LABY (1949) fits the following relation

$$P_{sat}(T_{dew}) - P_{sat}(T_s) = (5.0\ T_{dew} - 0.1\ T^2_{dew}) \times 10^{-4}\ g\ m^{-3}\ {}^{o}C^{-1} \quad \ldots 8.2$$

where T_{dew} and T_s are measured in °C.

So the rate of heat flow into a melting ice sphere falling at terminal speed may be obtained by substituting equation 8.2 into 8.3. Rate of heat flow = $4\pi b \left[C_h K_a T + C_m L_v D\ (P_{sat}(T_{dew}) - P_{sat}(0))\right]$ 8.3

Equation 8.3 was used to evaluate the rate of heat flow into the melting ice particles in the wind tunnel. The error in the rate of heat flow varies between approximately 40% for a heat flowrate of 30 mW to 25% at 100 mW. At low heat flowrates the dominant error is associated with the measurement of dew point which could only be estimated to $\pm \frac{1}{2}$°C despite an error of only $\pm 1\frac{1}{2}$% in the measurement of relative humidity. At high melting rates the chief source of error was the measurement of the radius of the particle which was estimated to ± 10%.

8.2 THE EFFECT OF MELTING RATE ON ELECTRIFICATION.

8.2.1 Mass correction for evaporation.

At low melting rates an appreciable fraction of the ice may evaporate during the 15 minutes it is in the airstream. The mass of ice actually melted was estimated in 2 stages. Firstly during the initial slow heating of the tunnel to 0°C the total amount of heat lost due to evaporation during

Fig. 8.2 The effect of melting rate on melting electrification

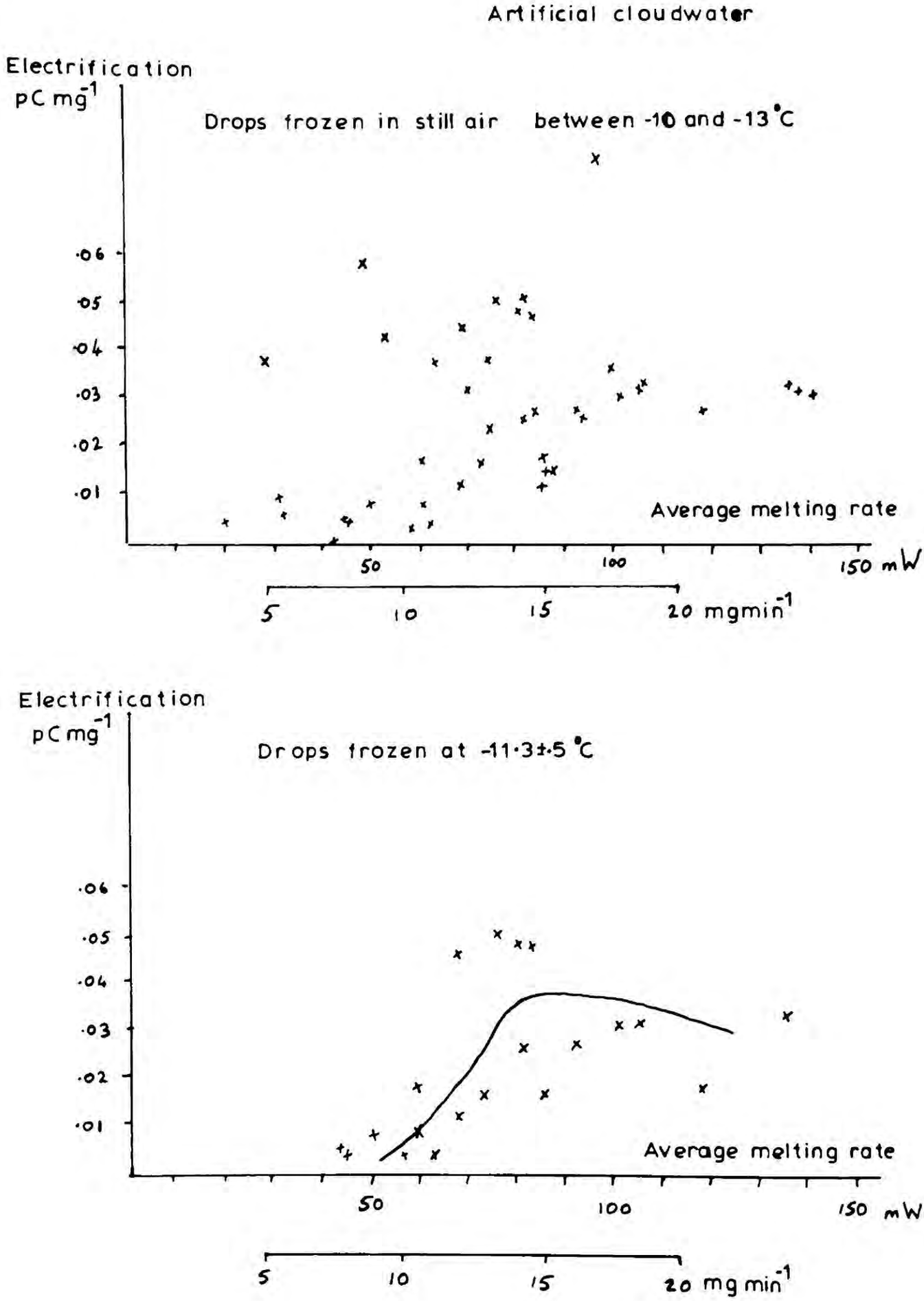

Fig. 8.3 The effect of melting rate on electrification

Artificial cloudwater

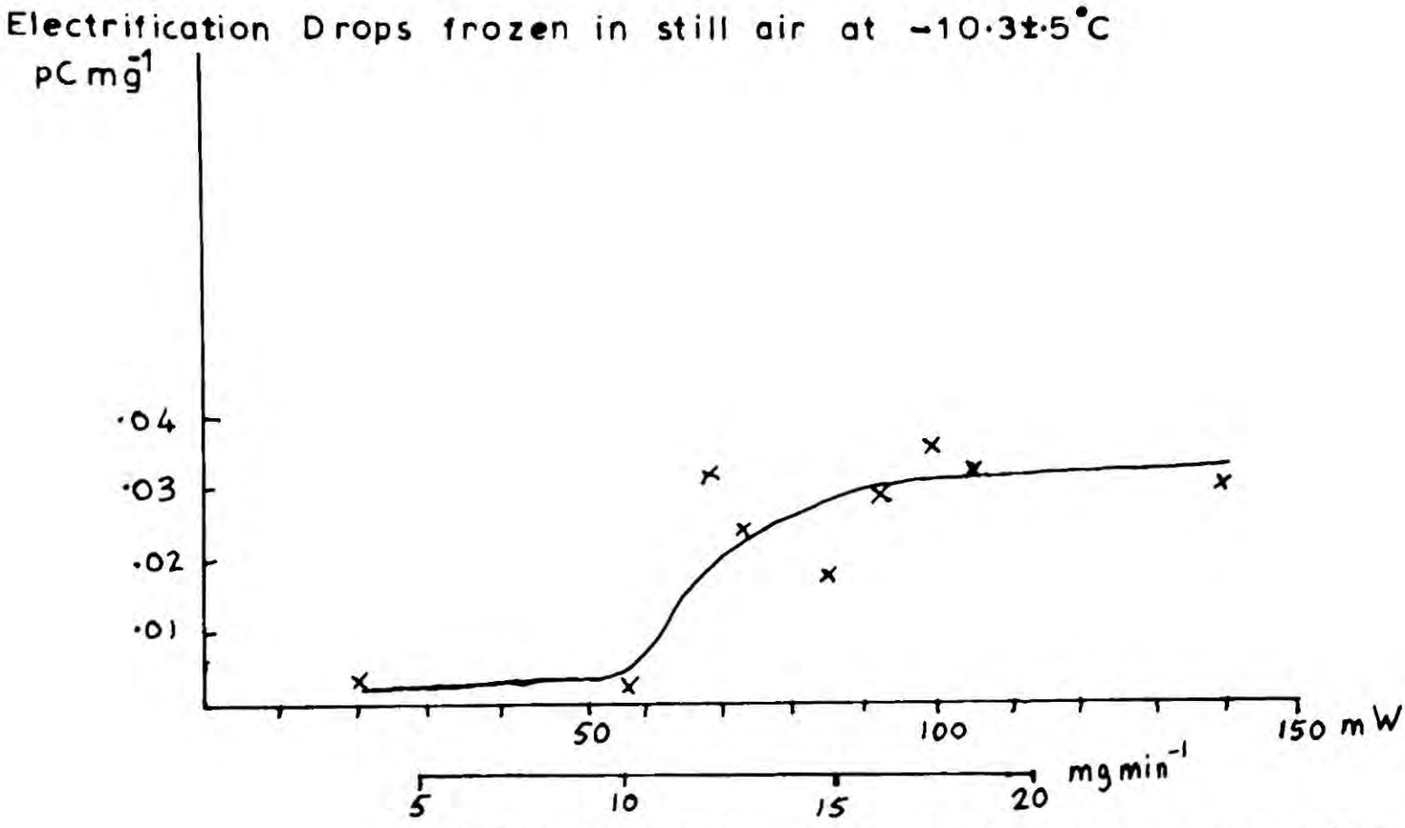

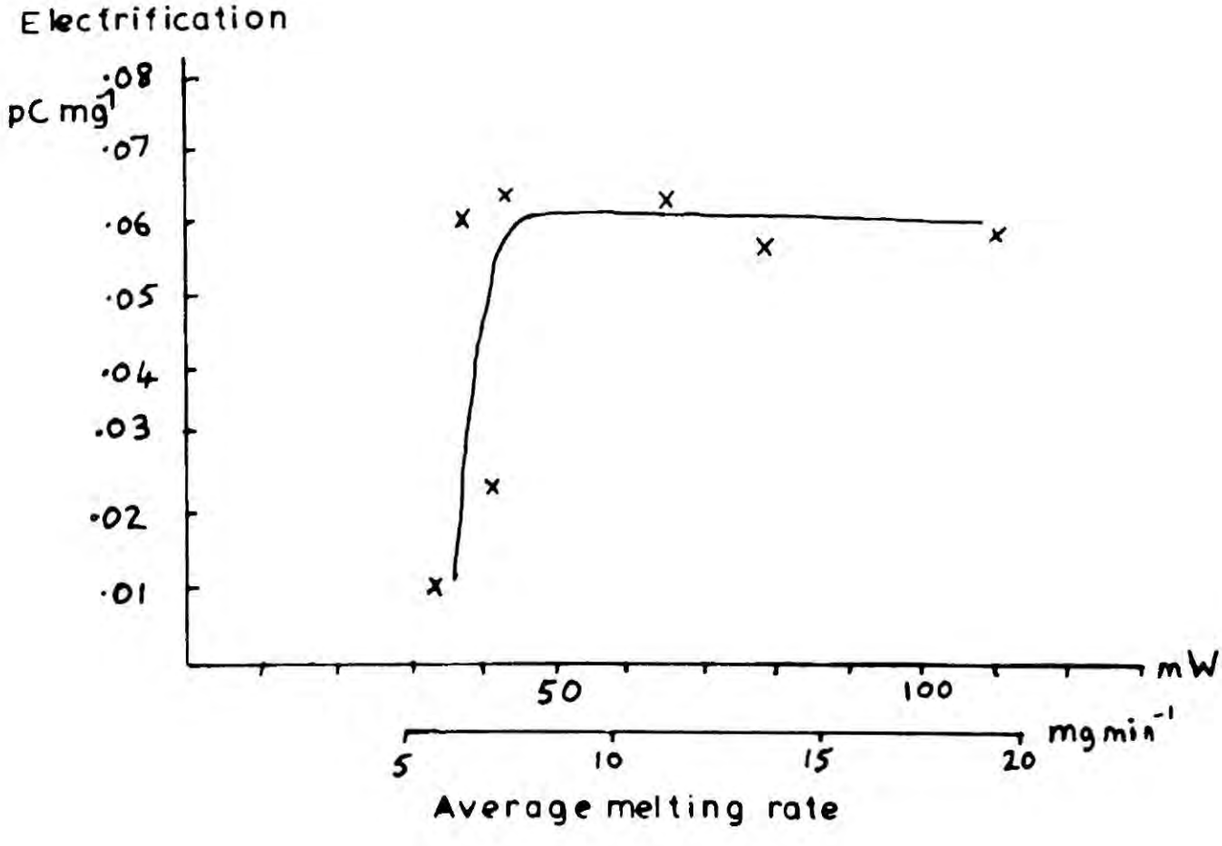

a time t, was

$$4\pi b \left[C_m L_v D \left(P_{sat}(T_{dew}) - P_{sat}\left(\tfrac{1}{2} T_{dew}\right)\right)\right] \quad \ldots\ldots\ldots 8.4$$

This follows from equations 8.1 and 8.2 assuming that the average difference in temperature between the dew point and the surface of the ice is $\frac{1}{2} T_{dew}$ During the melting process the temperature of the surface is approximately $0^{\circ}C$ so the heat lost, in time t_2, due to evaporation is simply

$$Ht = 3.9\ b\ t_2 \left[1.09\ T_{dew} + 0.022\ T^2_{dew}\right] \quad \ldots\ldots\ldots\ldots 8.5$$

Using equations 8.4 and 8.5 the total amount of water lost by evaporation was calculated for all the ice particles. At a melting rate corresponding to 20 mW, 50% of the mass evaporated and at 100 mW only 5% evaporated.

8.2.2. The results for artificial cloudwater.

The charge separated by the melting of the artificial cloudwater samples was always of the same sign, namely the meltwater became positively charged. If all the samples which were frozen in still air between -10 and $-15^{\circ}C$ were considered then there was no apparent relationship between maximum melting rate and charge separated. For the range -10 to $-13^{\circ}C$ there is a trend towards an increase in charging with increased melting rate (Fig. 8.2). If the range $-10\frac{3}{4}$ to $-11\frac{3}{4}\ ^{\circ}C$ is taken then the variation becomes more marked with almost a factor 10 increase in electrification between melting rates of 10 and 15 mg min^{-1} (Fig. 8.2). Fig. 8.3 shows similar though less well defined variations of electrification with melting rate for water drops frozen at about -10 and $-13^{\circ}C$. These results suggest that the temperature of freezing of the water drop has an important effect on melting electrification. The probable error in the ratio of charge to mass is in the region of 40 to 50% due to an uncertainty in the mass of $\pm$ 25% and in the charge of $\pm$ 20%. The error in the measurement of charge is due to the fact that the molten drops fall off the wire during the last stages of electrification.

Fig. 8.4 The effect of the type of support

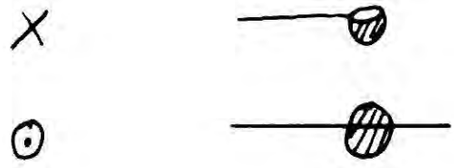

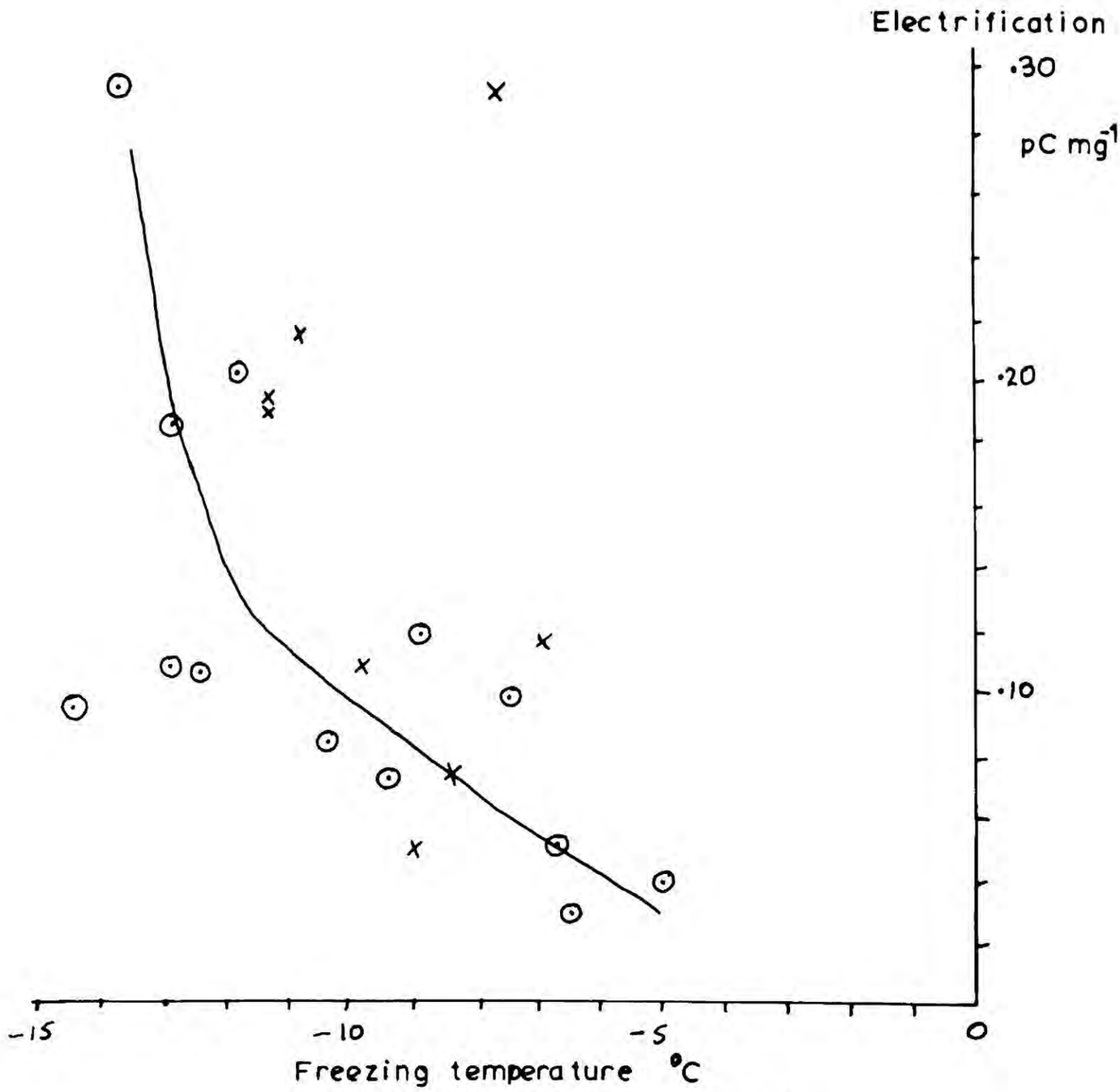

Conductivity of water 1·0 μmho cm^{-1}

Melting rate > 15 mg min^{-1}

Drops frozen in still air

8.2.3 Comparison with previous work.

These results agree qualitatively with the observations of DRAKE (1968) that the electrification increased by about an order of magnitude when the melting rate and wind speed became sufficient to cause vigorous convection in the melt water. DRAKE did not measure the melting rate absolutely so a direct comparison is not possible. There is some evidence from Figs. 8.2, 8.3 that the lower the freezing temperature the sharper the transition between the low and high electrification regions of the graphs. MASON (1956) has calculated that the average melting rate during the last minute of melting of a 4mm solid ice particle falling from the $0^{o}C$ level in a cloud is 14 mg min^{-1}. So it seems possible that such a particle would develop vigorous convection in the meltwater (cf Fig. 8.2). Unfortunately it was difficult to observe the particle clearly enough to verify that the increase in electrification coincided with the onset of convection.

DRAKE found that the total charging produced by melting particles of comparable purity (10^{-4}M) was about 0.4 pC mg^{-1} at high melting rates and 0.03 pC mg^{-1} in the absence of convection. Although he does not quote the actual melting rates it seems likely from the description of the experiment that the range of melting rates was similar to that in the present investigation. These values for the ratio of charge to mass are a factor of 10 greater than in Figs. 8.2 and 8.3. Two possible reasons for this difference are the different methods of supporting the particle and the fact that DRAKE froze the water drops in an airstream as opposed to still air.

8.3 THE EFFECT OF THE SUPPORT

To see whether the difference in the magnitude of charging was due to the different ways of supporting the ice particles 10 frozen waterdrops were melted on $1\frac{1}{2}$ mm diameter loops of platinum wire. These results were compared with those of a similar experiment with particles on the straight wire support used in the experiment described in Section 8.2. As can be seen in Fig. 8.4 there was no significant difference between the

Fig.8.5 Melting electrification and drop freezing temperature

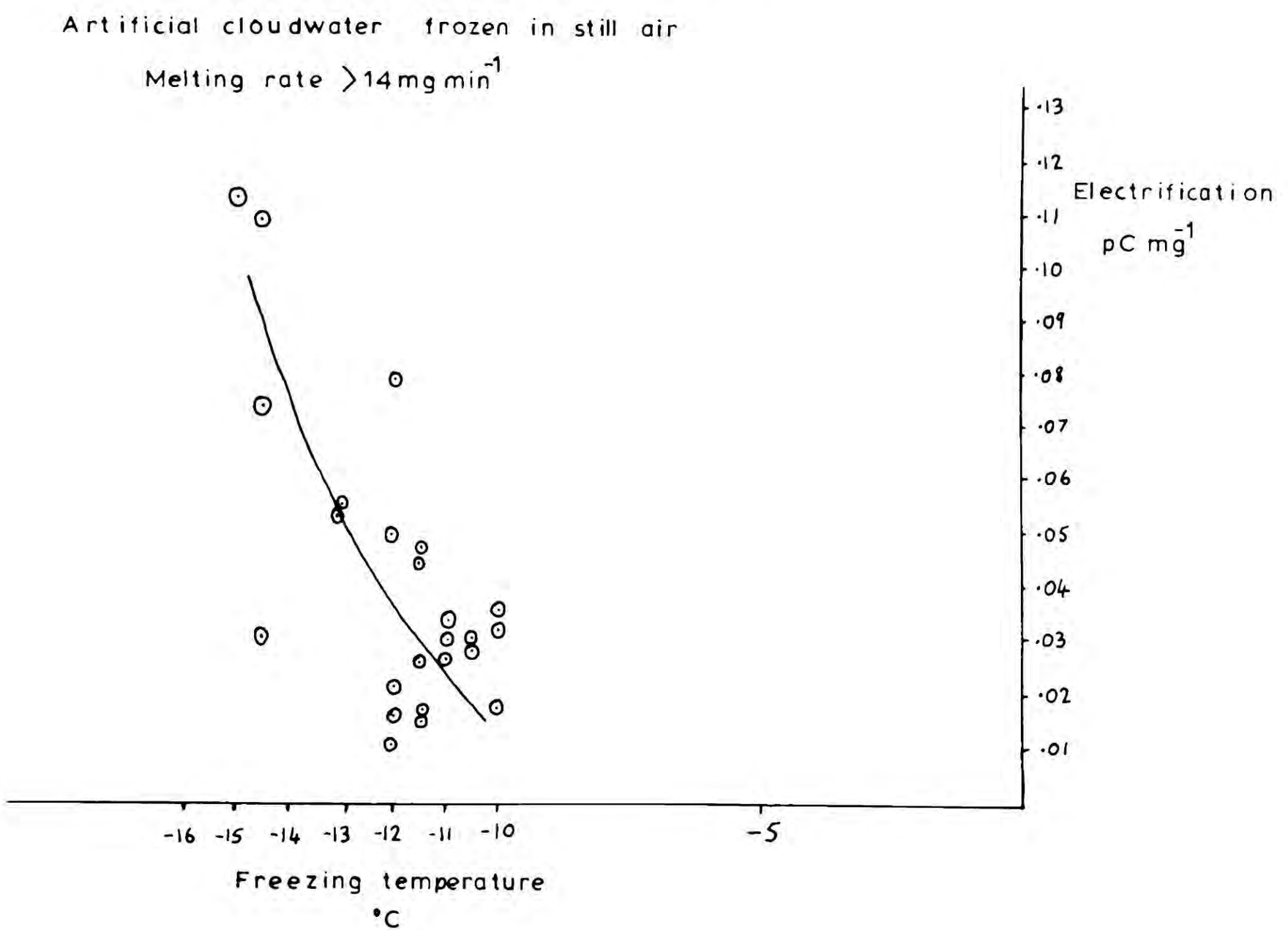

Fig.8.6 Heat flow from a water drop during freezing

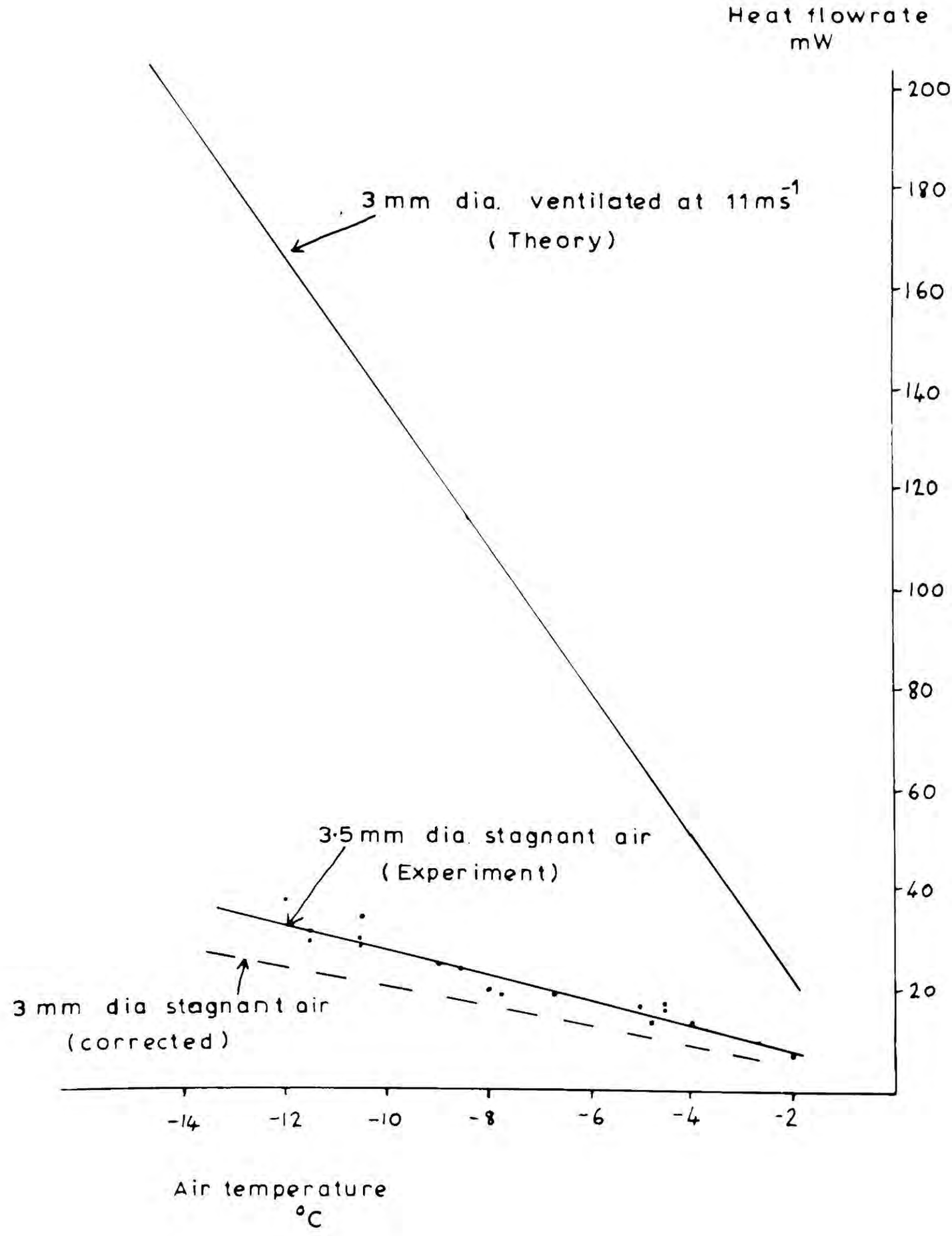

electrification produced by particles on either support. In both experiments the melting rates were judged to be high enough for vigorous electrification to have occurred. Clearly the different types of support do not cause an order of magnitude difference in electrification although possibly the higher turbulence present in DRAKE'S experiment could be important.

8.4 FREEZING RATE AND MELTING ELECTRIFICATION

8.4.1 Water drops frozen in still air - Pure water.

Fig. 8.4 shows that the temperature at which the drops were frozen has a marked effect on the electrification produced on melting. The probable accuracy of the freezing temperature was $\pm$ 1°C due to the thermometer and drop being located about 30 cm apart. There is some evidence that for freezing temperatures below - 12°C the charge separation increases rapidly with decreasing temperature. It was noted in Chapter 7 that below - 12°C the ice becomes more likely to be milky.

8.4.2. Water drops frozen in still air - Artificial cloud water.

The artificial cloud water samples showed a similar variation of melting electrification with freezing temperature (Fig. 8.5) provided that the melting rate was sufficient to ensure that small variations in melting rate were not important. Below a melting rate of 14 mg min^{-1} the effect of freezing temperature is altered by the sharp changes in the melting electrification - melting rate graphs (cf. Fig. 8.2, 8.3).

8.4.3 The freezing rate and the environement.

The freezing rate during the main part of the freezing process is governed by the rate of heat loss from the surface of the particle. The heat loss from the freezing water drops was determined by monitoring the drop temperature as described in Section 7.3.2. The variation of rate of heat loss with ambient temperature is plotted in fig. 8.6 for 3.5 mm drops. The dotted line shows a corrected value for 3 mm drops assuming that the heat loss is proportional to the surface area.

The heat loss for particles in an airstream was calculated from equation 8.1 assuming that the surface temperature of the sphere was at 0°C.

Fig.8.7 The effect of freezing rate on melting electrification

Deionized water 1·0 μmho cm^{-1}
Melting rate >14 mg min^{-1}

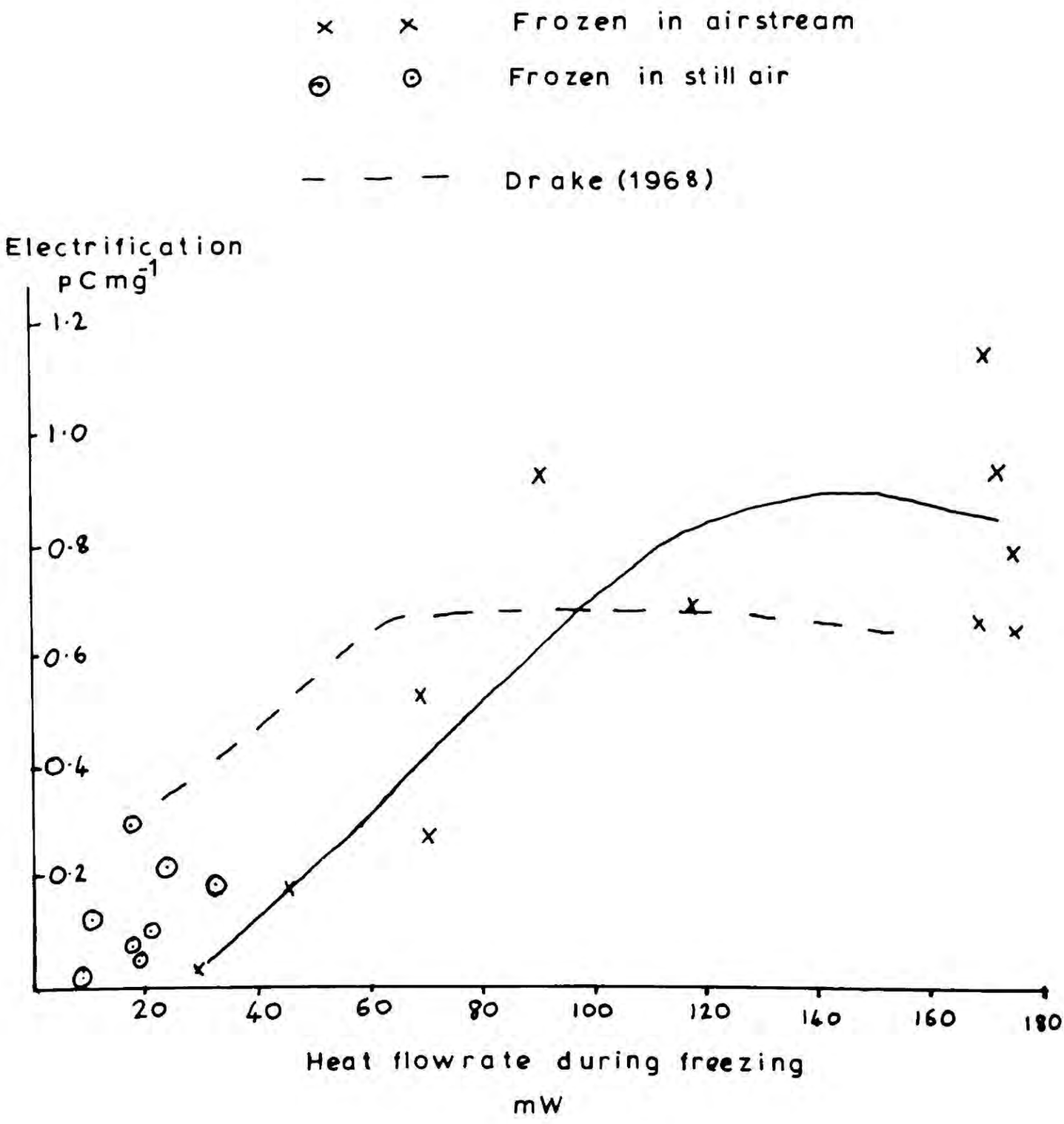

This overestimates the heat flow but as the surface temperature varies both with time and freezing rate in an undetermined manner a more accurate estimate was not made. It can be seen from Fig. 8.6 that a 3mm drop freezing in an airstream moving at 11 ms^{-1} dissipates 10 times as much heat as a similar particle in still air even if both are in an environment at $-12^{o}C$. A particle freezing at $-12^{o}C$ in still air dissipates as much heat as a similar particle in the airstream at $-2^{o}C$.

8.4.4. The dependence of melting electrification on freezing rate.

The electrification studies of the melting of water drops frozen in still air described in sections 8.4.1 and 8.4.2 have shown that there is a tendency for the charging to increase as the freezing temperature is lowered. The electrification measured in these experiments is an order of magnitude less than detected by DRAKE (1968) under similar conditions. As the particles melted by DRAKE were frozen in an airstream the difference between the 2 studies may be resolved by suggesting that the electrification was highly dependent on the rate of freezing of the water drops. The freezing conditions were therefore altered to test this theory.

The water drops were hung from a $1\frac{1}{2}$ mm loop of platinum wire and could be frozen in an airstream, using a vacuum pump. The air speed was 11 ms^{-1} and the air temperature could be monitored by means of a copper-constantan thermocouple. The rate of heat loss was calculated as described in the previous section assuming that the air was saturated. As the air was sucked from the bottom of the refrigerator where it was in equilibrium with ice, and was not heated, it seems probable that the air was saturated.

The electrification was found to increase rapidly with the increasing rate of heat loss from the freezing drop. At low values of heat dissipation there is a good agreement between the results of this experiment and the experiment with the drops frozen in still air (Fig. 8.7). As the values of heat flow rate were probably overestimates for the ventilated

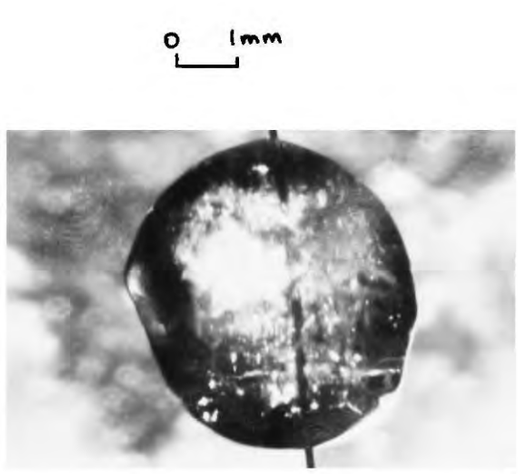

Frozen in still air at -6·5°C

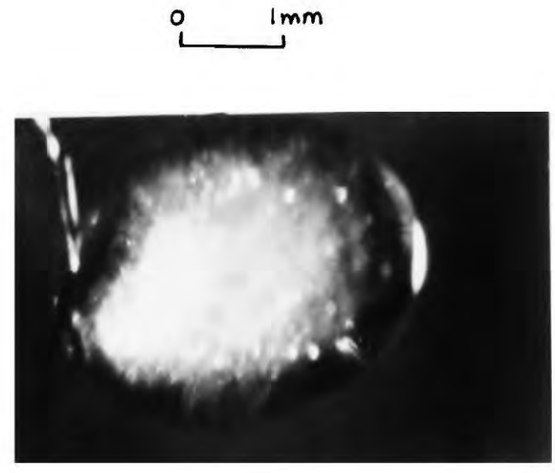

Frozen in still air at -12·5°C

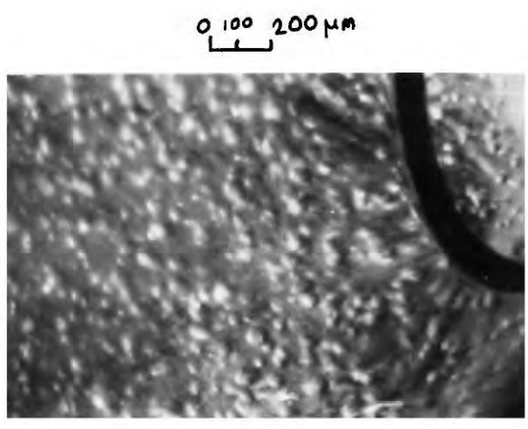

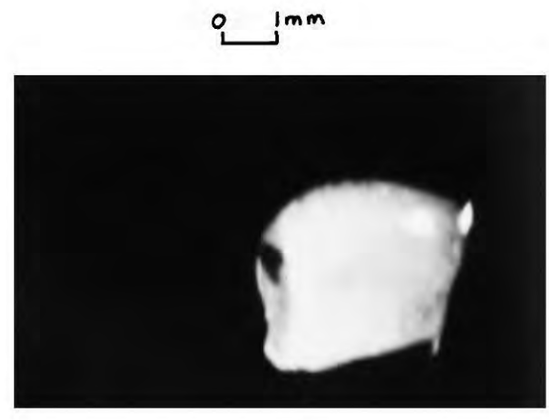

Frozen in an 11 ms^{-1} airstream at -12°C

Fig. 8.8 The frozen water drops

Fig. 8.9 Solubility of air in water
(Kaye and Laby, 1968)

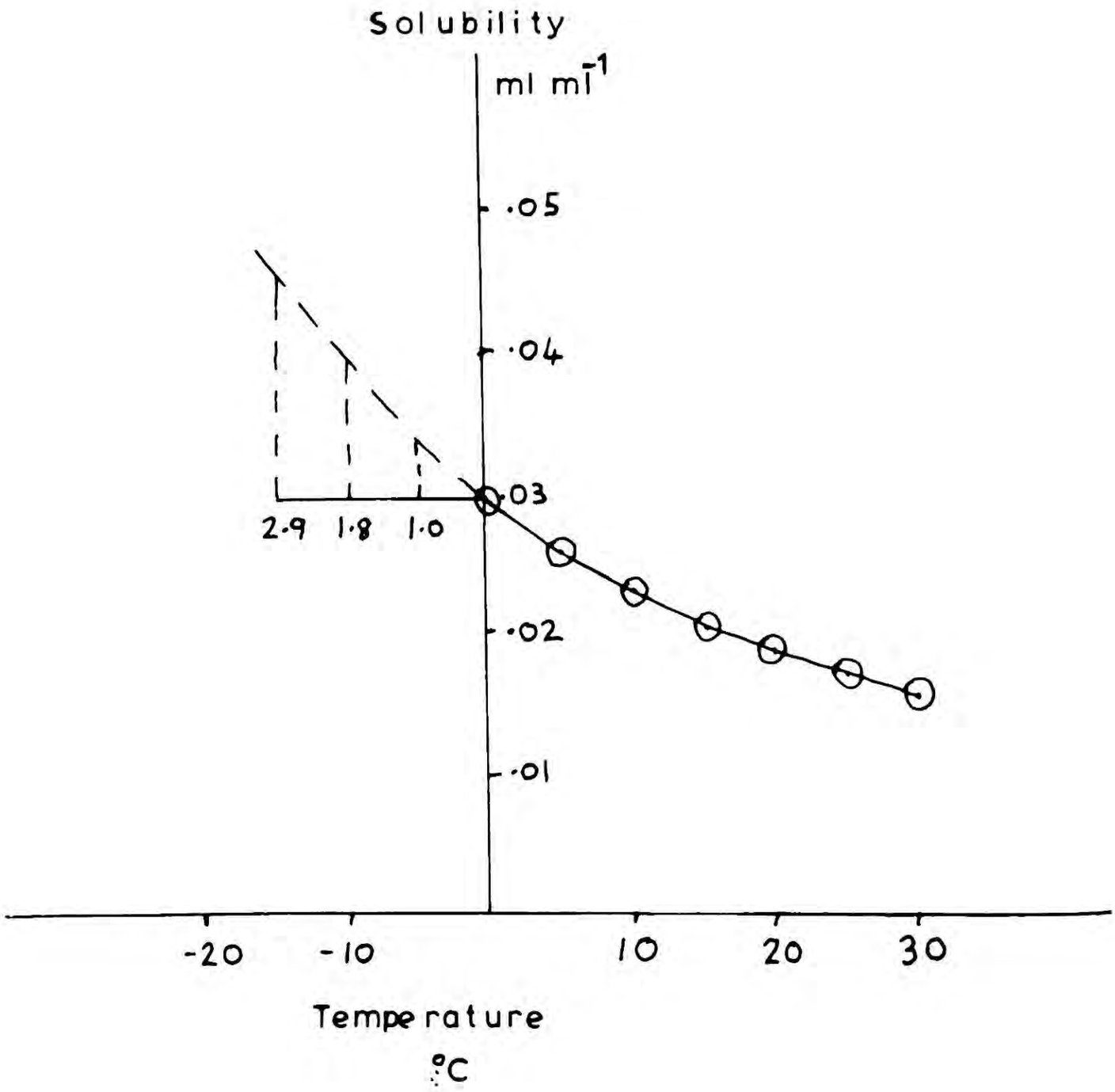

drops the agreement may be better than in fig. 8.7. For deionized water whose major source of impurity is atmospheric CO_2 the electrification increases from about 0.1 pC mg^{-1} when frozen in still air at about $-10^{\circ}C$ to 0.8 pC mg^{-1} when frozen in the airstream at the same temperature.

A direct comparison with the results of DRAKE is difficult because the actual size, airspeed and relative humidity were not given in his paper. Taking an average diameter of 3 mm and an airspeed of 7 ms^{-1} and assuming a saturated atmosphere during freezing it is possible to show that the variation of electrification with freezing rate is consistent with the results obtained at Durham (Fig. 8.7). If the air in DRAKE's experiment was not saturated then the freezing rates would be increased and the agreement would be better.

8.5 AIR BUBBLES AND MELTING ELECTRIFICATION

Water drops frozen in an airstream at low temperatures are completely white and opaque whereas drops frozen in still air near $0^{\circ}C$ are clear with a bubbly centre (Fig. 8.8). The effect of freezing rate on melting electrification may be due to differences in the air bubble structure of the particles.

8.5.1. The effect of the solubility of air on melting electrification.

The solubility of air in water increases rapidly as the temperature of the water decreases for temperatures above $0^{\circ}C$ (Fig. 8.9); the total amount of air trapped in the ice is probably greater in ice formed at lower temperatures. In the absence of data for supercooled water the values of solubility for temperatures below $0^{\circ}C$ have to be obtained by extrapolation. Provided no air escapes during freezing, the amount of air released at the surface of a melting ice sphere is proportional to the difference in solubilities of the air in water at $0^{\circ}C$ and at the initial supercooling temperature. The ratio of the volumes of air released by ice frozen at -15, -10 and $-5^{\circ}C$ as deduced from Fig. 8.9 is 2.9: 1.8: 1.0. As this variation is appreciably less than the variation in the amount of melting electrification for water frozen at similar temperatures (fig. 8.4 and 8.5) it seems likely that the increase of melting electrification with freezing temperature is due to different air bubble size spectra as well as the different amounts of air trapped in the ice. This conclusion

Fig. 8.10 Air bubbles in water drops frozen in still air

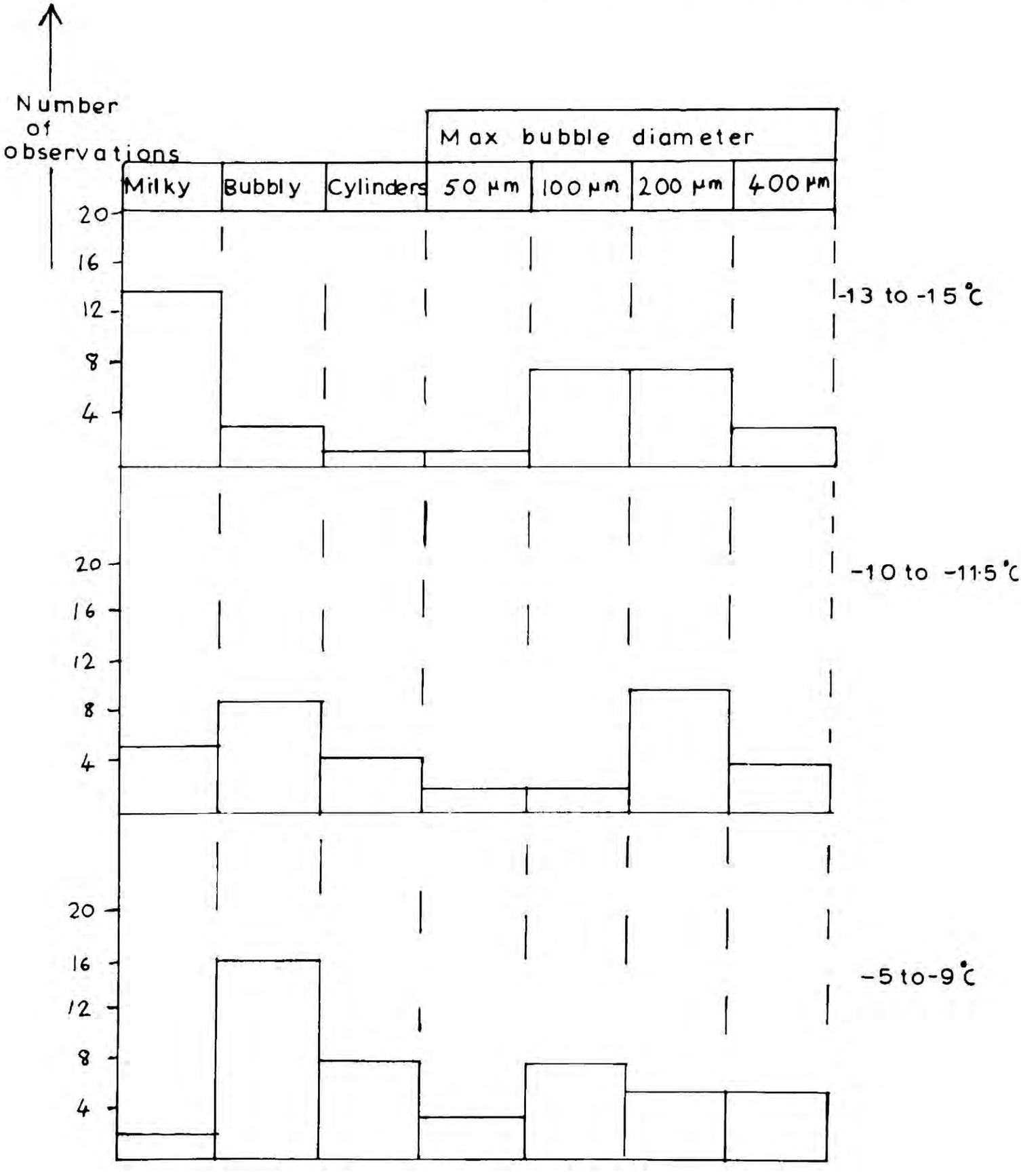

20 drops in each sample

is reinforced by fig. 8.7 which shows that the electrification is highly dependent on the rate of freezing rather than the temperature of freezing.

8.5.2. Air bubbles in water drops frozen in still air.

Generally the drops frozen in still air had an opaque centre surrounded by a shell of clear ice. The volume of the central region increased as the freezing temperature decreased. The ice samples could be classified as bubbly or milky. Milky samples had areas which were hazy even under the higher magnification range of the microscope and either consisted of bubbles smaller than 10 μm or areas of small crystals. In bubbly ice the bubbles were separated by clear ice and few were smaller than 40μm diameter. Fig. 8.10 shows that as the freezing temperature increases the ice particles are more likely to be bubbly than milky and in the range -5 to -9°C about 80% were bubbly and only 5% milky, whereas 70% of the drops frozen between -13 and -15°C were milky and only 15% bubbly.

The maximum size of bubbles did not vary appreciably with freezing temperature but at higher temperatures the mean size was nearer the maximum than for ice frozen at lower temperatures. The tendency for cylindrical bubbles of about 500 μm in length to form increased with the freezing temperature. Water drops frozen slowly were likely to lose air during freezing and air bubbles have been seen bursting through the thin ice shell during the first few minutes of freezing.

8.5.3 Air bubbles in water drops frozen in an airstream.

Water drops frozen in an airstream at 11 ms^{-1} and below about -9°C are completely opaque even under the microscope. They contain a large number of bubbles of the maximum diameter, which is in the range 25 to 40 μm. There are also a large number of smaller bubbles of all sizes down to the limit of resolution which was about 5 μm. As the freezing temperature increased the bubble size spectrum seemed to broaden and by -6°C there were a few bubbles of 100 μm and an appreciable number of 50 μm diameter. As the freezing rate decreased the drops became

Fig. 8.11 The charge separated per volume of bursting air bubbles

Iribarne and Mason (1967) theory

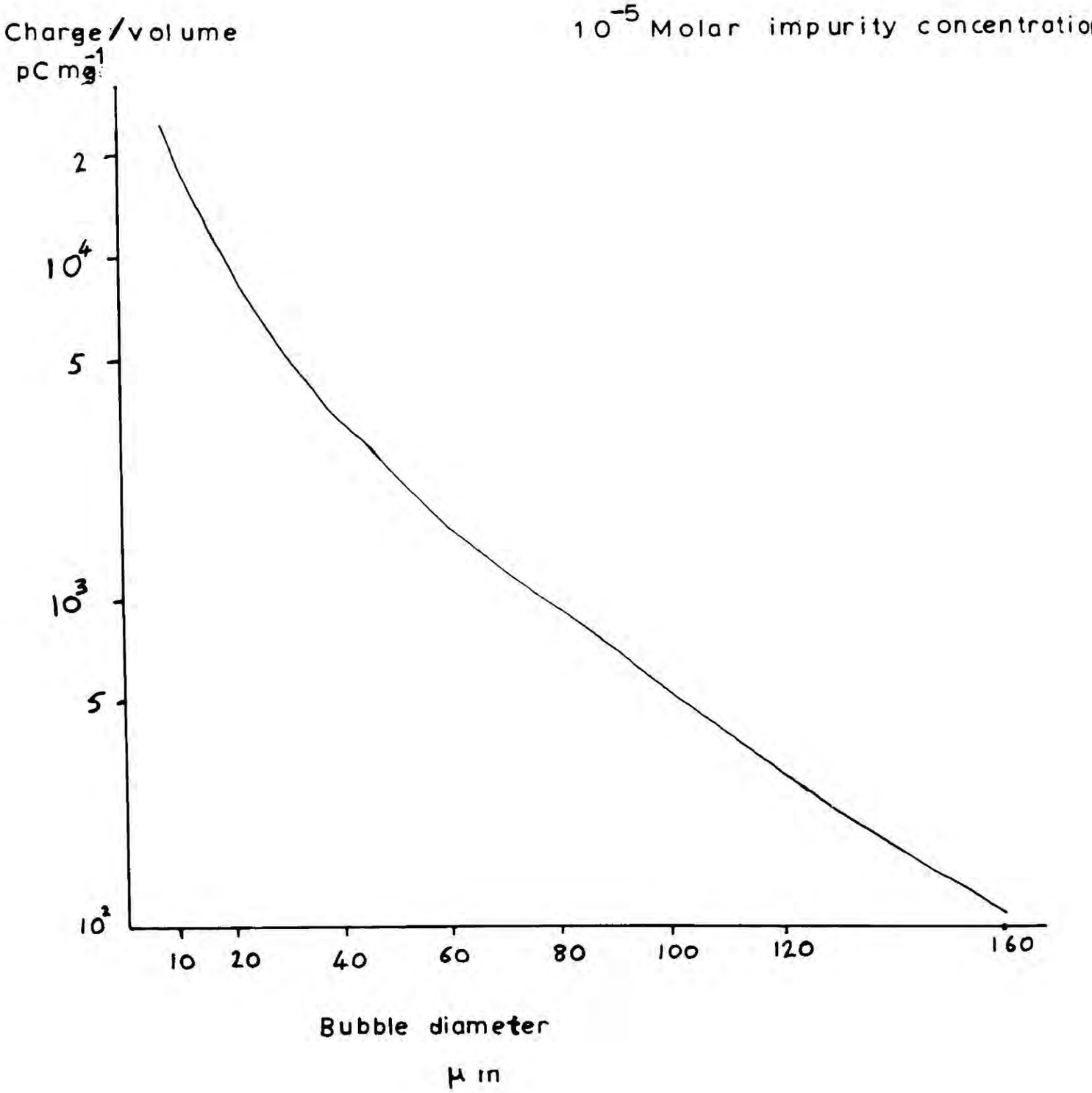

more clear and a drop frozen at -6°C was about 15% clear ice. This was about the percentage clear ice in a drop frozen at -15°C in stagnant air.

8.5.4 Melting electrification and air bubbles

The observed variation of the amount of melting electrification with freezing rate suggests that air bubbles smaller than about 50 μm diameter produce appreciably more charge separation than larger bubbles. If large enough concentrations of bubbles of 10 μm and less are present, then this size range will play an important part in the electrification of melting ice.

8.5.5. The bubble-bursting theory of melting electrification.

The bubble-bursting theory of IRIBARNE and MASON (1967) predicts (fig. 8.11) that the charge separated per unit volume of air falls off rapidly as the bubble diameter increases. For a 10^{-5} molar solution of ionic impurities corresponding to a conductivity of 1.0 μmho cm^{-1} the charge per volume increases by an order of magnitude over the bubble diameter range 80 to 20 μm. The measured variation of melting electrification with freezing rate and bubble structure is in qualitative agreement with this theory.

The volume of air released by the melting of a 4 mm diameter ice particle frozen at about -10°C is of the order of 1 mm^3. The charge on the particle was measured to be about 25 pC if the ice had a concentration of ionic impurity of 10^{-5} molar and were frozen in an 11 ms^{-1} air stream at -10°C. The maximum bubble diameter in such a particle would be about 50 μm. As bubbles of 100 μm diameter produce as much as 500 pC mm^{-3}, if all the bubbles trapped in the ice reach the surface the theory predicts a factor of 100 greater charging than is observed. One possible explanation is that many of the smallest bubbles will dissolve before reaching the surface and thebubble size spectrum will be greatly altered by the coalescence of bubbles. Furthermore the predictions of the theory may be in error for diameters as low as

20 μm as the theory depends on the bubble-bursting process remaining the same for widely different sizes of bubbles. The IRIBARNE and MASON theory has only been confirmed experimentally for bubble diameters greater than 160 μm.

8.5.6 Air bubble sizes and the rate of advance of the ice sheet.

According to BROWNSCOMBE and HALLETT (1967) the sizes and number of bubbles formed by the freezing of water depend on the rate of advance of the ice sheet and the extent to which pressure can build up. CARTE (1961) has measured the average diameter of bubbles formed by freezing layers of water at various freezing rates (Table 8.1).

TABLE 8.1. The rate of advance of the ice sheet and size of bubbles. CARTE (1961)

diameter μm	growth rate mm min^{-1}
400	0.2
200	0.5
100	2.0
50	5.0

The rate of advance of the ice sheet in a water drop freezing at $-12^{\circ}C$ in an airstream flowing at 11 ms^{-1} is 2.4 mm min^{-1}. According to Table 8.1 this rate of freezing corresponds to a mean bubble diameter of about 90 μm. This value is 3 to 4 times the mean bubble size observed in the frozen water drops but the difference may be due to the build-up of pressure during the final stages of freezing of the drop. For water drops freezing in still air a typical speed of the ice sheet would be 0.2 mm min^{-1} corresponding to a bubble diameter of 400 μm. It would be expected that the observations of CARTE would apply more closely to the freezing of a water layer on the surface of a hailstone.

8.6 COMPARISON WITH PREVIOUS EXPERIMENTS.

The magnitude of charge separated by the melting of artificial cloud water was found to be an order of magnitude less than that observed by DRAKE (1968). This may be explained by the different rates of freezing of the ice samples. Although vigorous convection in the melt water could not be observed it seems likely that this was the cause of the large difference in electrification at high and low melting rates described in figs. 8.2 and 8.3 There is some evidence that the higher the freezing rate, the lower the critical value of melting rate at which the increase of electrification is apparent. The results suggest that the effects of convection on the electrification are important for melting rates as low as 5 mg min^{-1} provided the ice contains enough air bubbles.

It has been shown in section 8.3 that the observations made using the loop support of DRAKE do not differ noticeably from those made with a more natural support which permits the particle to rotate. So DRAKE's observations can be used in assessing the importance of melting electrification for ice which has been formed at high freezing rates and which contains many bubbles smaller than 30 to 40 μ m diameter. The results obtained in the present investigation are applicable to the study of ice frozen at low freezing rates where an appreciable fraction of the trapped air is contained in bubbles larger than 40 to 50 μm.

The observed dependence of melting electrification on the size of air bubbles agrees qualitatively with the IRIBARNE and MASON (1967) theory of the electrification of bursting bubbles at a water surface. This confirms the view of DINGER and GUNN (1946) and DRAKE (1968) that the electrification of melting ice is due to the bursting of air bubbles.

CHAPTER 9

THE EFFECT OF CARBON DIOXIDE ON MELTING ELECTRIFICATION

9.1 CARBON DIOXIDE AND LABORATORY EXPERIMENTS

9.1.1 The Matthews and Mason experiment

One of the reasons put forward to explain why MATTHEWS and MASON (1963) failed to detect charging when ice and snow were melted has been the regular use of dry ice in the laboratory. Also in two out of three experiments the water was frozen in close proximity to dry ice. DINGER (1964) has pointed out that the presence of carbon dioxide near the apparatus was sufficient to reduce the electrification found in the Dinger-Gunn experiment (1946). However, as contamination of the water and the actual method of melting also have a large effect on the charge separated, the presence of carbon dioxide may not have been the only cause of the MATTHEWS and MASON null result.

9.1.2 The Dinger-Gunn experiment.

DINGER and GUNN (1946) found that water frozen in an atmosphere of carbon dioxide produced no electrification when melted. The ice samples had a typical volume of 2 ml and were melted in trays, with some ventilation.

9.1.3 Drake's experiment.

DRAKE (1968), in contrast to most of the previous workers, found that water frozen in the presence of carbon dioxide produced as much as +1.3 pC mg^{-1} on melting. The ice was made from small water drops and carbon dioxide was bubbled through the water before use. However, if vigorous convection did not develop in the meltwater, electrification was inhibited by the presence of carbon dioxide.

9.2 THE IMPORTANCE OF CARBON DIOXIDE IN MELTING ELECTRIFICATION

9.2.1 The double layer theory and the effects of carbon dioxide.

According to the electrical double layer theory of bubble-bursting electrification, the effect of dissolved carbon dioxide should be the same as that of a similar concentration of dissolved ions of any species. This has been confirmed by the experiment of IRIBARNE and MASON (1967). The reason for carbon dioxide being more active than most atmospheric gases is that it is highly soluble in water and forms carbonic acid which dissociates into hydrogen and bicarbonate ions. If melting ice electrification is caused by the release of trapped air bubbles, then one would expect the presence of carbon dioxide in the water would inhibit electrification.

9.2.2 The effect of atmospheric carbon dioxide.

GLUCKAUF (1944) gives examples of carbon dioxide concentration at the ground as 0.031 - 0.035% at Kew and 0.035 - 0.037% in central London. Inside the laboratory the concentrations tend to be higher and can range from 0.04 to 0.1%. Away from the ground, the concentration of carbon dioxide seems to be independent of altitude, certainly up to 10 km. GLUCKAUF gives an average value of 0.025% for 4 to 10 km over England and KEELING (1968) found concentrations of 0.031% over Hawaii and Antarctica between the 500 and 700 mb levels.

KAYE and LABY (1970) give the solubility of carbon dioxide in water as 1.0 ml of CO_2 per ml of water at 15°C and 1 atmosphere. Taking the concentration of atmospheric carbon dioxide as 0.03% and assuming all the CO_2 reacts with the water to form carbonic acid, this implies a typical equilibrium concentration of 5×10^{-6} Molar of carbonic acid. This value will remain nearly constant with altitude as the effects of decreasing pressure and temperature on the solubility tend to cancel out.

Unless carbon dioxide is more effective in reducing electrification than similar concentrations of other ionic species one would expect that, in the concentration found in the atmosphere, it would reduce the

electrification to about 60% of the value for purest water (IRIBARNE and MASON, 1967). The effect of dry ice in the laboratory may be more serious, because only a 3% concentration of carbon dioxide in the air is needed to reduce the charge produced by the bursting of a 100 μm radius bubble to an insignificant level.

9.3 AN EXPERIMENT TO DETERMINE THE EFFECT OF ATMOSPHERIC CARBON DIOXIDE.

9.3.1 Experimental details

Some of the dissolved carbon dioxide was removed from deionized water by bubbling with nitrogen and allowing the water to stand in a nitrogen atmosphere. The concentration of carbon dioxide could be regulated by exposing the water to the atmosphere. This water was used to make the ice spheres, which were then melted under constant conditions in the wind tunnel. Care was taken to nucleate the water drops 4 to 5 minutes after being placed in the refrigerator, in order to reduce the amount of carbon dioxide absorbed during the cooling of the drop. The ice sphere was then melted on a platinum wire support in the wind tunnel.

9.3.2 The use of electric conductivity measurements to evaluate the CO_2 concentration.

Carbon dioxide reacts with water to produce carbonic acid, which is partly dissociated into hydrogen and bicarbonate ions, thus

$$CO_2 + H_2O \rightleftharpoons H_2CO_3 \rightleftharpoons H^+ + HCO_3^-$$

As carbonic acid is weak acid, Ostwald's dilution law (Eqn. 9.1) may be used to evaluate the variation of conductivity with concentration of acid;

$$K = \frac{L^2 C}{L_o(L_o - L)} \qquad \ldots\ldots\ldots\ldots \quad 9.1$$

where K is the ionization constant (4.5×10^{-7} g equiv l^{-1} at 25°C) C is the concentration of carbonic acid, L_o the equivalent conductance at infinite dilution and L the equivalent conductance at concentration C. Equivalent conductance is defined as the conductance of a solution containing one gm equivalent of solute when measured between parallel electrodes which are 1 cm apart and large enough in area to contain the

Fig.9 1 The effect of dissolved CO_2 on conductivity deionized water

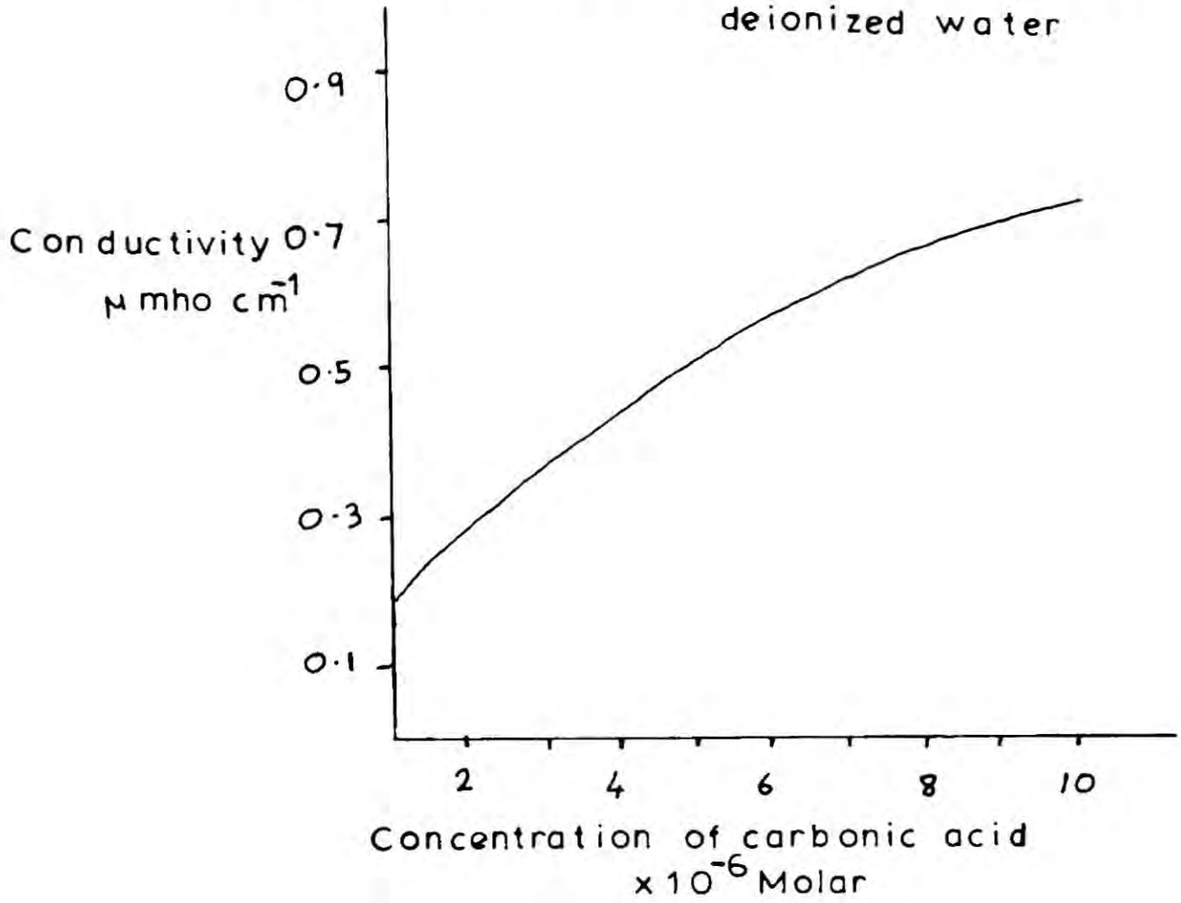

Fig.9·2 Charge on the meltwater of 4mm diameter ice spheres made from water with different CO_2 levels

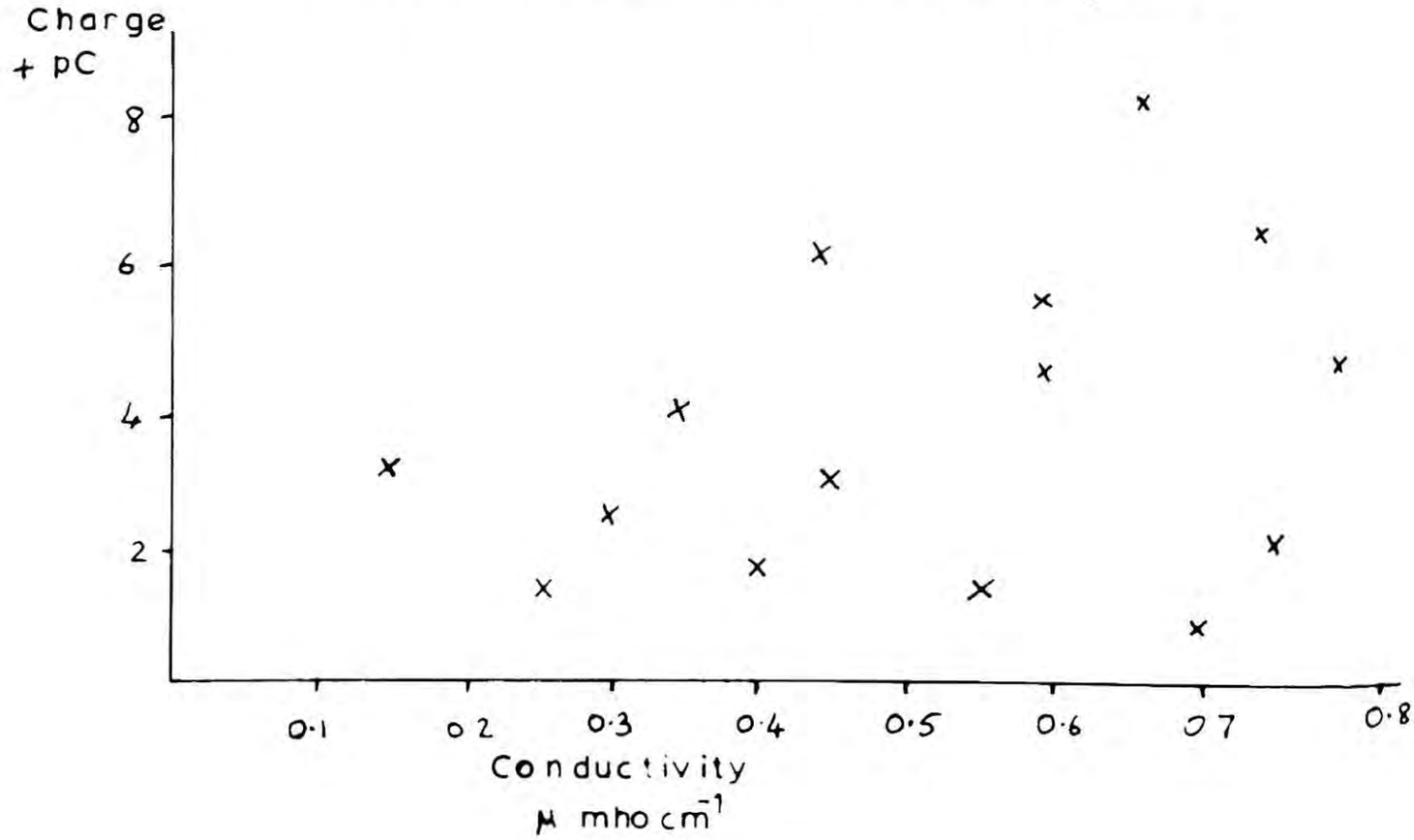

the necessary volume of solution.

By rewriting the Ostwald dilution law and substituting the value for L_o of 395 μmho cm^2 gm $equiv^{-1}$ quoted by MACINNES (1961);

$$L = -\frac{9 \times 10^{-5}}{C} \pm \sqrt{\frac{8 \times 10^{-9}}{C^2} + \frac{7 \times 10^{-2}}{C}} \quad \ldots\ldots 9.2$$

The specific conductivity can be obtained by multiplying the equivalent conductance by the concentration, enabling the variation of the conductivity of the solution of carbonic acid to be plotted against concentration (fig. 9.1). When nitrogen was bubbled through the deionized water samples to remove the CO_2, the conductivity fell from 0.75 μmho cm^{-1} to a minimum of 0.15 μmho cm^{-1} which implies that the conductivity due to carbon dioxide in equilibrium with the water was 0.6μ mho gm^{-1}. From fig. 9.1, the concentration of carbonic acid was 6×10^{-6} N which agrees with that calculated in section 9.2.2 caused by a 0.03% concentration of CO_2 in the atmosphere.

9.3.3 The effect of CO_2 concentrations on melting electrification.

The frozen water drops were made from water which contained from 7×10^{-6} M to less than 10^{-6}M carbonic acid. The actual value of the lower limit of the carbonic acid concentration could not be determined because the concentration of metal and non metal ions was not known. The icewas melted slowly, the 4 mm spheres taking about 8 minutes to melt.

The charge carried by the meltwater for water of different concentrations of carbon dioxide is plotted in fig. 9.2. There is little significant variation of the charging with carbon dioxide concentration. These results may be compared with earlier measurements made with water drops which had stood for about an hour before freezing and were therefore in equilibrium with atmospheric CO_2 (Table 9.1). The estimates of CO_2 concentration were derived by the method outlined in section 9.4.1.

TABLE 9.1 Effect of CO_2 concentration on melting electrification.

Percentage of the concentration of CO_2 present in equilibrium with water at +15°C	Charge pC	Number of drops
160	3.0 ± .8	7
180	4.0 ± 1.0	8
260	4.9 ± 1.0	17

Table 9.1 suggests that there is no significant difference between the charging produced by any of the 3 sets of melting ice spheres. However, if carbon dioxide does have an important effect on melting electrification these results could be explained by carbon dioxide being absorbed by a water drop during the melting process (cf section 9.4.2).

9.4 THE ABSORPTION OF CARBON DIOXIDE BY A WATER DROP

9.4.1 Absorption by a stationary drop.

A review paper by LEWIS and WHITMAN (1924) shows that the chief cause of resistance of a water drop to absorbing gaseous CO_2 is a thin film of liquid at the surface of the drop. Inside this film, which is typically 3 μm thick (WHITMAN, LONG and WANG 1926), the limiting factor is the diffusion of CO_2 through a relatively high concentration of carbon dioxide solution. The rate of mixing inside the drop only limits the absorption process by ~~reducing~~ increasing the concentration gradient across the surface film. By applying the theory of the diffusion of gases through a film of stagnant liquid (Appendix 2), the fraction f of the final equilibrium amount of CO_2 absorbed in a water drop can be derived.

For a 4 mm diameter drop for $t < 100$ s

$$f = \sum_{n=1}^{n=\infty} -2\left(\frac{-3}{r}\right)^n \left(\frac{D}{\pi}\right)^{n/2} t^{n/2} \quad \ldots\ldots\ldots 9.3$$

and for $t > 100$ s

$$f = 1 - 0.44 \exp -\left[\left(\frac{3k_{100}}{r}\right)(t-100)\right] \quad \ldots\ldots\ldots 9.4$$

Fig.9.3 The absorption of CO_2 by a 4mm water drop in still air

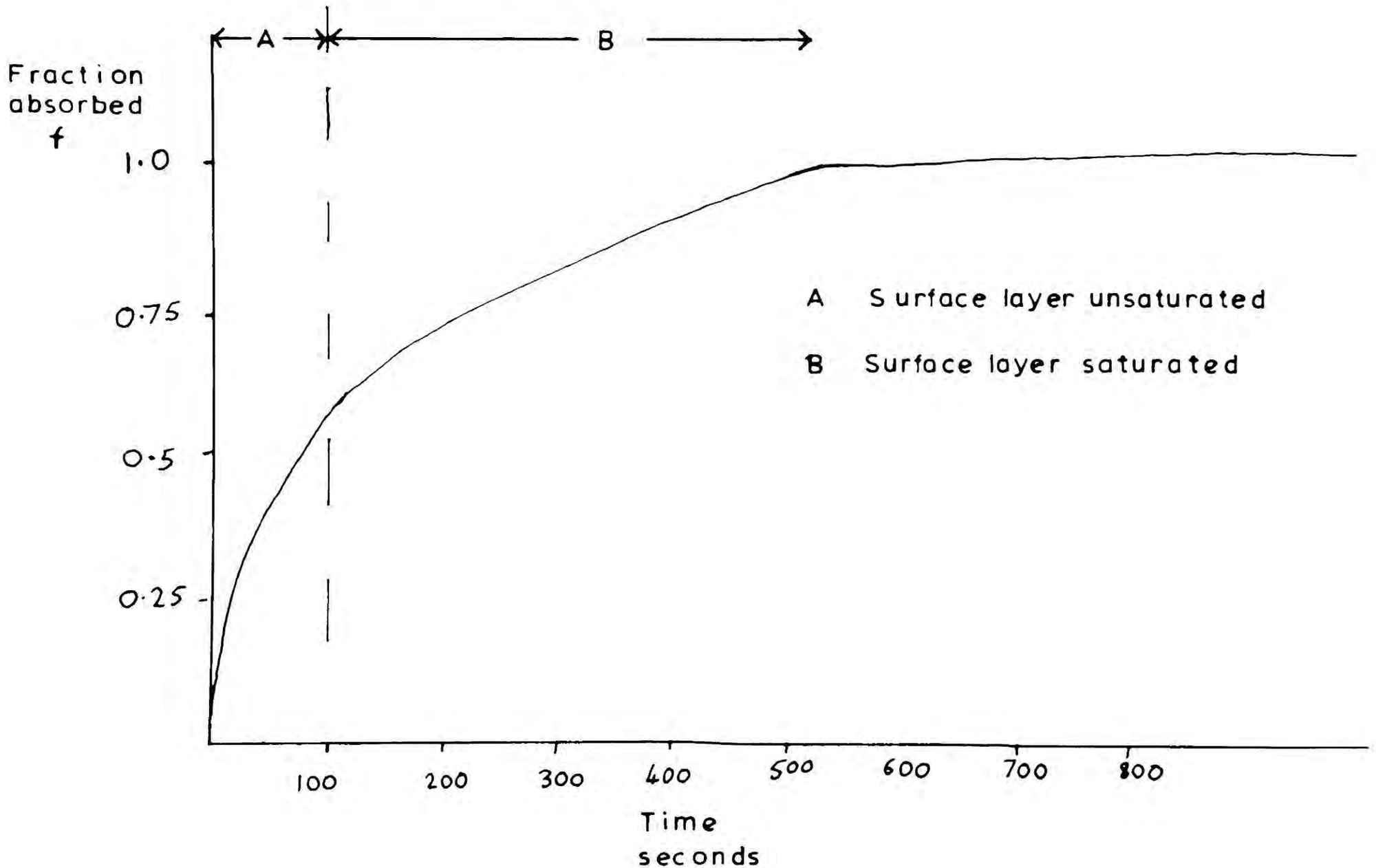

where the permeability coefficient $k_{100} = 2.8 \times 10^{-6}$ ms^{-1}, t is the time after the start of absorption and D is the diffusion coefficient.

The two equations 9.3 and 9.4 describe different stages in the absorption of gas. In the first stage, the permeability of the surface layer decreases as the CO_2 level rises, and in the second the layer is saturated with CO_2 and the permeability remains constant. These results are plotted in fig. 9.3, which shows that after 2.5 min the drop has absorbed 66% of its equilibrium value of CO_2, and after 7 min 90% of the CO_2 has been absorbed.

9.4.2. Absorption by a falling drop.

Much of the experimental work on absorption by water drops has been carried out on falling drops e.g. by GARNER and LANE (1959), LEWIS and WHITMAN (1924) and LEWIS et al. (1926). A typical value for the time taken for 90% absorption for a falling 4 mm diameter drop is 5 seconds (GARNER and LANE (1959). This is two orders of magnitude less than for a drop in stagnant air and is due to the presence of convection and the disturbed nature of the surface film in a falling drop.

9.5 CARBON DIOXIDE LEVELS IN PREVIOUS LABORATORY EXPERIMENTS

9.5.1 The Dinger-Gunn experiment.

If the rate of absorption of CO_2 is greatly enhanced by placing a water drop in a stream of the gas, the rate of desorption of CO_2 will also be increased in a ventilated atmosphere. The rate of desorption in the Dinger-Gunn experiment (section 2.1) may be estimated by considering a rectangular shaped volume of water, of depth d and surface area A, placed in a cubic container so that only the area A has access to the air. It seems likely that, because the water was sheltered from the fan by the sides of the small container, the surface film was not disturbed, and the CO_2 was transferred across the surface by molecular diffusion. From Appendix 2.2 the value of f is given by

$$f = 1 - e^{-kt/d} \qquad \text{.....9.5}$$

If we assume that the surface film is saturated with CO_2, then k = 2.8 x 10^{-6} $m^2 s^{-1}$. In this experiment the depth of ice was about 10 mm, so if one considers a layer of water 1 mm thick on the surface of the ice then, according to equation 9.5, the time constant d/k will be about 400 seconds. As the total time for all the ice to melt was of the order of 100 seconds it is suggested that the meltwater did contain approximately the same amount of CO_2 as the original water from which the ice was made. This experiment would therefore measure the effect of CO_2 on melting electrification.

9.5.2 The experiment of DRAKE.

The time constant for the absorption and therefore also desorption of CO_2 by a falling drop is less than 5 s, which is over a factor of 10 less than the melting time. So seems probable that the meltwater surrounding the bursting bubbles in DRAKE's experiment contained very little CO_2, even though the ice was made from water with a high CO_2 content. The rate of loss f of CO_2 from a small air bubble after release from the ice can be estimated (Appendix 2.3) using the film theory of gas absorption;

$$f = \exp\left(-\frac{6}{r}\sqrt{\left(\frac{D}{\pi}\right)t}\right) \quad \ldots\ldots\ldots\ldots \quad 9.7$$

where r is the radius of the bubble and D = 2 x $10^{-9} m^2 s^{-1}$.

For a typical 20μm bubble, 99% of the CO_2 is lost in the first 0.8 s after water comes in contact with the bubble. This suggests that the concentration of CO_2 in the meltwater will govern the CO_2 content of the double layer at the surface of the bubble on bursting, rather than the initial gas content of the bubble. As the meltwater loses most of its CO_2 in seconds, the concentration of CO_2 in the partly molten drop is probably very close to that due to the melting environment, and is not dependent on the freezing environment.

9.6 CONCLUSION

It is suggested that the reason for the failure of DRAKE to find that CO_2 inhibits melting electrification may be due to the absence of CO_2 in the meltwater of his samples. The apparatus of DINGER and GUNN would

measure the effect of CO_2. The MATTHEWS and MASON null results were obtained with ice in bulk form, where any CO_2 introduced during the formation of the ice would not easily leak away during melting. In order to confirm this theory, ice spheres should be melted in an atmosphere of CO_2 when, according to the double layer theory of melting electrification, the charging should be reduced. It is hoped to carry out this experiment at Durham shortly.

C H A P T E R 10

THE ELECTRICAL EFFECTS OF THE MELTING OF REAL PRECIPITATION

10.1 THE LOCATION OF THE LOWER POSITIVE CHARGE

10.1.1 The location deduced from laboratory experiments.

The way in which real ice particles melt while falling from the 0°C level in convective clouds is similar to the behaviour of the melting ice particles in the wind tunnel. In both cases the temperature rises during the course of melting although the temperature of the air in the wind tunnel increases more slowly during the first minute of melting. Typically 40% of the ice is melted in the last minute of melting in the tunnel compared to 50% as calculated by MASON (1956) for a 4 mm solid ice sphere falling in a saturated atmosphere from the 0°C level.

In the laboratory between 50 and 90% of all the charge was separated during the last minute of melting when the average melting rate ranged from 7 to 18 mg min^{-1}. As MASON calculated this average value to be 14 mg min^{-1} for a 4 mm particle melting in a cloud, it seems that most of the charge separation on such a particle occurs during the last minute of melting Certainly the laboratory results show that the amount of charging during the first minute of melting is likely to be negligible (cf. fig. 7.9).

For a 4 mm solid ice particle MASON estimated that the last 50% of the mass melted below the $+6\frac{1}{2}$°C level or 1km below the 0°C level. One might therefore expect the centre of charge separation to lie at about + 8°C and 1.2 km below the 0°C level. The smaller the melting particle, the higher in the cloud it will melt, so 2 mm particle will have half melted by 450 m below the 0°C level. However small ice particles which melt higher in the cloud will melt at a lower rate due to the cooler environment, so they may contribute less to the cloud electrification. Graupel will also melt higher in the cloud; according to MASON a 3 mm diameter graupel pellet of specific gravity 0.3 will lose the last 50% of its mass between 300 and 600 m below the 0°C level. Clearly the location of the charged

Fig.10·1 The location of the lower positive charge

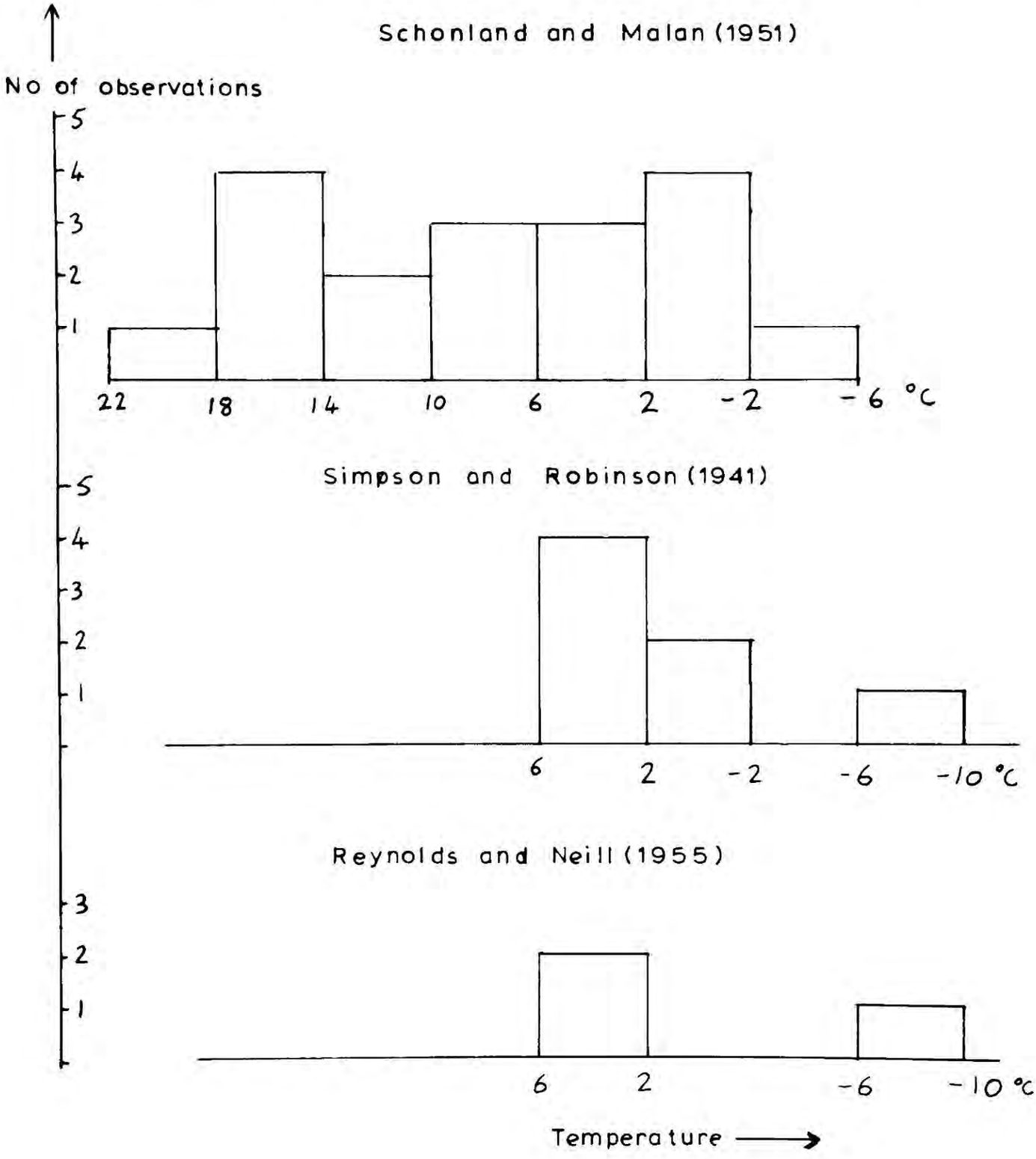

ALSO

Kuettner (1950) 12 out of 50 higher than +2°C level

Clarence and Malan (1957) 40 observations average +8°C

region caused by melting precipitation depends very much on the size and density of the ice particles.

10.1.2 The effect of the downdraught.

If the melting particles are falling in a downdraught which may be up to 10 ms^{-1} (BYERS and BRAHAM, 1953) then the position of the charged region produced by the melting ice may be lower than if the particles melted in the updraught. In the downdraught the negatively charged droplets will be carried down below the 0°C level and will tend to neutralize the positive charge on the melting precipitation. The speeds of the downdraught measured by BYERS and BRAHAM were in the range 5 to 10 ms^{-1} which is of the same magnitude as the fallspeeds of particles of 2 to 5 mm diameter, so this effect may well be important. If the downdraught is inclined to the vertical the melting precipitation may fall clear either into the updraught or into a relatively motionless part of the cloud.

10.1.3 The measured location of the lower positive charge.

A summary of some experiments in locating the lower positive charge in thunderclouds is outlined in Table 1.3. The mean temperatures at which the charge was found varied from -3 to +8°C. A direct comparison of these results is difficult because of the different methods of measurement and because the variation of temperature with altitude was usually inferred from distant radiosonde measurements and an estimate of the height of cloud base. These temperature measurements are likely to be about 2°C too high according to BYERS and BRAHAM (1949) if the charge region is located in the downdraught and 2°C too low if in the updraught. Fig. 10.1 shows the distribution of locations of the charge found by 3 observers who published individual as well as mean values. The results of SCHONLAND and MALAN (1951) point towards a charge distribution which can occur at any level near and below the 0°C level and perhaps is best explained by rising point discharge ions caught in the updraught (MALAN (1952).) The results of REYNOLDS and NEILL (1955) certainly do not justify placing the mean location of the charge at -3°C as in Table 1.3. KUETTNER (1950) has provided

perhaps the most reliable estimate of the position of the charge by studying the sign of the potential gradient in the centre of precipitation or lightning activity in thunderclouds on the Zugspitze. On 50 occasions the charge was located above the +8°C level and on 12 above the +2°C level. It is possible that the mountain may have affected the thunderstorm but these results point to a theory of electrification that does not involve the melting of ice. CLARENCE and MALAN (1957) only quote average results for the location of the lower positive charge.

10.14 Conclusion

From the previous section it appears that it is not possible to state a location for the lower positive charge or even be sure that there is only one type of lower positive charge. It may be that the South African measurements have described a cloud of point discharge ions whereas the European and American observations have described a charge carried by the precipitation. Clearly it is not possible to say that the measured location of the charge precludes or supports a melting ice theory.

If melting ice is responsible then the location of the charge will depend on the mean density and diameter of the melting particles. The motion of the air in the region of the precipitation may also be important and the mechanism should be more active at the edge of the downdraught or in the updraught. This location agrees with the position of the lower positive charge deduced by WILLIAMS (1958) from a study of lightning flashes to ground.

10.2 SOLID PRECIPITATION IN THUNDERSTORMS

10.2.1 Classification of solid precipitation.

There is some confusion in the literature concerning the classification of solid precipitation and in particular the word graupel. The Japanese e.g. NAKAYA and TERADA (1935), describe graupel as having a mean specific gravity of 0.13 agreeing with the American ARENBERG (1941) who gives a value of 0.2 WEICKMANN (1953) and KEUTTNER (1950) refer to graupel as having a specific gravity of about 0.6 and LIST (1965) suggests an

upper value of 0.8. As LIST's studies of the structure of ice particles were a main part of his work his classification will be used in this thesis.

Snow pellets These are light and opaque either roughly conical or spherical particles of specific gravity 0.1 to 0.3. They are formed according to ARENBERG (1941) and NAKAYA and TERADA (1935) by the accretion of cloud droplets onto a falling snow crystal.

Graupel Graupel pellets are white and opaque and roughly spherical in shape with specific gravity up to 0.8 and diameters up to 5mm. They differ from snow pellets in having an ice framework in which a crystalline structure can be identified. WEICKMAN (1953), from his experiences on Mount Hohenpeissenberg considers that the following description of LITTLE (1940) describes them well. "All the stones (average diameter some 5 mm) examined showed a definite crystalline structure, being in the approximate form of a sector of a sphere, the angle subtended at the centre being 90°. It was not possible to identify the form of the individual crystals, but they radiated out from the apex of the stone giving a streaky appearance at the spherical face as if the stone were composed of a bundle of fibres". Graupel can either be formed on a crystal or a frozen cloud droplet.

Small hail LIST (1965) describes small hail as being semi-transparent particles of similar size to graupel but with a more rounded appearance and a specific gravity of 0.8 to 0.99. They may consist partly of liquid water and grow from graupel by the intake of water into the air capillaries of the ice framework.

Hailstones Hailstones generally have a layered construction and are larger than small hail. They may take a variety of shapes sometimes with lobes.

10.2.2. Observations of solid precipitation in thunderclouds.

There are very few observations of precipitation particles which were made in thunderclouds and the descriptions that are available were usually made as a subsidiary part of an electrical or dynamical study. The observations fall into two types, those made from mountain stations which were immersed in thunderclouds, and aircraft observations.

WEICKMANN (1953) observed that graupel was the most common form of solid precipitation in thunderclouds. KUETTNER (1950) noted that graupel was present in 60% of the thunderstorms on the Zugspitze, small hail in 20%, liquid precipitation in 20% and hail in only 10% of the storms. Snow was present in 70% of the storms. KUETTNER concluded that hail was relatively rare and was by no means necessary for the production of lightning.

BYERS and BRAHAM (1953) found that snow and snow pellets were the most common form of solid precipitation above the 0°C level in summer thunderstorms over Ohio. However, graupel and small hail below 3 mm diameter were practically unidentifiable but in only 10% of the storms could the precipitation be classed as hail. BRAHAM (1963) found that the most common solid precipitation in convective clouds over Missouri was graupel which gave the appearance of having grown by the riming of cloud droplets. The average specific gravity of the graupel was 0.88 and all the 110 graupel pellets collected had specific gravities greater than 0.7. BRAHAM also found clear ice pellets of specific gravity 0.9 usually near the tops of updraughts.

WEICKMANN and AUFM KAMPE (1953) found that the liquid water content of cumulonimbi varies from 1 to 6 g m^{-3}. The actual value will depend on the part of the cloud studied and the temperature of cloud base and the amount of air entrained by the updraught. From the observations of KUETTNER, WEICKMANN and AUFM KAMPE and BYERS and BRAHAM it seems that the most common form of solid precipitation in thunderclouds is smaller than 5 mm diameter and can be classified as graupel or snow. The density and structure of the ice will depend on the conditions under which it is formed and may be different in thunderstorm with different cloud base heights, updraught speeds and liquid water contents.

10.2.3 The effect of growth conditions on the structure of solid precipitation

If the rate at which supercooled water drops arrive at an ice surface is greater than the rate at which the water is frozen then water will be present on the surface and the growth can be said to be wet. The transition from wet to dry growth has been studied by LUDLAM (1950)

by calculating the heat balance at the ice surface. He deduced the temperature at which the growth becomes wet for different sized particles in clouds with bases at 10 and 20°C. 4 mm diameter ice spheres will grow in the dry phase at heights above the -10°C level in both clouds while particles of 10 mm diameter can grow by wet growth up to the -25°C level. It seems unlikely that a particle of 4 mm diameter will have grown by wet growth in a cumulonimbus provided that the growth did not start on top of a frozen water droplet. One might expect a particle of less than 4 mm to have a liquid layer if it was surrounded by enough cloud droplets as it fell towards the 0°C level.

10.2.4 Air bubbles in natural solid precipitation.

Air bubbles can either be formed by the release of dissolved air at an advancing ice-water interface or can originate in the spaces between individual cloud droplets which froze on impact with the growing particle.

Wet growth The rate of advance of the ice is governed by the rate of loss of heat to the environment. For a 4 mm diameter particle falling at terminal speed at -10°C the heat loss as computed from equation 8.1 is approximately 170 mW, corresponding to a rate of advance of the ice sheet of 2.4 mm min^{-1}. CARTE (1961) found that this rate of freezing produced bubbles of about 80 μm diameter. At -20°C the mean bubble diameter would be about 50 μm. As the air would be free to escape from the surface the concentration of air bubbles may be greatly reduced.

Dry growth. The air bubbles released by the freezing of individual supercooled cloud droplets are likely to be a few μm as typical cloud droplets in cumulonimbus clouds have diameters in the range 20 to 40 μm. (WEICKMANN, 1953). A more important source of trapped air bubbles is probably the gaps between adjacent frozen droplets. MACKLIN (1962) explains the formation of rime of specific gravity less than 0.5 as being due to different degrees of close packing of frozen water droplets. BROWNSCOMBE and HALLETT (1967) suggest that the increasing densities of rime of specific gravity greater than about 0.6 can be explained by the

increasing deformation of the cloud droplets on impact. Lighter rime will be formed when the droplets freeze before they have had time to spread out over the surface.

The air bubbles trapped in rime of specific gravity less than 0.6 will probably be in the diameter range 2 to 200 μm assuming a range of cloud droplet diameters of 5 to 40 μm. At very low densities the gaps between frozen droplets will tend to be interconnected. Ice of higher density probably contains smaller air bubbles trapped between the frozen droplets due to the effect of deformation on the droplets. As the freezing rate will be less the bubbles trapped inside the droplets may become larger and as the growth becomes more like wet growth the bubble size will increase as adjacent droplets coalesce before freezing.

10.3 MELTING ICE AND THE MAGNITUDE OF THE LOWER POSITIVE CHARGE.

The charge separated by melting ice has been shown to depend on the size of the air bubbles, the melting rate and the purity of the ice. All these properties would be expected to have a range of values for different thunderstorms. A figure for the magnitude of charge that can be produced by melting ice under perfect conditions can however be obtained.

10.3.1 Electrification under ideal circumstances.

We will assume that the ice present in the thundercloud contains a large number of bubbles smaller than 50 μm diameter and has been formed at high enough freezing rates to eliminate an appreciable loss of air during freezing. The range of concentrations of impurities in cloudwater has been estimated in chapter 5 as 2 to 20 mg l^{-1}. Certainly the level cannot be less than that due to an equilibrium concentration of atmospheric carbon dioxide. Ice made from water in equilibrium with atmospheric carbon dioxide and containing an additional ionic impurity concentration of no more than 0.2 mg l^{-1} was found to produce 0.8 pC mg^{-1} of electrification at the maximum melting rates likely to be found in the atmosphere (fig 8.7). This corresponds to a charge density of 0.8 C km^{-3} if the melting precipitation is present in a concentration of 1 gm^{-3}. In precipitation of 5 gm^{-3} this corresponds to

4 C km^{-3}. SIMPSON and ROBINSON (1941) estimated that the lower positive charge of -4 C could be considered as being located in a region 500 m in radius. This corresponds to a charge density of 8 C km^{-3}.

DRAKE (1968) found that the charge separated by melting a 10^{-4} Molar sodium chloride solution (5.8 mg l^{-1}) at high melting rates was 0.4 p C mg^{-1} which would produce a charge density of 0.4 C km^{-3} for a concentration of melting precipitation of 1 gm^{-3} and 2 C km^{-3} for 5 g m^{-3}. This value of purity of the water is probably realistic especially as the measurements made by SIMPSON and ROBINSON were made at Kew which was not an area of low pollution.

TABLE 10.1 Maximum charge densities due to melting ice as predicted by laboratory experiments

Concentration of ionic impurities	concentration of melting precipitation	Charge Density
10^{-5} M (0.6 mg l^{-1})	1 g m^{-3}	0.8 C km^{-3}
" "	5 g m^{-3}	4.0 C km^{-3}
10^{-4} M (6 mg l^{-1})	1 gm^{-3}	0.4 C km^{-3}
	5 g m^{-3}	2.0 C km^{-3}
SIMPSON and ROBINSON (1941)		8 C km^{-3}

10.3.2 The effect of the nature of the precipitation.

As has been discussed in section 8.1 the density of a solid precipitation particle affects the melting rate of the ice as denser particles fall faster and reach warmer levels before finally melting.. Smaller particles also melt slower for the same reason. There will be a limiting density and size below which the melting rate is insufficient to sustain the enhanced electrification associated with vigorous convection in the meltwater. Such particles will produce an order of magnitude less charge separation than particles with higher melting rates and will not contribute significantly to the lower positive charge. DRAKE (1968) suggests a minimum diameter of 1 mm for frozen water drops as these will melt after falling 500 m from the 0°C level according to DRAKE and MASON (1966).

Fig.10·2 The effect of water purity on melting ice electrification in clouds

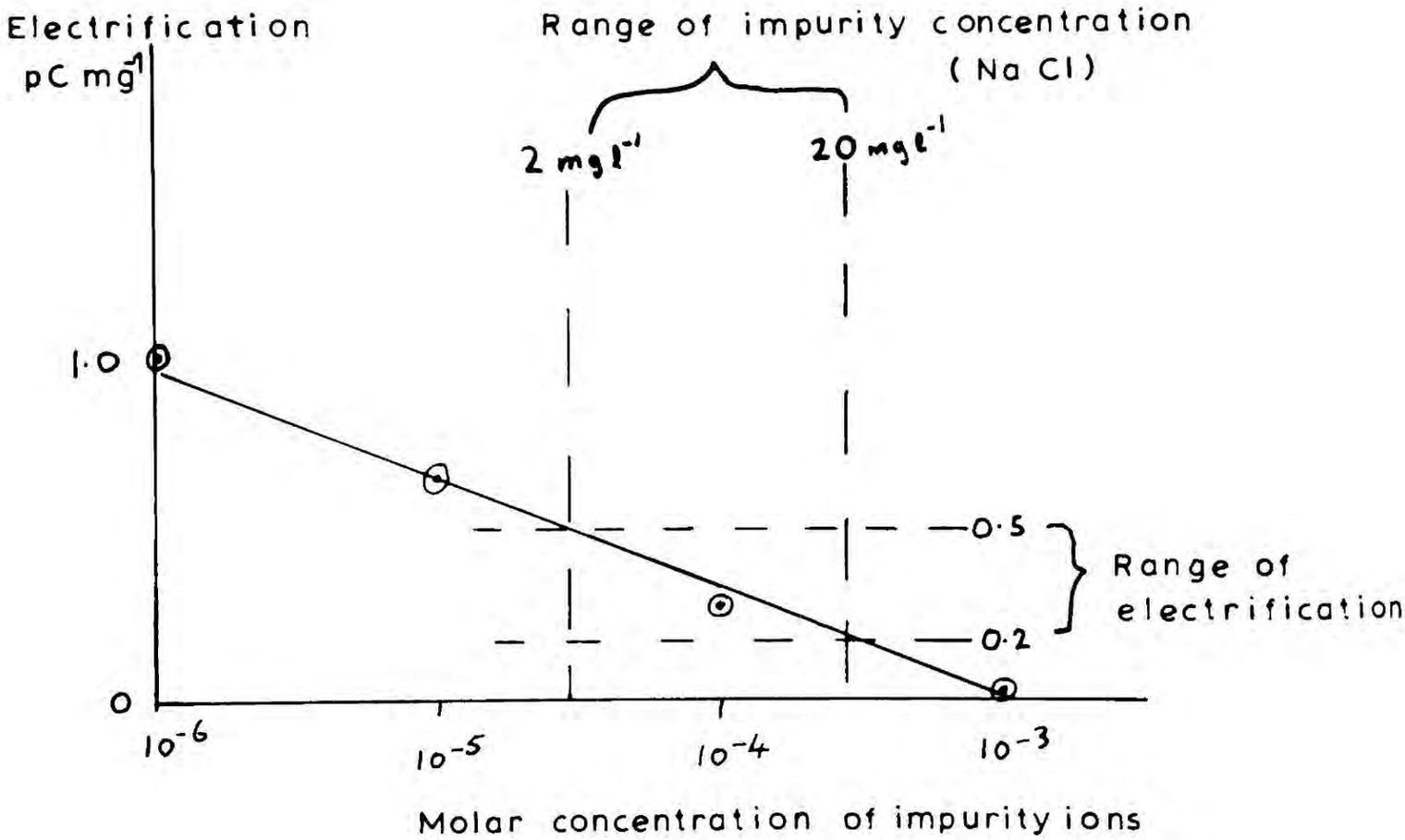

DATA Drake(1968)

Particles frozen in airstream
Convection in meltwater

MASON (1956) has calculated that 3 mm diameter particles of specific gravity 0.3 will melt in a similar distance. Snowflakes have fall speeds less than 1 ms^{-1} and are unlikely to melt at a high enough rate to charge significantly by this process.

Hail and small hail which are often made of clear or milky ice with most of the air trapped in bubbles larger than 50 μm diameter are on the basis of the work described in chapter 8, unlikely to contribute significantly to the charging process. Opaque ice containing many bubbles smaller than 40μm diamter would however be expected to produce electrification up to 0.4 pC mg^{-1} if made of water with an impurity concentration of about 5 mg l^{-1}. In chapter 5 an estimate for the range of impurity concentrations in thunderclouds was given as 2 to 20 mg l^{-1}. Under the ideal conditions discussed in section 10.3.1 this corresponds to a range in electrification of 0.2 to 0.5 pC mg^{-1} (fig. 10.2) The observations described in chapter 8 confirm the magnitude of charging observed by DRAKE for water of impurity concentration 10^{-5} M.

10.3.3 The effect of the electric field due to the negative charge centre.

MATTHEWS and MASON (1964) observed that water drops shattering in an electric field can produce as much as a factor of 100 more charge separation in an electric field than in the absence of the field. The fields used were about 3×10^{4} V m^{-1} which is appreciably less than the expected breakdown field in thunderclouds.

BLANCHARD (1963) studied the electrification produced by bursting bubbles in an electric field. The charge on the jet drops from a 200μm diameter bubble could be reversed by a field of about 3×10^{3} V m^{-1} for a 10^{-4} M sodium chloride solution. However, from the theory of IRIBARNE and MASON (1967) and the conclusions reached in chapter 8 it seems unlikely that 200 μm bubbles will play an important part in melting electrification for water of this purity. As BLANCHARD observed that the induction charging fell off rapidly with decreasing jet drop size and hence bubble diameter, this mechanism will not be so effective in altering the charge separated by bubbles of about 20 μm diameter in cloud water.

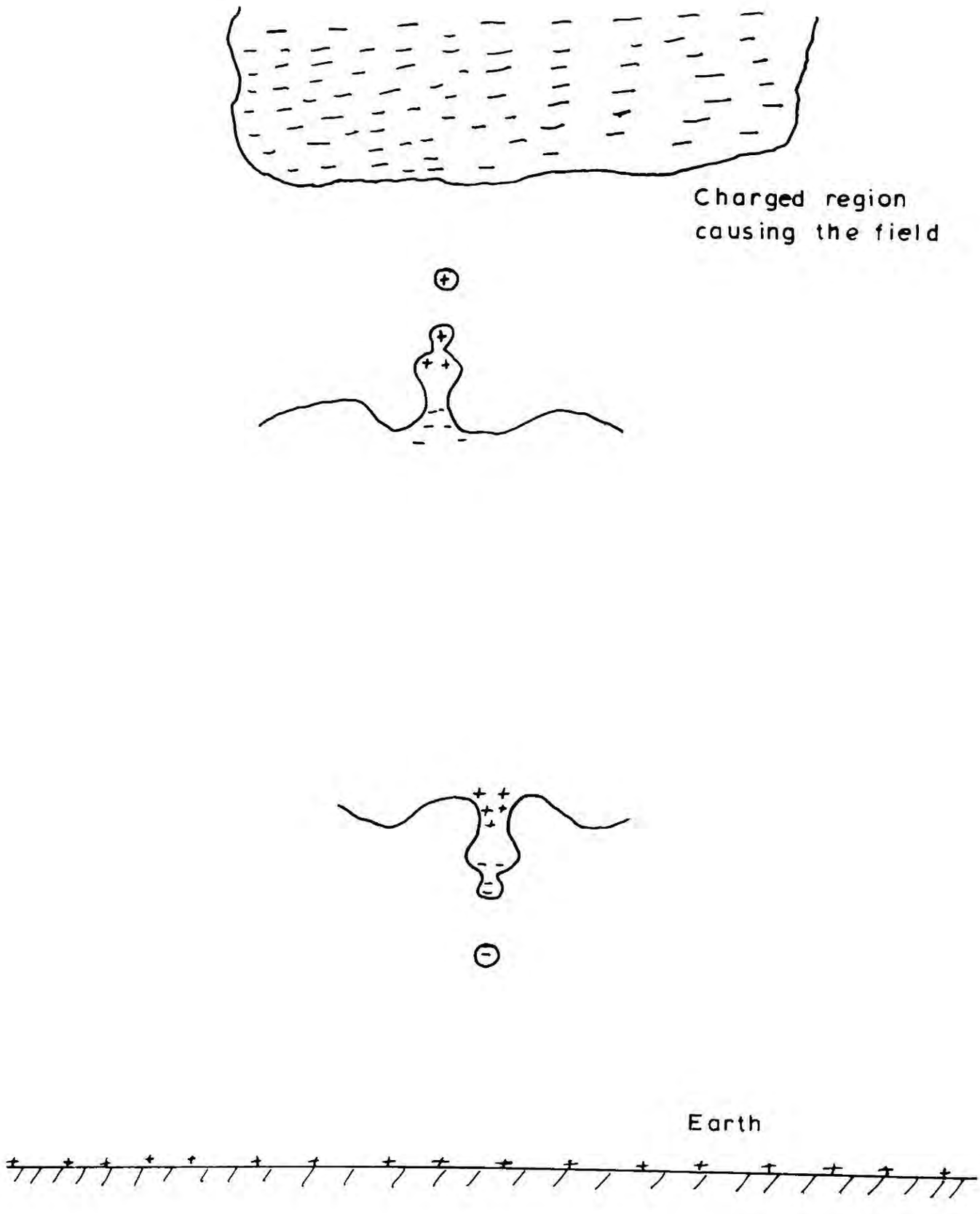

Fig.10·3 Schematic view of the effect of orientation of the bubble on an induction charging mechanism

An induction mechanism would also be influenced by the way in which the bursting bubbles were distributed over the surface of the melting particle (Fig. 10.3). If the bubbles burst at all points on the surface with equal frequency, then an induction mechanism would be ineffective as the sign of charge produced at the bottom of a melting particle would be opposite to that obtained at the top. DRAKE and MASON (1966) have observed that air bubbles of less than 100 μm diameter tended to go to the bottom of melting ice spheres whereas larger bubbles generally went to the top. If the field in the region of the melting hail were due to the negative charge centre above, then the induction charging would then increase the melting electrification by giving the ejected jet drops from the small bubbles more negative charge. The magnitude of this effect is unknown for bubbles less than 100μm diamter.

CHAPTER 11

THE ELECTRIFICATION OF EVAPORATING ICE SPHERES

11.1 PREVIOUS WORK

LATHAM and MASON (1961) have shown that ice possesses a thermoelectric property which causes the warmer end of a piece of ice to be negatively charged. When an ice specimen evaporates, its surface temperature is usually lower than the interior and one would expect the surface to acquire a positive charge. As this surface is lost by evaporation the remaining ice should acquire a net negative charge.

LATHAM and STOW (1965) evaporated an ice shell surrounding a copper sphere and found a good qualitative agreement with the predictions of the Latham and Mason temperature gradient theory. In a later paper LATHAM and STOW (1966) showed that the probability of a charged molecule leaving the ice surface was 10^{-57} times less than for an uncharged molecule. The charging attributed to evaporation could be explained if the charged molecule left the surface in the centre of a cluster of about 1000 neutral molecules.

CROSS and SPEARE (1969) monitored the electric charging of a polycrystalline ice specimen due to evaporation in vacuo and showed the electrification to be negligible compared to that found by LATHAM and STOW (1965). The largest current recorded was -0.0011 fA mm^{-2} with an evaporation rate of 45 $\mu g s^{-1}$ and a temperature gradient in the surface of 0.3°C mm^{-1}. The mean value of current for evaporation rates between 35 and 70 $\mu g s^{-1}$ and temperature gradients of 0.3 to 0.6°C mm^{-1} was - 0.004 fA mm^{-2}. For an evaporation rate of 54 $\mu g s^{-1}$ the results of the Latham and Stow experiment predict a charging current of - 38 fA for the sample used by Cross and Speare (3.5×10^3 mm^2). The largest current observed by Cross and Speare at this evaporation rate was -7 fA and the mean value -2.7 fA.

Cross and Speare also found that polycrystalline ice evaporating in vacuo is characterized by the development of a fibrous or whiskery surface. They suggest that the presence of an airstream will fracture these whiskers

Fig.11·1 Electrification of evaporating ice spheres

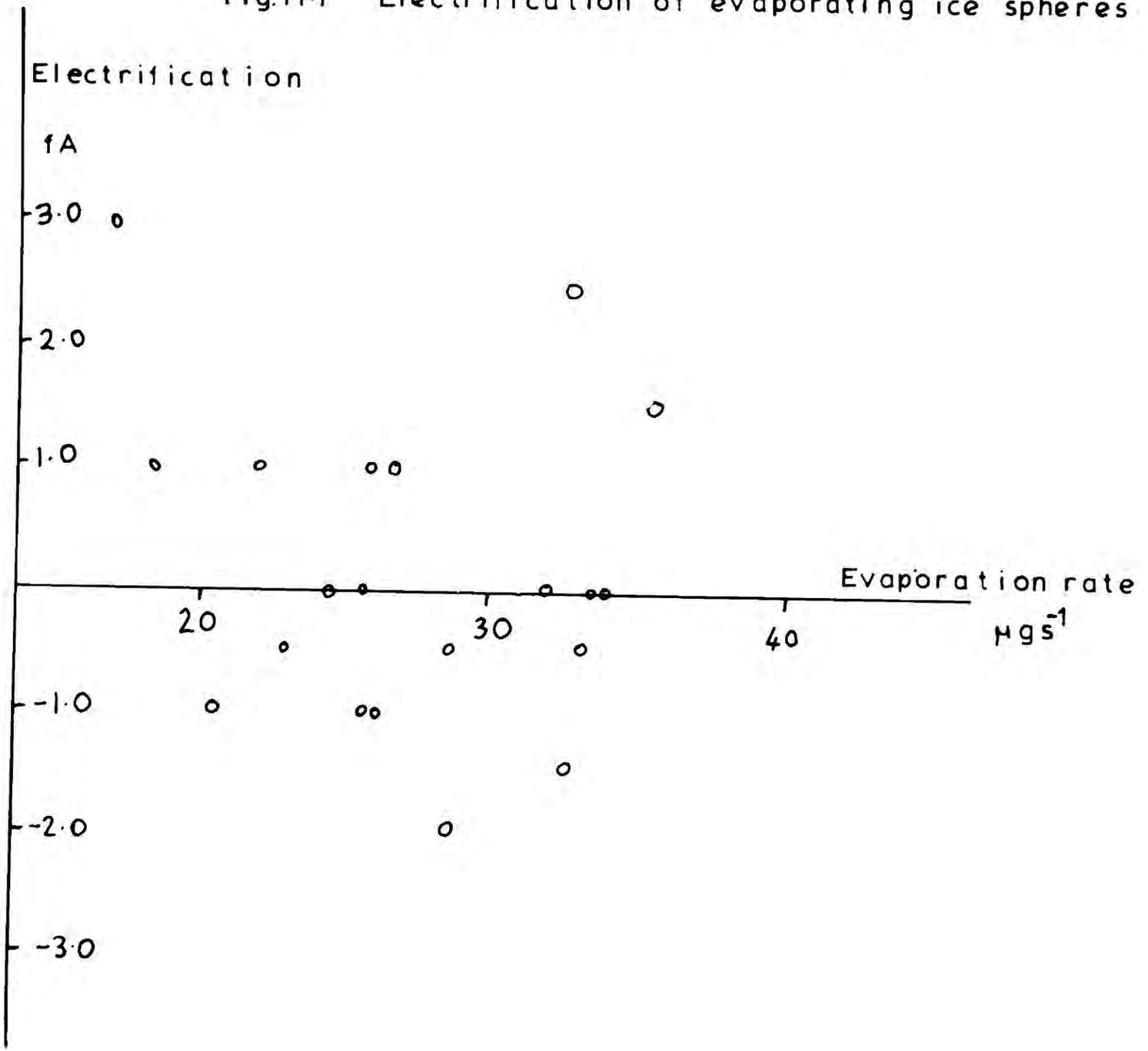

and cause them to be carried away. They also suggest that these fragments will be charged by a temperature gradient mechanism in a similar way to that proposed by LATHAM (1963) for the electrification of frost deposits.

11.2 THE ELECTRIFICATION OF ICE PARTICLES EVAPORATING IN THE WIND TUNNEL

Ice spheres of about 4 mm diameter were frozen onto 120 μm platinum wires and allowed to evaporate in the wind tunnel. The ice was made from artificial cloudwater of sodium chloride content 4.5 mg l^{-1}. The dry bulb temperature of the air was about 0°C and the relative humidity ranged from 50 to 70%. The wet bulb depression was sufficient to prevent the ice melting. The values of electrification described in fig. 11.1 are averages over a 2 min period of the current output from the V.R.E. which was used with a $10^{12}\Omega$ input resistor. The maximum average current was + 3 fA and themean + 0.1 fA. The average rate of evaporation was computed by equation 8.5 to be 27 μg s^{-1} corresponding to a rate of heat loss of 68 mW. As the surface area of the ice spheres was about 50 mm^2, the maximum current density corresponds to + 0.06 fA mm^{-2} and the mean to + 0.002 fA mm^{-2}. These values are of the same order as the background currents with no ice present in the working section of the tunnel. No correlation is apparent between rate of evaporation and the V.R.E. reading.

11.3 INTERPRETATION OF THE WIND TUNNEL EXPERIMENT

The wind tunnel experiment has enabled the electrification of simulated solid precipitation particles to be studied in conditions which are probably similar to the environment of evaporating graupel and small hail in the a atmosphere. The amount of charging is clearly of little importance in cloud electrification, as even at the maximum charging rate the particle would take 50 min to attain a charge equivalent to that due to its melting (0.3 pC mg^{-1} or 1 esu g^{-1}).

The values of the temperature gradients expected are likely to be considerably less than the 9°C mm^{-1} value estimated by LATHAM and STOW (1965) for the ice shell on the copper sphere used in their experiments.

MASON (1956) has calculated the thermal relaxation time of a 4mm diameter ice sphere falling at terminal speed to be 7s. It seems likely that such a precipitation particle would soon reach a constant temperature while evaporating in an isothermal atmosphere. If the evaporating particle is falling in a real atmosphere where the temperature increases as the particle falls, the outer surface will be warmer than the centre. If the particle is falling at 7 ms^{-1} through an atmosphere with the dry adiabatic lapse rate of 10°C km^{-1} the increase in temperature of the environment during a period equal to the relaxation time of the particle will be 0.5°C. Assuming this is the temperature difference between the centre and the surface of a 4 mm diameter particle, the mean temperature gradient will be approximately 0.25°C mm^{-1} or a factor of 30 less than in the Latham and Stow experiment.

One would also expect the sign of the charge separation to be opposite to that found by Latham and Stow and the evaporating particle to become positively charged. A temperature gradient should also develop in the whiskers of ice formed during the evaporation, due to a greater evaporation rate occurring at the tips of the whiskers than near the surface of the particle. This gradient would be of the same sign as in the Latham and Stow experiment.

It is suggested that the one reason for the low level of charging produced by the evaporation of the small ice spheres was the low temperature gradients in the ice samples. This condition is likely to be found in the evaporation of particles smaller than 10 mm diameter in the real atmosphere. While it is not know whether whiskers did develop on the surface during evaporation, if they did form, then presumably the temperature gradients in them were insufficient to produce a measureable electrification.

CHAPTER 12

CONCLUSIONS AND SUGGESTIONS FOR FURTHER WORK

12.1 THE DESIGN OF A WIND TUNNEL TO STUDY THE ELECTRIFICATION OF PRECIPITATION

The design of the wind tunnel which supported small ice spheres has enabled some of the problems associated with this type of research to be studied. The design of a windtunnel which will support both solid and liquid particles is clearly more difficult than a system which will support only water drops, as the way in which these particles react to pressure gradients and shear forces is different. As no small wind tunnel appears to have been designed which will support a particle throughout its melting period, the additional constraints to design caused by the need to measure small electric currents and to keep the particles very clean make the design of such a tunnel even more difficult.

Even with a wind tunnel working section as small as 40 mm diameter the rate of flow of air was so great that the air in the cold room of volume $4m^3$ was heated to about $2^{o}C$ after a melting run lasting 10 min. This limited the rate of performing experiments to one every 3 hours, as the cold room temperature had to be restored to below freezing. Stringent precautions to avoid contamination also slow down the experimentation and some results were rejected because of possible contamination. In the present work, on average only 2 experiments per day gave useable results. These problems would arise with almost any system of supporting ice particles in a tunnel. Another problem associated with the high flow rate of air is the difficulty in regulating the relative humidity if the air is heated considerably to enable the ice particles to melt. The humidification of air flowing at the rate of 10 l s^{-1} was found to require more sophisticated equipment than a heated tray of water. Probably the best method would be to use a commerical humidifying unit. Clearly, trying to attain realistic conditions by flying or supporting particles in a relatively laminar

flow environment does severely limit the versatility of the apparatus and the conclusions that can be drawn from such experiments. The difficulty of measuring the mass of irregular ice particles, which also had to be kept very clean, introduced an error of about 30% into the final value of the charge to mass ratio. This error necessitates a large number of experiments to deduce the effect of environmental conditions on the melting electrification. Furthermore the slow rate of experimentation with a large wind tunnel can be a great hindrance to getting meaningful results in the time available. It may well be that these disadvantages of a large tunnel capable of freely flying a melting particle make such a system of less use than the more simple and versatile system used by DRAKE (1968).

12.2 THE ELECTRIFICATION OF MELTING ICE

The electrification of melting ice has been shown to be highly dependent on the rate at which the ice was formed initially. Water drops frozen in still air were found to produce an order of magnitude less charging on melting than drops frozen in an airstream flowing at 11 ms^{-1}. The distribution and sizes of the bubbles were found to be different for the drops frozen in moving and still air. It appeared that at low freezing rates less air was trapped because the air could escape whilst the ice shell was still thin. Ice frozen in the airstream below about $-8^{o}C$ contained no air bubbles greater than 50 μm diamter, whereas if the ice were formed in still air the largest bubbles were usually from 100 to 200 μm in diameter. The observations that a large number of small bubbles of diameter less than 50 μm will produce considerably more electrification than a smaller number of larger bubbles agrees well with the IRIBARNE and MASON (1967) theory of the electrification of bursting air bubbles.

Evidence was found that carbon dioxide was rapidly absorbed by a melting water drop falling in air and it was suggested that the different results of the effect of CO_2 on melting electrification noted by DRAKE (1968) and DINGER and GUNN (1946) can be explained by the way in which

CO_2 escaped from the ice during melting. A rapid increase of an order of magnitude in melting electrification over a small range of melting rates was observed, and this may be the same as that observed by DRAKE to be due to the onset of vigorous convection in the meltwater. It was shown that this increased electrification could occur at melting rates likely to be found in the atmosphere. No significant difference was noted between the electrification of ice melted on straight 100 μm platinum wires and 1.5 mm loops of wire. As the loop support is easier to use this is probably the best type of support.

Further work on the electrification of melting ice should include an evaluation of the effects of electric fields. The effect of CO_2 on the electrification should be reexamined in order to see whether its behaviour is consistent with a bursting bubble mechanism. Work on the electrification produced by the bursting of bubbles of less than 100 μm diamter would enable the IRIBARNE and MASON theory to be checked for the range of bubbles sizes likely to be found in small solid precipitation particles. The present work, and that of DRAKE, strongly suggest a bubble bursting mechanism for the formation of the positive charge on the meltwater.

12.3 THE ROLE OF MELTING ICE IN CLOUD ELECTRIFICATION

Using the information gained in the present investigation and the work of DRAKE (1968), the effect of some of the important variables influencing melting electrification can be assessed. It has been shown that precipitation particles of approximately specific gravity 0.9 and diameter 4 mm melting in a cloud will probably display the enhanced electrification which Drake associated with vigorous convection in the meltwater. It was found that the volume of air and the size of the air bubbles trapped in the ice could influence the electrification by an order of magnitude. Ice which was milky in appearance and which was formed in still air produced ten times less charging than completely opaque ice formed in an airstream. It is therefore suggested that the air bubble structure of the ice is very important in influencing the

the amount of electrification produced by this mechanism, and that ice formed by dry growth may be more effective than ice formed by wet growth.

The melting rate and particle size can influence the development of enhanced electrification which may be associated with vigorous convection in the meltwater. The melting rate depends on the speed of the downdraught and the density of the particles, as well as the size of the particles and the actual lapse rate of the temperature in the cloud. The effect of impurities in the cloudwater may be less than the effect of the air bubble structure and melting rates, according to the experiments described in Chapter 8. If the contribution of the melting ice to the electrical structure of a thunderstorm is to be assessed, then more information is needed of the actual melting ice particles and the melting environment.

It was pointed out in Chapter 10 that the amount of information of the location, magnitude and frequency of occurrence of the lower positive charge is very small. It is not even possible to say that there is only one type of lower positive charge. Certainly there is insufficient information to rule out a melting ice origin, but on the evidence available it was suggested that such a mechanism could only explain the charge under the best circumstances possible, unless the mechanism was more effective in the presence of electric fields.

The process of melting electrification and the conditions that might cause it to be an effective means of charge production in clouds are relatively well understood. However it is not possible to decide on the mechanism for the formation of the lower positive charge until more information is available on the magnitude and position of the charge, on the nature of the precipitation and the evironmental conditions associated with the charge. This laboratory investigation has suggested several properties of clouds which may well influence the cloud electrification. These properties must now be studied in detail if the physics of the lower positive charge is to be understood.

APPENDIX 1

A1.1 THE ELECTRIFICATION OF ICE SPHERES MELTING ON PLATINUM WIRES

Ice frozen in stagnant air

ARTIFICIAL CLOUD WATER - 4.5 mg l^{-1} sodium chloride.

Conductivity 8.4 μmho cm^{-1}

No	Dry Bulb Temperature °C	Dew Point - °C	Melting Heat mW	Initial Mass mg	Mass Melted mg
1	12.5	5.7	96	64	56
2	10.0	5.8	49	32	25
3	10.1	6.5	43	32	24
4	10.6	7.8	34	32	22
5	11.6	7.9	47	48	35
6	11.3	8.4	38	32	21
7	11.4	9.1	27	32	19
8	9.8	7.3	31	32	21
9	10.4	7.0	44	36	26
10	10.1	4.6	63	32	27
11	8.7	6.2	32	32	22
12	11.5	6.3	60	32	25
13	9.2	4.5	68	40	34
14	10.6	7.4	42	48	35
15	10.9	3.9	86	40	36
16	9.8	3.7	75	41	43
17	11.0	4.1	85	48	43
18	11.2	9.5	21	36	17
19	12.0	9.2	26	60	20
20	9.8	8.5	20	48	23
21	9.8	3.8	85	48	45
22	8.9	3.8	58	36	32
23	8.8	2.8	73	40	38
24	11.6	6.4	66	48	39
25	9.6	4.6	83	40	34
26	10.0	3.5	73	36	33
27	11.2	4.5	83	48	43
29	9.5	6.4	44	48	37
30	6.6	2.6	50	40	36
31	8.8	3.5	60	32	29
32	10.4	4.5	74	40	34
33	9.3	3.5	72	32	29
34	9.8	3.7	69	32	29
35	11.2	4.7	81	40	35
36	8.4	4.5	44	24	20
37	10.0	4.4	80	64	56
38	10.1	2.5	92	48	45
39	10.5	2.0	101	40	38
40	10.0	2.2	84	36	34
41	10.9	3.1	99	48	44
42	10.4	4.6	73	48	41
43	10.4	5.9	53	36	28
44	9.0	7.9	18	40	18
45	9.6	3.5	75	40	35
46	10.6	4.5	69	36	31

No	Dry bulb Temperature °C	Dew point -°C	Melting Heat mW	Initial Mass mg	Mass Melted mg
47	10.1	3.8	81	48	43
48	10.4	3.9	80	40	36
49	10.4	2.5	95	40	38
50	10.5	2.9	96	48	45
51	11.6	1.8	105	48	46
52	11.6	1.6	118	40	39
53	14.0	2.7	142	48	46
54	11.1	1.6	112	48	46
55	12.6	2.0	125	40	38
56	10.6	2.7	99	48	44
57	13.1	1.9	136	40	38
58	11.2	2.7	93	36	33
59	14.9	1.7	141	36	35
60	11.9	2.1	106	32	31

No	Freezing Temp - °C	Charge + pC	Charge/mass pC mg^{-1}
1	12	4.5	0.08
2	12	0.2	0.008
3	11.5	0	0
4	13	0.2	0.009
5	12.5	2.0	0.058
6	13	1.3	0.060
7	12.5	0.7	0.038
8	12	0.2	0.009
9	11.5	0.1	0.004
10	11.5	0.1	0.004
11	12	0.1	0.005
12	11.5	0.2	0.008
13	11.5	0.4	0.012
14	13	0.8	0.023
15	12	0.6	0.016
16	11.8	2.2	0.051
17	11.5	0.7	0.016
18	14.5	1.0	0.057
19	14	0	0
20	10.5	0.1	0.004
21	10	0.8	0.018
22	10	0.1	0.003
23	10.5	0.9	0.024
24	13	2.4	0.062
25	12	1.3	0.038
26	10.5	4.2	0.129
27	11.5	2.0	0.047
28	14	3.1	0.106
29	13	2.3	0.063
30	11	0.3	0.008
31	11	0.5	0.017
32	12.5	1.3	0.038
33	11.5	0.5	0.017
34	11	1.3	0.045
35	11.5	0.9	0.026
36	11	0.1	0.005

No	Freezing Temp $-^{o}$ C	Charge +pC	Charge/mass pC mg^{-1}
37	13	3.1	0.055
38	10.5	1.3	0.029
39	11	1.2	0.031
40	12	0.4	0.012
41	10	1.6	0.036
42	11	0.7	0.017
43	12	1.2	0.043
44	14	1.6	0.088
45	14.5	1.0	0.028
46	10.5	1.0	0.032
47	12	2.2	0.051
48	11.5	1.7	0.048
49	14.5	4.1	0.109
50	12	1.0	0.022
51	11	1.5	0.032
52	11.5	0.7	0.018
53	14.5	3.4	0.074
54	13	2.6	0.056
55	15	4.4	0.114
56	14.5	1.4	0.031
57	11	1.3	0.034
58	11	0.9	0.027
59	10.5	1.1	0.031
60	10	1.0	0.033

A1.2 THE ELECTRIFICATION OF ICE SPHERES MELTING ON PLATINUM WIRES

Ice frozen in stagnant air.

DEIONIZED WATER Conductivity 1.0 μmho cm^{-1}

No	Dry Bulb Temperature ^{o}C	Dew Point $-^{o}$C	Melting Heat mW	Initial Mass mg	Mass Melted mg
61	13.0	1.2	138	40	39
62	13.7	3.3	119	36	34
63	14.0	2.0	154	48	46
64	14.1	2.5	138	40	38
65	14.3	2.4	141	40	38
66	13.2	0.8	157	48	47
67	13.5	2.5	131	40	38
68	12.0	1.4	125	46	45
69	13.6	2.5	126	32	30
70	13.7	2.5	121	32	31
71	15.0	2.6	154	48	46
72	13.8	2.5	140	48	46
73	13.2	2.2	130	46	44
74	14.7	3.2	137	40	38
75	14.0	2.8	133	46	44

No	Freezing Temperature $-^{o}C$	Charge +pC	Charge/mass pC mg^{-1}
61	12	5.7	0.15
62	9	3.9	0.12
63	9.5	3.2	0.069
64	11.5	4.6	0.12
65	14	11.1	0.29
66	10.5	3.8	0.08
67	12	7.6	0.20
68	13	8.2	0.18
69	7.5	2.9	0.10
70	50	1.1	0.036
71	6.5	1.2	0.026
72	6.8	2.2	0.05
73	14.5	4.0	0.09
74	12.5	3.8	0.10
75	13.0	4.5	0.10

A1.3 THE ELECTRIFICATION OF ICE SPHERES MELTING ON PLATINUM LOOPS

NO	Dry Bulb Temperature ^{o}C	Dew Point $-^{o}C$	Melting Heat mW	Initial mass mg	Mass Melted mg
76	12.5	1.0	115	24	24
77	14.0	2.4	100	18	17
78	12.3	2.5	90	18	17
79	14.2	4.7	94	21	19
80	13.7	1.1	127	27	27
81	13.2	1.7	118	24	23
82	13.5	1.5	109	18	18
83	13.7	1.3	99	14	14
84	12.0	2.0	81	14	14

No	Freezing Temperature $-^{o}C$	Charge +pC	Charge/mass pC mg^{-1}
76	11	5.0	0.21
77	9	0.8	0.046
78	8.5	1.2	0.07
79	10	2.0	0.11
80	11.5	5.0	0.19
81	11.5	4.4	0.19
82	7	2.0	0.11
83	4	0.1	0.007
84	8	3.9	0.29

A1.4 THE ELECTRIFICATION OF ICE SPHERES MELTING ON PLATINUM LOOPS

DEIONIZED WATER Conductivity 1.0 μmho cm^{-1}

Drops frozen in an airstream moving at 11 ms^{-1}

No	Dry Bulb Temperature ^{o}C	Dew Point $-^{o}C$	Melting Heat mW	Initial Mass mg	Mass Melted mg
85	12.0	2.0	86	18	17
86	11.0	1.5	81	18	17
87	14.5	4.5	82	14	13
88	11.8	6.2	48	16	13
89	14.0	1.3	108	18	18
90	12.0	2.5	82	18	17
91	12.8	2.0	87	14	13
92	13.1	2.0	89	14	13
93	12.7	1.2	98	18	18
94	13.1	2.0	95	18	17
95	11.2	1.3	85	18	18

NO	Freezing Temperature $-^{o}C$	Charge +pC	Charge/mass pC mg^{-1}
85	12.0	11.2	0.65
86	12.5	13.5	0.77
87	5.2	6.9	0,54
88	12.3	12.2	0.94
89	8.5	12.0	0.68
90	3.5	2.9	0.17
91	11.5	15.3	0.14
92	6.6	12.5	0.93
93	2.4	0.4	0.023
94	5.3	4.6	0.27
95	12.5	11.1	0.63

Melting heat is defined as the heat flow rate to the melting sphere which causes the ice to melt and is corrected for the loss of heat due to evaporation using equation 8.1. The value of mass melted, melting heat and charge/mass were worked out on the N.U.M.A.C. I.B.M. 360 computer using the program outlined in A1.5.

A1.5 FORTRAN PROGRAM USED TO PROCESS THE MELTING ELECTRIFICATION DATA

```
      DIMENSION TW (100), HTM (100), TIME (100), TIMM (100), AMASS (100), Q (100),
                TDEW (100), RAD (100), HMELT (100), TF (100)
1.    FORMAT (12 F 5.1)
2.    FORMAT (8 x, 'TEMPW', 2x, 'HT. MELT', 2x, 'TIMM', 2x, 'HT,EVAP', 2x,
        'TIME', 4x, 'INMASS', 2x, 'CHARGE', 2x, 'FRACTM', 2x, 'MASS MLT',
        2x, 'RATE', 4x, 'QPM', 5x, 'RAD', 6x, 'TDEW', 3x, 'TEMPF')
3.    FORMAT (2x, I3, 14 F 8.3)
      READ (5,1) (TW(I), HTM(I), TIME (I), TIMM (I), AMASS (I), Q(I), I =1,36)
      READ (5,1) (TDEW (I), RAD (I), TF (I), I = 1,36)
      WRITE (6,2)
      DO 10 I = 1,36
      HT MELT (I) = 3.9 * RAD (I) * (TW (I) * 1.34 - 1.09 * TDEW (I) -
        0.022 * TDEW (I) * * 2.
      HTE = 3.9 + RAD (I) * (1.0( * TDEW (I) + 0.022 * TDEW (I) * * 2.)
      A  = H MELT (I) * 8. * TIMM (I)
      B  = HTE * TIMM (I)
      C = 3.9 * RAD (I) * (.55 * 7 DEW (I) + .005 * TDEW (I) * * 2.)
      D = C * (TIME (I) - TIMM (I))
      FRACTM = A/ (A+B+D)
      AMELT = FRACTM * AMASS (I)
      RATE - AMELT/TIMM (I)
      QPM = Q (I) / AMELT
10.   WRITE (6,3) I, TW(I), H MELT (I), TIMM (I), HTE, TIME (I), AMASS (I),
        Q (I), FRACTM, AMELT, RATE, QPM, RAD (I), TDEW (I), TF (I)
      STOP
      END
```

In the above program the names of the variables are as follows

I index number of the ice particle

TW average dry bulb temperature during last minute of melting ^{o}C

HTM melting heat mW

TIME Time particle was evaporating min.

TIMM Time particle was melting min.

(This is defined by the time between the moment when the air temperature has been raised halfway between $0^{o}C$ and its final value at the end of melting and the end of the melting process).

AMASS The initial mass of the particle as deduced from its dimensions mg.

Q The charge on the meltwater at the end of melting pC

(This was calculated by integrating the current over the melting period using the U.V. chart record).

TDEW Modulus of the dew point temperature of the air in the tunnel during the last minute of melting. ^{o}C

RAD Mean radius of the particle mm

TF Modulus of the temperature of the freezing environment ^{o}C

FRACTM Fraction of the ice actually melted.

AMELT Mass of ice actually melted mg

QPM Charge/mass melted pC mg^{-1}

APPENDIX 2

THE ABSORPTION AND DESORPTION OF CARBON DIOXIDE BY WATER

A2.1 Absorption by a stationary drop.

The chief cause of resistance to the diffusion of CO_2 into a water drop in stagnant air is the thin surface film of liquid. This film has a permeability which rapidly decreases after the initial exposure to CO_2 due to the increasing saturation of the layer. When the film is saturated the permeability remains constant. The rate of absorption can be related to the concentration gradient in the surface film by

$$\frac{\partial W}{\partial t} = k\,A\,(Cg - C_1) \qquad \text{.....} \qquad \text{A2.1}$$

where W is the volume of gas absorbed, A the surface area, k the permeability coefficient and C the concentration of CO_2. The subscript 1 refers to the liquid remote from the film and g to the gas/liquid boundary.

RIDEAL and DAVIES (1963) show, by solving the diffusion equation for a stagnant liquid of infinite extent, that the permeability coefficient is related to the diffusion coefficient D by

$$k = \sqrt{\frac{D}{\pi t}} \qquad \text{.....} \qquad \text{A2.2}$$

provided that the film is not saturated. After the film becomes saturated at a time t_s

$$k = \sqrt{\frac{D}{\pi t_s}}$$

By integrating A2.1 with respect to time and substituting for k we have, for a water drop of radius r,

$$W = \int_0^t \left(4\pi r^2 (Cg - C_1) \sqrt{\frac{D}{\pi t}}\right) dt \qquad \text{.....} \qquad \text{A2.3}$$

After a time t, the fraction f of the amount of CO_2 absorbed at equilibrium may be written as

$$f = \frac{W}{(4\pi r^3 Cg/3)} = \frac{3}{rC_1} \int_0^t (Cg - C_1) \sqrt{\left(\frac{D}{\pi t}\right)}\, dt \quad \text{...A2.4}$$

If we assume that once the CO_2 has passed through the surface film it is rapidly distributed throughout the drop

then $C_1 = f\ Cg$

so $$f = \frac{3}{r}\sqrt{\left(\frac{D}{\pi}\right)}\int_o^t \frac{1-f}{\sqrt{t}}\,dt \quad \ldots\ldots\ A2.5$$

This equation has a solution

$$f = \sum_1^{n=\infty} -(-1)^n \cdot 2\left(\frac{3}{r}\right)^n \left(\frac{D}{\pi}\right)^{n/2} t^{n/2} \ldots\ A2.6$$

which converges rapidly if $t \ll \frac{r^2}{D}$. but tends to infinity if $t > \frac{r^2}{D}$. The value of $t = \frac{r^2}{D}$ corresponds to the time when the permeability has reached a minimum value due to the saturation of the layer and may be designated as t_s. WHITEMAN et al (1926) quote the permeability coefficient for $t > t_s$ as $2.8 \times 10^{-6} ms^{-1}$, which approximately corresponds to a saturation time t_s of 100s.

For $t > 100$ s f can be expressed in terms of f_{100}, the value of f at t = 100s, and k_{100}, the permeability coefficient for $t \geq 100_s$

$$f = f_{100} + \frac{3k_{100}}{r}\int_o^T (1-f)\,dT \ldots\ldots A2.7$$

where T = t -100.

Differentiating A2.7 and writing $a = \frac{3}{r} k_{100}$

$$\frac{df}{dT} = a\,(1-f) \quad \ldots\ldots\ A2.8$$

This has the solution

$$f = 1 - (1-f_{100})\exp(-a(t-100)) \quad \ldots\ldots\ A2.9$$

For a 4 mm diameter water drop A2.6 gives $f_{100} = 0.56$. Equations A2.6 and A2.9 are plotted in fig. 9.3.

A2.2 The desorption of a thin water layer in a container.

The desorption of a thin water layer on the surface of a block of ice in a container can be treated in a similar way to the absorption of gas by a water drop, provided that the process is by molecular diffusion

through an undisturbed surface film. If the surface film has been present for longer than 100s then it can be said to be saturated and the permeability can be taken as constant.

For a layer of area A and depth d, f may be written in a similar way to equation A2.5:

$$f = \int \frac{kA(1-f)}{Ad}\,dt = \int \frac{k}{d}\,(1-f)\,dt \quad \ldots\ldots\ldots \text{A2.10}$$

The solution of A2.10 will be

$$f = 1 - \exp - (kt/d) \quad \ldots\ldots\ldots \text{A2.11}$$

The time constant of the desorption of a layer d due to its formation from Co_2 saturated ice will be d/k. For a 1 mm layer with $k = 2.8 \times 10^{-6}$ ms^{-1} WHITMAN et al. (1926), the time constant will be approximately 400s.

A2.3 The release of carbon dioxide from a bubble immersed in an unsaturated liquid.

If one assumes that the gas will diffuse through the bulk liquid faster than through the surface film, and if the concentration of CO_2 in the water is negligible compared to that in the bubble, the volume of CO_2 removed from the bubble is

$$Q = \int k\,A\,Cg\,dt \quad \ldots\ldots\ldots \text{A2.12}$$

where A is the surface area of the bubble and Cg the concentration of CO_2 inside the bubble. The fraction f of the intial concentration Co of Co_2 in the bubble is given in a similar way to A2.5 as

$$f = \frac{3}{Co.4\pi r^3} \int \sqrt{\frac{D}{\pi t}}\; 4\pi r^2\, Co\, f\, dt \quad \ldots\ldots\ldots \text{A2.13}$$

Differentiating both sides of A2.13 by t we have

$$\frac{df}{dt} = \frac{3}{r}\sqrt{\frac{D}{\pi t}}\,.f$$

which may be expressed as

$$\frac{df}{f} = \frac{3}{r}\sqrt{\frac{D}{\pi t}}\,dt \quad \ldots\ldots\ldots \text{A2.14}$$

Integrating equation A2.14 we have

$$f = \exp\left(\frac{-6}{r}\sqrt{\frac{Dt}{\pi}}\right) \quad \ldots\ldots\ldots \text{A2.15}$$

REFERENCES

ALTY, T.	1926	The origin of the electric charge on small particles in water Proc. Roy. Soc. A, 112, 235-51
ARENBERG, D.L.	1941	The formation of small hail and snow pellets. Bull. Amer. Met. Soc. 22, 113-6
BENT, R.B.	1964	The electrical space charge in the lower atmosphere. Unpublished Ph.D thesis, University of Durham.
BEST, A.C.	1951	Drop-size distribution in cloud and fog. Quart. J.R. Met. Soc. 77, 418-26
BLANCHARD, D.C.	1950	The behaviour of water drops at their terminal velocity in air. Trans. Amer. Geophys. Union, 31, 836-42.
BLANCHARD, D.C.	1957	The supercooling, freezing and melting of giant waterdrops at their terminal velocity in air. in Artificial stimulation of Rain, Pergamon Press (Woods Hole conference Report - 1955)
BLANCHARD, D.C.	1963	Electrification of the atmosphere by particles from bubbles bursting in the sea. Progress in Oceanography 1, 73-202 Pergamon Press.
BRAHAM, R.R.	1963	Measurements of snow pellet bulk densities. J. App. Met. 2, 498-500.
BROCAS, J. and DELWICHE, R.	1963	Chloride, potassium and sodium concentration in Antarctic snow and ice. J.G. Res. 68, 3999-4000
BROWNING, K.A. and LUDLAM, F.H.	1962	Airflow in convective storms. Quart. J.R. Met. Soc. 88, 117-135
BROWNSCOMBE, J.L. and HALLETT, J.	1967	Experimental and field studies of precipitation particles formed by the freezing of supercooled water. Quart. J.R. Met. Soc. 93, 436-74.
BYERS, H.R. and BRAHAM, R.R.	1948	Thunderstorm structure and circulation. J. Met. 5, 71-86.
BYERS, H.R. and BRAHAM, R.R.	1949	The Thunderstorm, U.S. Department of Commerce, Washington. (Report of the Thunderstorm Project)

BYERS, H.R. and BRAHAM, R.R. 1953 Thunderstorm structure and dynamics. in Thunderstorm Electricity pp 46-65. University of Chicago, Byers Ed.

BYERS, H.R. 1965 Elements of cloud physics University of Chicago Press.

CARTE, A.E. 1961 Air Bubbles in ice. Proc. Phys. Soc. 77, 753-68.

CHALMERS, J.A. 1965 The role of melting in atmospheric electricity. Proceedings supplement 152-56 Int. Conf. Cloud physics. Tokyo and Sapporo.

CHALMERS, J.A. and PASQUILL, F. 1937 The potential difference at an air-water interface. Phil.Mag.Ser 7, 23, 88-96

CHAPMAN, S 1953 Thunderstorm electrification in relation to rain and snow particles. In Thunderstorm Electricity pp207-231. Byers-Ed. University of Chicago Press.

CLARENCE, N.D. and MALAN, D.J. 1957 Preliminary discharge processes in lightning flashes to ground. Quart. J.R. Met. Soc. 83, 161-72.

COTTON, W. and GOKHALE, N. 1967 Collision, coalescence and break-up of large waterdrops in a vertical wind tunnel. J.G. Res. 72, 4041-51

CROSS, J.D. and SPEARE, P.A. 1969 Electrical aspects of the evaporation of ice. Brit. J. App. Phys. 2, 1021-5.

DAY, J.A. 1964 Production of droplets and salt nuclei by the bursting of air bubble films. Quart. J.R. Met. Soc. 90, 72-8

DINGER, J.E. 1964 Electrification accompanying the melting of ice and snow - correspondence. Quart. J.R. Met. Soc. 90, 208.

DINGER, J.E. and GUNN, R. 1946 Electrical effects associated with a change of state of water. Terr. Magn. Atmos.Elect. 51,477-94.

DRAKE, J.C. 1968 Electrification accompanying the melting of ice particles. Qurt.J.R. Met. Soc. 94, 176-91.

DRAKE, J.C. and MASON, B.J. 1966 The melting of small ice spheres and cones. Quart. J.R. Met. Soc, 92, 500-9.

DROZDOVA, V and PETRENCHUK,O.	1966	On the chemical composition of cloudwater Tellus 18, 280.
FETERIS, P.J.	1952	Detailed observations of thunderstorms. Weather 7, 35-9
FISHER, D and GAMBELL,A	1964	Occurrence of sulphate and nitrate ions in rainfall. J.G. Res. 69, 4203-10.
FOSTER, H.	1950	An unusual observation of lightning. Bull. Amer. Met. Soc. 31, 140-1 .
FRÖSSLING, N	1938	Über die Verdunstung fallender tropfen. Beiter.Geophys. Leipzig. 52, 170-216
GARNER, F.D and KENDRICK, P	1959	Mass transfer to drops of liquid suspended in a gas stream. Trans. Inst. Chem. Eng. 37, 155-170
GISH, O.H and WAIT, G.R.	1950	Thunderstorms and the earth's general electrification. J.G. Res. 55, 473-84.
GLUCKAUF, E.	1944	CO_2 content of the atmosphere Nature 153, 620-1
GREENFIELD, S.M.	1957	Rain scavenging of radioactive particulate matter from the atmosphere. J. Met. 14, 115-25.
GUNN, R.	1950	Free electric charge on precipitation inside an active thunderstorm. J.G. Res. 55, 171-8.
HELMHOLZ,H	1879	Wied. Ann. 7, 337
H.M.S.O	1938	Admiralty weather manual 487pp.
IRIBARNE, J.V. and KLEMES, M	1970	Electrification associated with the breakup of drops at terminal velocity in air. J. Atmos. Soc. 27, 927-35.
IRIBARNE, J.V. and MASON, B.J	1967	Electrification accompanying the bursting of bubbles in water and dilute aqueous solutions Trans. Farad. Soc. 163, 2234-45.
JUNGE , C.	1953	Die rolle der aerosole und der gasförmingen beimengungen der luft in spurenstoffhaushalt der troposphäre. Tellus 5, 1-26.

KAYE, G.W and LABY, T.H — 1968 — Tables of physical and chemical constants 13th ed. Longmans

KEELING, G — 1968 — Concentration of atmospheric CO_2 at 500 and 700 mb. J.G. Res. 73, 4511 -

KIKUCHI, K — 1965 — On the positive electrification of snow crystals in the process of their melting (3). J. Met. Soc. Jap. 43, 343-50.

KIKUCHI, K. and MAGONO, C. — 1965 — On the positive electrification of snow crystals ih the process of their melting (2). J. Met. Soc. Jap. 43, 331-42.

KINZER, G.D and GUNN, R. — 1951 — The evaporation, temperature and thermal relaxation time of freely falling water drops. J. Met. 8, 71-83.

KOENIG, L. — 1965 — Drop freezing through drop breakup. J.Atmos. Sc. 22, 448-51.

KRAMERS, H — 1946 — Heat transfer from spheres to flowing media. Physica, Hague, 12, 61.

KUETTNER, J. — 1950 — The electrical and meteorological conditions inside thunderclouds J. Met. 7, 322-32.

LANE-SMITH, D — 1969 — Electrical processes in heavy rain in the tropics. Unpublished Ph.D thesis, University of Durham.

LATHAM, J. — 1963 — The electrification of frost deposits. Quart. J.R. Met. Soc. 89, 265-70.

LATHAM, J. and MASON, B.J. — 1961 — Electric charge associated with temperature gradients in ice. Proc. Roy. Soc. A. 260, 523-37

LATHAM, J. and STOW, C.D. — 1965 — Electrification associated with the evaporation of ice. J. Atmos. Sc. 22, 320-4.

LATHAM, J. and STOW, C.D. — 1966 — The mechanism of charge transfer associated with the evaporation of ice. J. Atmos. Sc. 23, 245-7.

LEWIS, W. and WHITMAN, W. — 1924 — Principles of gas absorption. Indust. Chem. Eng. 16, 1215-20

LIST, R. 1959 Design and operation of the Swiss hail tunnel. Physics of Precipitation, IP, pp. 310-6. Proceedings of cloud physics conference, Woods Hole, American Geophysical Union.

LIST, R. 1965 The mechanism of hailstone formation. Proceedings of the International Conference of Cloud Physics, Tokyo and Sapporo, 481-92.

LITTLE, E.W.K. 1940 Observations on hail Quart. J.R. Met. Soc. 66, 21-2.

LUDLAM, F.H. 1950 The composition of coagulation elements. Quart. J.R. Met. Soc. 76, 52-8.

McINNES, D.A. 1961 The principles of electrochemistry. Dover.

McCREADY, P.B. and PROUDFIT, A. 1965 Self charging of melting ice Quart. J.R. Met. Soc. 91, 54-60.

McTAGGART, H. 1914 The Electrification of liquid-gas surfaces. Phil. Mag. 6th ser. 27, 293-314.

MALAN, D.J. 1952 Les décharges dans l'air et la charge inferieure positive d'un nuage orageux. Ann. de Geophys. 8, 385-401.

MALAN, D.J. and SCHONLAND, B.F.J. 1951 The distribution of electricity in thunderclouds. Proc. Roy. Soc. A. 209, 158-77.

MASON, B.J. 1954 Bursting of air bubbles at the surface of seawater. Nature 174, 470-1

MASON, B.J. 1956 On the melting of hailstones. Quart. J.R. Met. Soc. 82, 209-16.

MASON, B.J. 1957 The physics of clouds. Oxford. University Press.

MASON, B.J. and MATTHEWS, J.B 1964 Correspondence Quart. J. R. Met. Soc. 90, 208-9.

MATTHEWS, J.B. and MASON, B.J. 1963 The electrification accompanying the melting of ice and snow. Quart. J.R. Met. Soc. 89, 376-80.

MATTHEWS, J.B. and MASON, B.J.	1964	Electrification produced by the rupture of large water drops in and electric field. Quart. J.R. Met. Soc. 90, 275-87.
MICHNOWSKI, S.	1963	On the observation of lightning in warm clouds. Ind. J. Met. Geophys. 14, 320-2.
NAKAYA, U and TERADA, T.	1935	Simultaneous observations of mass falling velocity and form of individual snow crystals. J. Fac. Sc. Hokkaido Univ. 1. 191.
NEWITT, D.M. DOMBROWSKI, N, and KNELMAN, F.H.	1954	Liquid entrainment., The mechanics of drop formation from gas or vapour bubbles. Trans. Inst. Chem. Eng. 31, 244-61
NEWTON, C.W.	1967	Severe convective storms. Advances in Geophysics 12, 257-308.
NEWTON, C.W. and NEWTON, H.R.	1959	Dynamical interactions between large convective storms and environment with vertical wind shear. J. Met. 16, 483-96.
ODDIE, B.	1962	The chemical composition of precipitation at cloud levels Quart. J.R. Met. Soc. 88, 535-8.
PETRENCHUK,O. and SELEZNEVA	1970	Chemical composition of precipitation in regions of the Soviet Union. J.G. Res. 75, 3629-34.
PIERCE, E.T.	1955	Electrostatic field changes due to lightning discharges. Quart. J.R. Met Soc. 81, 211-28
POPE, A and HARPER, J.J.	1966	Low-speed wind tunnel testing Wiley
PRANDTL, L.	1952	Essentials of fluid mechanics Blackie.
PROBERT, S.D. and HUB, D.R.	1968	Thermal Insulation Elsevier
PRUPPACHER, H. and NEIBURGER, M.	1968	Design and performance of the U.C.L.A. cloud tunnel. Proc. Toronto Conf. 389-92.
RAMSAY, M.W. and CHALMERS, J.A.	1960	Measurements of the electricity of precipitation Quart.J.R.Met. Soc. 86, 530-39

REITER, R.	1965	Precipitation and cloud electricity. Quart. J.R.Met.Soc. 91, 60-72.
REYNOLDS, S.E. and NEILL, H.W.	1955	The distribution and discharge of thunderstorm charge centres. J. Met. 12, 1-12
RIDEAL, E.K. and DAVIES, J.T.	1963	Interfacial Phenomena. Academic Press. 2nd Edition
ROGERS, L.N.	1967	The electrification of water drops on freezing or melting at terminal velocity. Unpublished Ph.D. Thesis. University of Durham.
SARTOR, J.D.	1970	Accretion rates of cloud drops, raindrops and small hail in mature thunderstorms. J.G. Res. 75, 7547-58.
SIMPSON, G.C.	1909	On the electricity of rain and its origin in thunderstorms. Phil.Trans.A, 209, 379-413
SIMPSON, G.C.	1927	The mechanism of a thunderstorm Proc. Roy. Soc.A, 114, 376-401.
SIMPSON, G.C. and ROBINSON, G.D	1941	The distribution of electricity in thunderclouds (2) Proc. Roy. Soc. A, 177, 281-329.
SIMPSON, G.C. and SCRASE, F.J.	1937	The distribution of electricity in thunderclouds. Proc. Roy.Soc. A, 161, 309-52
SPILHAUS, A.F.	1947	Raindrops size, shape and falling speed. J. Met. 5, 109 -
TAHAHASHI, T.	1969	Electric potential of liquid water on an ice surface. J. Atmos. Sc. 26, 1253-8.
WEICKMANN, H.K.	1953	Observational data on the formation of precipitations cumulo-nimbus clouds. in Thunderstorm Electricity, Ed. Byers. University of Chicago Press 66 - 138.
WEICKMANN, H.K. and AUFM KAMPE, H.K.	1953	Preliminary results concerning the charge generation in thunderclouds J. Met. 10, 204-811
WHIPPLE, F.J.W.	1938	Modern views on atmospheric electricity. Quart. J.R. Met. Soc. 64, 199-214.

WHITMAN, W.
LONG, L
and
WANG, H.
1926
Absorption of gasses by a liquid drop
Indust. Chem. Eng. 18, 363-7.

WILLIAMS, J.C.
1958
Some properties of lower positive charge in thunderclouds.
Proc. New Hampshire Conf. 425-9
Pergamon Press.

WOODCOCK, A.H.
KIENTZLER, C.F
ARONS, A.B.
and
BLANCHARD, D.C.
1953
Giant condensation nuclei from bursting bubbles.
Nature 172, 1144-5

WORMELL, T.W.
1939
The effect of thunderstorms and lightning on the earth's electric field.
Phil. Trans. A, 238, 249-303.